

The Institute of Electrical and Electronics Engineers (IEEE)
The Tomsk IEEE Chapter & Student Branch
The IEEE GOLD Affinity Group
of the Russia Siberia Section

IEEE INTERNATIONAL SIBERIAN
CONFERENCE ON CONTROL
AND COMMUNICATIONS

SIBCON-2005

PROCEEDINGS

RUSSIA, TOMSK, OCTOBER 21–22, 2005

IEEE International Siberian Conference on Control and Communications (SIBCON-2005). Proceedings. – Tomsk: The Tomsk IEEE Chapter & Student Branch, Russia, Tomsk, October 21–22, 2005.

Copyright and Reprint Permission: Abstracting is permitted with credit to the source. Libraries are permitted to photocopy beyond the limit of U.S. copyright law for private use of patrons those articles in this volume that carry a code at the bottom of the first page, provided the per-copy fee indicated in the code is paid through Copyright Clearance Center, 222 Rosewood Drive, Danvers, MA 01923. For other copying, reprint or republication permission, write to IEEE Copyrights Manager, IEEE Operations Center, 445 Hoes Lane, P.O. Box 1331, Piscataway, NJ 08855-1331. All rights reserved. Copyright © 2005 by the Institute of Electrical and Electronics Engineers, Inc.

Sponsor



Russian Foundation for Basic Researches (RFBR),
project # 05-07-93013

Technical co-sponsors



IEEE The Institute of Electrical and Electronics Engineers



Com.Soc

The IEEE Communications Society



The IEEE Microwave Theory and Techniques Society

Co-sponsors



Tomsk
IEEE
Chapter

The Tomsk IEEE Chapter & Student Branch



Tomsk Polytechnic University

IEEE Catalog Number: 05EX1091

ISBN: 0-7803-9219-1

Library of Congress: 2005925121

Welcome Message from the General Chair

Dear Colleagues,

On behalf of the Tomsk IEEE Chapter & Student Branch it is an honor and pleasure to cordially invite you to participate in the IEEE International Siberian Conference on Control and Communications SIBCON-2005, jointly organized by the Tomsk IEEE community and Russian Foundation for Basic Researches. The meeting celebrates its tenth anniversary continuing traditions of international conference SIBCON holding since 1995.

The technical challenges and opportunities in communications and control are progressing at an unprecedented pace. The merging of technical research and business applications is increasingly important as traditional circuit and data services are intertwined with the Internet. Communication and control systems will be a major player in the global word market. Extending communication technologies to wideband services stimulates the development of new types of circuits and systems oriented toward the realization of low-cost, low-voltage, and portable devices. These reasons have determined the choice of the conference topics.

With the assistance of an excellent Technical Program Committee, we have been able to put together a very interesting technical program. The Technical Committee has carefully considered submissions to design a comprehensive program of technical papers that spans most of the key areas. Among the topics receiving the largest numbers of papers for this year's conference were information security, signal processing, and QoS for wireless systems. As is evident from just those categories alone, the technical program will almost assuredly provide some topics of interest for all attendees. In the opinion of the Organizing Committee, session topics include the main part of perspective questions and problems, for example, detectors for nondestroying control.

When we first planned the SIBCON conference, we envisioned a meeting that engineers and scientists would gather and openly discuss all aspects of control and communications. Thus, it would be more inclusive than the traditional event in material physics, microwave and wireless circuits and systems, electron devices and transistors, and radar. Instead, aspects from each of these different, individual symposia would be brought together under one symposium to unify a single community of engineers interested in developing the next generation technique. Furthermore, we wanted to include the contributions from engineers throughout the world since progress is always accelerated when

everyone's ideas are heard. We believe this tradition conference succeeded to meet both of these goals.

We also encourage you to take advantage of the wonderful opportunity to meet and exchange ideas with colleagues. I think that's the spirit of good technical conferences to share as by-products. Once we are here in the hope of meeting old acquaintances to know what they are doing, and above all, of making new friends with similar technical expertise and interests.

No event can be successful without the support and encouragement of commercial sponsors. So, thanks go to AlparSoft R&D. This inaugural collaboration between the Tomsk IEEE Chapter and AlparSoft promises to be a milestone event promoting the interaction of our researchers with leading software companies.

The success of any event is due to the efforts of many people, and this conference is no different. Gratitude is also deserved for the Russian Foundation for Basic Researches, the IEEE Microwave Theory and Techniques Society, and the IEEE Communications Society for providing technical and financial support. I would like to welcome all the participants, and especially, to express the warmest gratitude to all the paper presenters for sharing their valuable experiences with us, on behalf of the organizing committee of the conference. My special thanks go to my good friends and reviewers, without whose help this conference would not have taken place.

Welcome to SIBCON 2005 and welcome to Tomsk!

Oleg Stukach

The Usage of Mobile Agents for Management of Data Transmission in Telecommunications' Networks

M. Sc. Tomasz Orzechowski

*Department of Telecommunications, AGH University of Science and Technology, al. Mickiewicza 30, 30-059 Cracow, Poland
phone: +48 501426360; fax. +48 122699011; e-mail: to@ieee.org*

Abstract — Mobile Agent Technology potentially has a very wide spectrum of the utilization. It is often used in these network's areas where making operations without any user's attendance is seen as benefits [3,5,6,7]. This article focuses on the possibility of the usage mobile agents (MAs) for data transmission management. Mobile agents, in described system, are responsible both for splitting and merging data stream that is created between target service and end-user. This process is fully hidden from end-users. The system is the part of MAO Service (Mobile Agent Offering Service), which the main purpose is to allow end-users to "pay and enjoy" the contents located on remote hosts (i.e. pay not only for the access to the information but also for the maintenance of the data stream that fulfils all end-users' requirements like QoS parameters).

Index Terms — mobile agents, data transmission, QoS

1. INTRODUCTION

A development in Internet services, network protocols and a progress of commercialization deliver a wider spectrum of Internet utilization to end-users. They can not only send e-mails, exchange files, but often get access to live streams of video (films, video-conferences, etc.) or voice (radio, telephony, etc.) contents. Nowadays users potentially have a possibility to choose a quality of data transmission that is required. However, how to change the bandwidth only for the short period at the local network provider when someone decides to see the video film via Internet in real time?

It is still rather impossible...

The Mobile Agent Oriented Service (MAO Service) is a solution for it. It could be seen as a kind of a "travel bureau" where end-users can see an offer, choose, pay for it and then enjoy it.

2. GENERAL CONCEPT OF THE SERVICE

Each (MAO) service can process primarily gathered information (concerning the structure of network, i.e. existing connections, their characteristics, costs of utilization, etc.) and subsequently deliver a real offer (complied with sets of rules: costs, QoS, etc.) to all end-users.

MAO Services could be seen as a kind of middle layer between

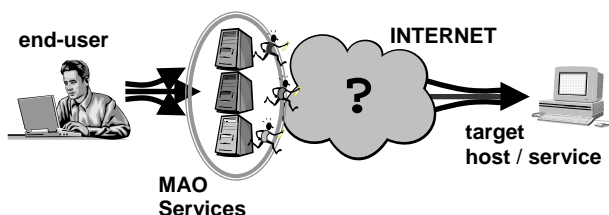


Fig. 1. Location of MAO Services

end-users and remote resources (Fig.1). The process of gathering information is accomplished by mobile agents. The MAs can negotiate with gateway static agents for costs of data transmission. The whole process was presented in detail in another article [4].

3. DATA TRANSMISSION MANAGEMENT

It was assumed that providers could add their own routers into current networks, or/and create alternative connections between existing gateways. Moreover, either end-users or remote services can be attached to more than one network (Fig.2).

When end-users want to connect to any remote resources, they can do it on their own or just by using MAO Service. Proposed Service is responsible for proper maintenance of sold offer. This offer includes not only costs of accessing to remote resources but also creation of the data stream between end-users and target resources (QoS parameters are guaranteed). The process of buying complete offer is presented at figure 3 – steps I-III.

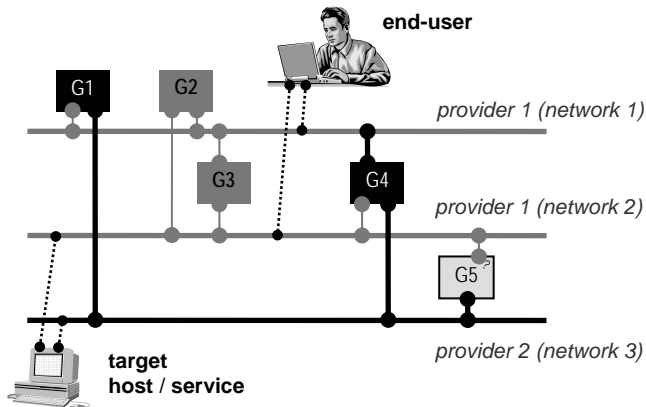


Fig. 2. Assumed structure of networks and connections among them

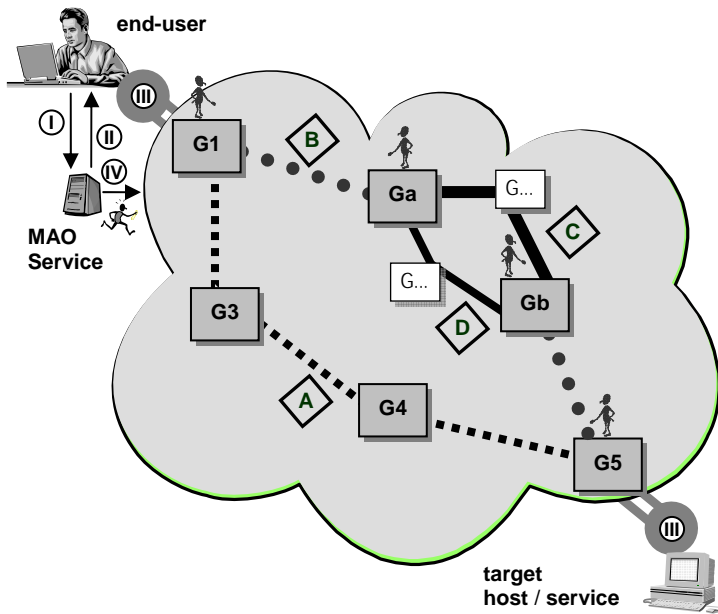


Fig. 3. Access to remote resources as invisible split stream

From end-users side it could be seen as a holiday package purchase in a travel bureau. The full booking process consists of following steps:

- to choose a travel bureau;
 - to choose an offer;
 - to accept regulations;
- } ①

- to make payments;
 - to receive a voucher;
 - to make connection to remote resources using voucher.
- } ②
 } ③

From MAO Service side situation is much more complicated. The simplest process consists on reservation resources without mobile agents. If routers support mobile agent technology, connections will be established by the usage of mobile agents, but data transmission doesn't need any assistance from MAs. In the most advanced case data transmission is fully managed by mobile agents. It means that specific mobile agents are sent to edge routers where they become both traffic generator and receiver and they are responsible for splitting and merging data streams. (*The edge router means a place where splitting or merging streams taking place.*) Of course each of a single partial stream can be sent different ways. Familiar topics were described by other authors [1,2].

In my opinion the best solution should have mixed character. If it is only possible MAs should be exclusively used during the process of connection establishing. When we need to split data stream mobile agents should be sent to the edge routers. They will capture user data stream, split it and change user's voucher to cover it by their own vouchers (each new stream needs its own voucher) [Fig.3, A & B streams]. There is no problem to split the stream that was previously split [Fig.3 C & D streams].

Splitting and merging techniques allows us to create virtual channel with better parameters of QoS (i.e. higher bandwidth), lets us decrease costs of data transmission and enables stability of transmission when redundant streams are created.

4. CONCLUSIONS

This article presents the recent trends in the development of global network. It focuses on creation integrated services where user might receive access to remote resources under guaranteed parameters of connections. The most important in presented system is that if only there are no hardware restrictions end-user, after payment, will receive a special channel to remote resources so often also temporary parameters of connection in local network will improve (i.e. bandwidth). The MAO Service was generally designed for P2P transmissions, but the usage of the service for multicast transmissions will be also taken under consideration in future. Moreover, all cumulated information could also be used by provider to observe network traffic, or prepare proposals for

the reconfiguration of the current network structure in real-time.

REFERENCES

- [1] S.S.Manvi i P. Venkataram, *QoS Management By Mobile Agents in Multimedia Communication*, The IEEE 11th International Workshop on Database and Expert Systems Applications (DEXA'00).
- [2] N. Minar, K. H. Kramer, P. Maes, *Cooperating Mobile Agents for Dynamic Network Routing*, The ACM Mobile Computing and Communications Review (SIGMOBILE), April 1999, vol. 3/2, pp. 12-16.
- [3] T. Orzechowski, *Ontology oriented systems of the access to information*. The IEEE-Siberian Conference on Control and Communications, 1-2 Oct. 2003, pp. 3-9.
- [4] T. Orzechowski, *The usage of mobile agents for making services in telecommunications' networks*, KKRRiT, Cracow 17-2 June. 2005.
- [5] T. Orzechowski, *Updating System for Distributed Databases*, The IASTED CATE'2002, Cancun, Mexico, ACTA Press, pp. 421-425.
- [6] Vu Anh Pham i A. Karmouch, *Mobile Software Agents - An Overview*, IEEE Communications Magazine, vol.3, July 1998; pp. 26-37.
- [7] S. Rayan, R. Pradeep, N. Paramesh, *Network management platform based on mobile agents*, Int. J. Network Mgmt 2004; 14: 59–73.

A Convolutional Code Decoder Design Using Viterbi Algorithm with Register Exchange History Unit

Vasily P. Pribylov, *Member, IEEE*, Alexander I. Plyasunov

*Siberian State University of Telecommunications and Informatics,
86, Kirova str., 630102, Novosibirsk, Russia
Tel.: +7 3832 661478, E-mail: v.pribylov@ieee.org*

Abstract — In this paper, results of a design of a convolutional code decoder using Viterbi algorithm with path-history unit based on register-exchange architecture are considered. Some functional simulation results for the design are given. Various uses of a designed scheme are possible, mainly in communication systems.

Index Terms — Data transmission, error-control coding, convolutional codes, Viterbi algorithm, register-exchange architecture, Verilog.

I. INTRODUCTION

It is known that noise-immunity is one of the basic attributes of information transmission systems. Since errors are possible in communication channels during the data transmissions we must apply error-correcting codes to combat these errors. In most of applications the convolutional codes [1] are used for this purpose. Convolutional code definition parameters are the following: code rate R , generating polynomials $\{g\}_n$, constraint length K . The rate is the number of transmitted bits per input bit, e.g., a rate $1/2$ encodes 1 bit and produces 2 bits for transmission. A code can be punctured to increase its rate, by deleting some of the encoded bits according to some pattern. One generating polynomial stands for one output. The constraint length is the length of the generating polynomial in bits. The higher it is the more robust is the code.

Three exist basic convolutional codes decoding techniques: sequential [2], threshold [3] and maximal-likelihood, which is best known as the Viterbi algorithm [4]. The sequential algorithm can provide very strong correcting capabilities while it needs relatively large memory, which strongly depends on communication channel error density. The threshold algorithm is extensively good for channels with mid-to-good signal-to-noise ratios (SNR). The Viterbi algorithm is an

asymptotically optimum decoding technique. It is also the relatively “straight” algorithm to implement in hardware. However, the complexity of the Viterbi decoder increases exponentially with the constraint length, so it is impractical to use codes with constraint lengths more than $K > 15$ (3 to 9 is common practice [5]). Useful description of the Viterbi algorithm can be found in [6].

The receiver can deliver either hard or soft symbols to the Viterbi decoder. A hard symbol is equivalent to a bit $\{0,1\}$. A soft symbol is multi-bit symbol (usually from 3 to 8 bits, [5]), least-significant bits (LSBs) representing the confidence in the bit being positive or negative, e.g., if the channel is Gaussian, the output of a matched filter quantized to a given number of bits can present a soft input for a decoder. Soft decision offers approximately a 3 dB increase in coding gain over hard-decision decoding, but its implementation has a significant cost in terms of chip area.

Until now, the trace-back [7] and the register-exchange [8] approaches are the two major techniques used for the path history management in the chip designs of Viterbi decoders. The former takes up less area [9] but requires much more time than the latter, since it needs to search the trace of the survivor path back sequentially. The recommended value of the trace-back length for non-punctured decoding is at least $6 \cdot K$ [10]. For punctured coding or external erasure, a larger value trace-back length is required, usually at least $10 \cdot K$ in order to obtain optimal bit-error rate (BER) performance. The major disadvantage of the latter approach is that its routing cost is very high especially in the case of long-constraint code. However, it has minimal latency, that is, one clock cycle.

In this paper some results of a design of a convolutional code decoder using Viterbi algorithm with path-history unit based on register-exchange architecture and hard decisions are considered. In Section II description of decoder architecture is presented. In Section III some functional simulation results for the design are given. Section IV presents some comparison results for implementation of the decoder in programmable logic devices of different vendors. Section V concludes the paper.

II DECODER ARCHITECTURE

We have chosen to implement a four state Viterbi decoder for $R=1/2$ (5,7) convolutional code with free distance $d_f=5$, which is capable of correcting up to two errors within $4 \cdot K$ distance.

The entire chip can be divided into five distinct functional units: branch metric unit (BMU), add-compare-select unit (ACS), normalization unit (NU), register exchange path history unit (RE), and majority unit (MJ). Complete architecture of a decoder is presented in fig.1.

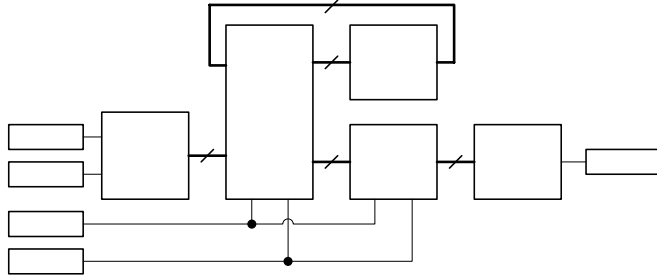


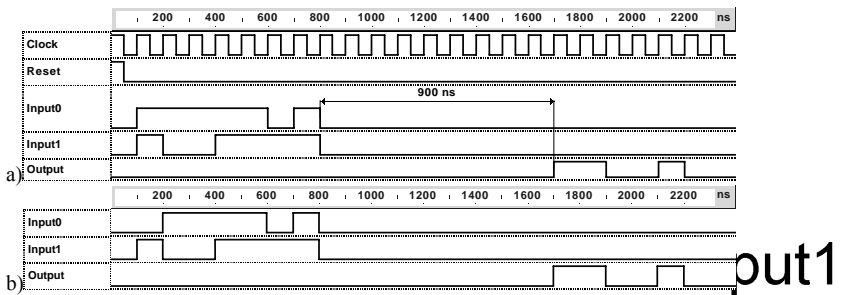
Fig.1. Viterbi decoder RE architecture

Decoder interface can be described as follows. The chip is clocked with external clock and at the beginning of the burst sequence decoder will be reset to the beginning state. There are two bit parallel inputs and one bit serial output.

Decoder has been implemented mostly using Verilog HDL. Some blocks have been designed in schematics editor directly.

III FUNCTIONAL SIMULATION

Functional simulation was done with the following parameters. Clock frequency is equal to $F_{clock}=10$ MHz. We consider the case of 5 transmitted information bits with 2-bit tail (for forcing coder register to zero state) $I=11001.00$ with different error patterns. This gives us the encoded sequences $C0=1111101$ (polynomial 5), $C1=1001111$ (polynomial 7), which corresponds to Input0 and Input1 of the decoder, see fig. 2a.



input1
input0

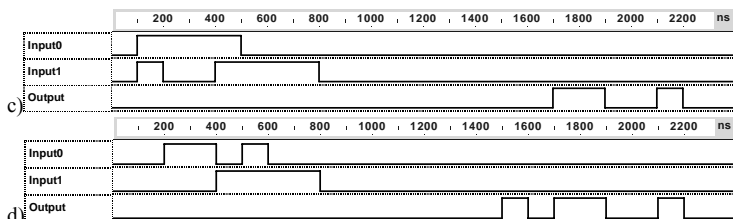


Fig.2. Functional simulation of decoding process:
 (a) no errors, (b) 1 error, (c) 2 errors, and (d) 4 errors

Decoding delay is equal to $T_d = 900$ ns that is 9 clock cycles. Results of fig.2d show the necessity of closing the output prior to the decoded sequence exit the RE-MJ that is after 9 clock cycles in our example. One can see that decoder works fine in all of the cases since the decoded sequence is the same as the transmitted information sequence $D = I = 11001.00$. It is also worth to mention that, at maximum, every 3rd-bit (one in K) error in one input can be corrected, see Input0 at fig.2c and fig.2d. Two consecutive errors are correctable also, see fig.2d, first bits at Input0 and Input1. Some more complex error patterns can be corrected, as it is shown in fig. 2d. To find the regularity of the correctable error patterns the more careful investigation is needed. And it is believed that the generating polynomials of encoder as well as the length of RE unit will be important in this investigation.

IV CHIP SELECTION FOR DECODER IMPLEMENTATION

Many alternatives for chip selection exist, some of them are considered in this Section. In our opinion there are 3 basic factors for chips which must be considered at this point: maximal clock frequency (determines the maximal data rate), number of gates and pins available, the price.

The decoder model synthesized for different chips has shown the estimated number of equivalent logic gates: ≈ 1200 -1400. The number of pins needed does not exceed 5 in-out pins plus a few pins for VDD and GND. That is almost all the existing chips are suitable for the implementation. Some speed results are presented in Table 1 for both area and speed optimization.

Table 1

Vendor	Altera		Xilinx		
Chip	FLEX10K	APEX20K	Coolrunner	VirtexE	Spartan2
Area opt.	12.64 MHz	-	26.32 MHz	-	124 MHz

Speed opt.	13.79 MHz	45 MHz	30.30 MHz	44 MHz	133 MHz
------------	-----------	--------	-----------	--------	---------

Thus the speed varies significantly from chip to chip. The main two factors are the chip technology process and its architecture. So it is up to the system architect to choose between the variants. In any case our design uses little (except FLEX10K) portion of chip area and thus some additional units can be implemented on a chip.

V CONCLUSIONS

In this paper, results of a design of a code rate $R=1/2$ constraint length $K=3$ convolutional code decoder using Viterbi algorithm with path-history unit based on register-exchange architecture are considered. Some functional simulation results for the design are given. Various uses of a designed scheme are possible, mainly in communication systems.

REFERENCES

- [1] P. Elias, "Coding for Noisy Channels," *IRE Conf. Rec.*, vol. 3, pt. 4, pp. 37-46, 1955.
- [2] J. M. Wozencraft, "Sequentlal decoding for reliable communication," *IRE Nat. Conv. Record*, vol. 5, pt. 2, pp. 11-25, 1957.
- [3] J.L.Massey, *Threshold Decoding*. Cambridge, Mass.: M.I.T. Press, 1963.
- [4] A. J. Viterbi, "Error Bounds for Convolutional Codes and an Asymptotically Optimum Decoding Algorithm," *IEEE Transactions on Information Theory*, vol. IT-13, April, 1967, pp. 260-269.
- [5] The Xilinx LogiCORE: Viterbi Decoder v3.0. Product Specification DS247 (v1.0), March 28, 2003.
- [6] A. A. Makarov, V. P. Pribylov. *Error-correction coding in telecommunications systems*. Monograph. SibSUTI, Novosibirsk, 2005, 186 p. (in Russian).
- [7] G. C. Clark, J. B. Cain. *Error-Correction Coding for Digital Communications*. Russian ed. / Editor B. S. Tsybakov, Moscow, "Radio i svyaz," 1987. – 392 p.
- [8] C. M. Rader, "Memory Management in a Viterbi Decoder," *IEEE Trans. Communications*, vol. COM-29, pp. 1399 - 1401, Sept. 1981.
- [9] G. Feygin and P. G. Gulak, "Architectural Tradeoffs for Survivor Sequence Memory Management in Viterbi Decoders," *IEEE Trans. Communications*, vol. COM-41, pp. 425-429, March 1993.

- [10] Viterbi Decoder from Amphion Semiconductor, Ltd., online at <http://www.altera.com/>.

Vasily P. Pribylov (S'01-M'03) was born in Kemerovo, Russia, in 1977. He received the B.Sc. and the Eng. degrees in radio engineering from the Siberian State University of Telecommunications and Informatics (SibSUTI), Novosibirsk, Russia, in 1998 and 1999, respectively. He received the Candidate of engineering sciences (Ph.D.) degree from the same university in 2004. He has been teaching at SibSUTI since 1999. Currently he is Asst. Prof. of Radio engineering systems department, SibSUTI. Dr. Pribylov is an active member of the IEEE Communications Society. He is the author more than 30 publications. His research interests include mobile communications, WLAN/WPAN integration, error-control coding and efficient data transmission over energy-constrained communications channels.

Alexander I. Plyasunov was born in Novosibirsk, Russia, in 1979. He received the Eng. degree in radio communications, broadcasting and television from SibSUTI, Russia, in 2005.

Formal Interpretation of Network Tasks of Model OSI

A. A. Kiselev, *Member, IEEE*, S.N. Novikov, *Senior Member, IEEE*

*Siberian State University of Telecommunications and Informatics
630102, Novosibirsk, Kirova str., 86, SibSUTI, MDT&M,
Tel: (383-2) - 66-50-59, e-mail: a.kiselev@ngs.ru*

Abstract — The purpose of paper-development of mathematical model which irrespective of type of cooperating open systems and used technologies information transformations of the at a network level and the appropriate planes of generalized model open system interconnection (GMOSI) are describes.

Index Terms — OSI, QoS, NGN, PP, data transformation

BACKGROUND

Based on the concept of interconnection of telecommunication and information systems the 7-level model of Open System Interconnection – OSI) is fixed [1]. For optimum interconnection of open systems developers of network technologies the process transformation functions of levels on planes have entered [2]. In [3] GMOSI is offered which transformation functions of system interconnections on levels and planes, and also process of transformations of the data which are carried out by levels and planes of model is submitted. The further development of model OSI [4] in most degree concerns not verbal, but the mathematical description system interconnection executed with detailed elaboration of functional transformations of the transmitted data on each of levels, for the description of these transformations the matrix equations are used.

1. VERBAL ROUTE MODEL

In paper [5] the verbal route model in a next generation network (NGN) (fig. 1) is offered. This model has some planes, each of which carries out complicated problems.

As the main goal of telecommunication system is intended for transmitting of the user information with required QoS (Quality of Service) all NGN resource is divided into two parts – service (R_S) and user (R_U). The user part of a resource for transmission only the user information with a required QoS is intended.

The service plane should solve the problem QoS transmission of the user information and by means of the appropriate types of protocols is realized:

- a) protocols of a signal system plane – allocate resource NGN for transmission of the user information with guaranteed QoS on probability – time characteristics (PTC) and a security degree; and a product of protocol functioning of the this plane are switch tables (ST QoS) and a protection profile (PP QoS);
- b) protocols of a definition of set of routes plane – evaluation NGN resources for transmission of the user information with guaranteed QoS; protocols of the this planes form databases (DB) about a condition of NGN elements, in result the set of route tables (RT) for various kinds of user services (RT QoS_i is formed; where n is quantity of kinds of the service this to the user) [5].

Enter the following designations:

P_i is the formation method of information distribution plan IDP

(wave, logic, game);

V_i is the method of a choice proceeding message transmission route (MTR) in switch node (gradient, diffusion, parallel, etc);

$\lambda_{\nu}=(\Delta M)$ is parameters of the user traffic acting in NGN;

R_{NGN} is a NGN common resource;

R_U is a NGN user plane resource;

R_S is a NGN service plane resource;

R_{RP} for a protocol stack of routing NGN allocated resource;

R_{SS} for a protocol stack of the signaling system NGN allocated resource;

R_{PP} for formation PP of the user information NGN allocated resource;

$Q_{BBX} = \{q_{BBX}^i\}_{i=1, \overline{n}}$ is the user to QoS NGN in PTC requirements;

$Q_3 = \{q_3^j\}_{j=1, \overline{m}}$ is the user to QoS NGN on security degree of information transmitted requirements;

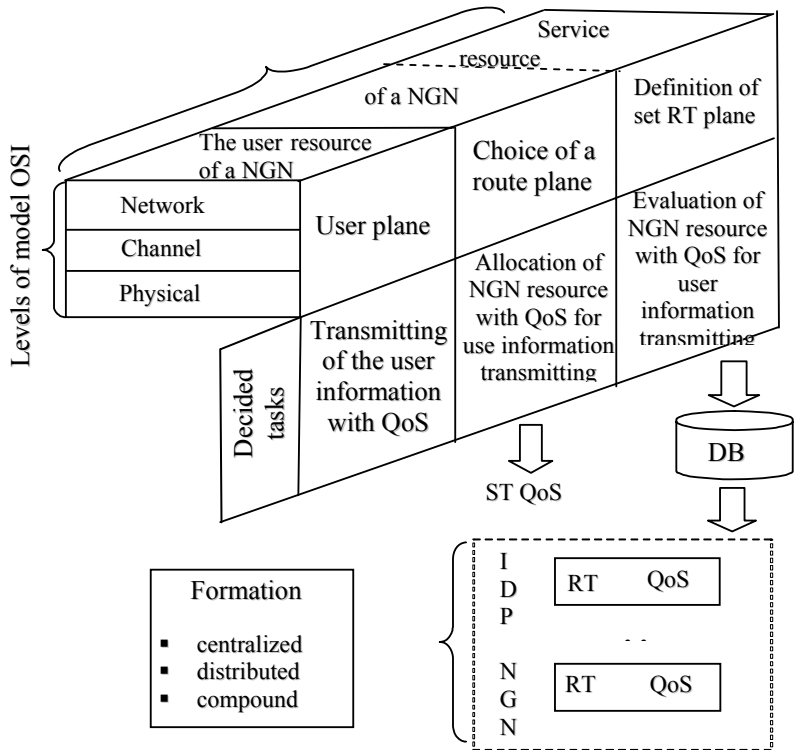


Fig.1. Verbal route model in NGN

The following ideas are fair

$$R_{NGN} = R_U + R_S; \quad R_S = R_{RP} + R_{SS} + R_{PP}. \quad (1)$$

Thus routing should provide required user QoS in PTC and security degrees the information transmission at the maximal effective utilization of user resources and service planes

$$\{Q_3, Q_{66x}\} = F \{ \max R_n, \min(R_{NM}, R_{CC}, R_{N3}), \lambda_O \}. \quad (2)$$

2. INTRASYSTEM TRANSMISSION INTERACTIONS

The direction of an arrow in the top index transformation functions that transformation occurs at progress of data “down”-↓ or “up”-↑.

Let's consider progress of the data through network level of model OSI, taken as the basic. $S_i^{(3)}$ is a stream of the data at 3rd level j -planes (subplanes). We shall express the matrix communication between streams on an input and an output of 3rd system level:

$$\begin{bmatrix} S_1^{(3)} \\ S_2^{(3)} \\ S_3^{(3)} \end{bmatrix} = \begin{bmatrix} F_{11}^{(3)\downarrow} & F_{12}^{(3)\downarrow} & F_{13}^{(3)\downarrow} \\ F_{21}^{(3)\downarrow} & F_{22}^{(3)\downarrow} & F_{23}^{(3)\downarrow} \\ F_{31}^{(3)\downarrow} & F_{32}^{(3)\downarrow} & F_{33}^{(3)\downarrow} \end{bmatrix} \begin{bmatrix} S_1^{(4)} \\ S_2^{(4)} \\ S_3^{(4)} \end{bmatrix}, \quad (3)$$

where $F_{ki}^{(3)\downarrow}$ is transformation functions of 3rd level, the matrix equation (3) enters the name in the brief form:

$$S^{(3)\downarrow} = F^{(3)\downarrow} S^{(4)\downarrow}, \quad (4)$$

where $S^{(4)\downarrow}$ is a matrix of data stream on output of 4th level, $F^{(3)\downarrow}$ is a transformation matrix of 3rd level.

Independence of model OSI planes

Generally quality of work of one plane may influence on quality of work another plane (it is reflected by elements of a matrix, not dispose in the main diagonal, having not zero values). However in real systems this influence may be insignificant what to accordance to zero values transformation function, at these approximation the equation (3), connecting data streams on input and output of 3rd level, becomes simpler:

$$S^{(3)\downarrow} = \begin{bmatrix} F_{11}^{(3)\downarrow} & 0 & 0 \\ 0 & F_{22}^{(3)\downarrow} & 0 \\ 0 & 0 & F_{33}^{(3)\downarrow} \end{bmatrix} S^{(4)\downarrow} \quad (5)$$

3. INTRASYSTEM INTERACTIONS AT RECEIVING OF THE DATA STREAM

Let's consider progress of the data “upper” from the bottom level to top. The index transformation functions at this progress have a direction “up”. Similarly (4) we shall write down the formula which connects streams of the data on input and output of 3rd level at movement “up”:

$$S^{(4)\uparrow} = F^{(3)\uparrow} S^{(3)\uparrow}. \quad (6)$$

Independence of model OSI planes

Take into consideration positions of item 2, we shall receive zero values transformation functions located outside of the main diagonal. In this case the equation (6) connecting data streams on an input and an output of 3rd level at data progress “up” will become:

$$S^{(4)\uparrow} = \begin{bmatrix} F_{11}^{(3)\uparrow} & 0 & 0 \\ 0 & F_{22}^{(3)\uparrow} & 0 \\ 0 & 0 & F_{33}^{(3)\uparrow} \end{bmatrix} S^{(3)\uparrow} \quad (7)$$

4. INTRASYSTEM INTERACTIONS AT RECEIVING OF THE DATA STREAM

The formulas (1)–(7) describe data transformation by cooperating levels within the bounds of one system. Using these formulas, we shall describe transformation of the data stream at interaction between network levels of different systems A and B.

Let $S^{(3)\uparrow}$ be the matrix of the data stream B systems at progress “up”, accordingly the data stream at a network level of system A will signify $S^{(3)\downarrow}$ (progress “up”). Being based on principles of deducing of formulas of transformation data stream (1)–(7), it is possible to receive the formula of transformation data stream at data transmission from input of 3rd level of system A to output of 3rd level of B system:

$$S^{(4)\uparrow} = \left[\prod_{i=1}^3 F^{(i)\uparrow} \right] \left[\prod_{i=0}^3 F^{(3-i)\downarrow} \right] S^{(4)\downarrow} \quad (8)$$

Independence of model OSI planes

Independence in work of separate planes simplifies transformations, as matrixes $F^{(3)\downarrow}$ and $F^{(3)\uparrow}$ transformation functions of 3rd level become diagonal, i.e. transformation functions $F_{kl}^{(3)\uparrow} = 0$ for all $k \neq l$. We shall consider interaction of 3rd level of system A and 3rd level of system B:

$$S^{(4)\uparrow} = \begin{bmatrix} \prod_{i=1}^3 F_{11}^{(i)\uparrow} & 0 & 0 \\ 0 & \prod_{i=1}^3 F_{22}^{(i)\uparrow} & 0 \\ 0 & 0 & \prod_{i=1}^3 F_{33}^{(i)\uparrow} \end{bmatrix} \times \begin{bmatrix} \prod_{i=0}^3 F_{11}^{(3-i)\downarrow} & 0 & 0 \\ 0 & \prod_{i=0}^3 F_{22}^{(3-i)\downarrow} & 0 \\ 0 & 0 & \prod_{i=0}^3 F_{33}^{(3-i)\downarrow} \end{bmatrix} S^{(4)\downarrow} \quad (9)$$

Note that in (8) and (9) for exception of double transformation of signals at the zero level the bottom bounds of multiplying transformation functions of system describing transformations at progress of data streams “up” are changed.

CONCLUSIONS

1. Formalized mathematical description GMOSI allows to state a qualitative/ quantitative evaluation of interaction of any open systems

among themselves and at any level GMOSI in particular; translates understanding of interaction processes on qualitatively new level.

2. This approach allows to define a calculation task characteristics of telecommunication systems interconnection in a new fashion: now it is reduced to a finding of values transformation functions at levels.

3. Use generalized information model allows to simplify processes of the analysis and synthesis of systems, and as consequence and procedures of routing without dependence from considered technologies.

4. The mathematical model and graphic representation does transparent the processes which are taking place in cooperating systems.

5. Work of each independent plane is characterized with multiplying of lines transformation functions.

REFERENCES

- [1] Recommendation X.200 Information technology. Open Systems Interconnection. Basic Reference Model: The basic model. – ITU-T, 1994.
- [2] Recommendation 1.321. B-ISDN protocol reference model and its application. – ITU-T, 1991.
- [3] P.P.Vorobienko . The concept of the generalized reference model OSI, *Elektrosvyaz*, Vol. 10, 2001, pp. 14–15.
- [4] P.P.Vorobienko., M.I. Stukalo. “The generalized mathematical model of telecommunication systems interconnection“, *Elektrosvyaz*, Vol. 11, 2003, pp. 44–46.
- [5] S.N. Novikov. “Routing methods in digital broadband networks“. V.1. Novosibirsk: 2000. 84 p.

Anton A. Kiselev (S’01-04, M’05) was born in 1980. He has received bachelor diploma in 2002 on “Protection to information of sets of access». He has graduated from SibSUTI in 2003. Now he is the second year Ph.D. student of SibSUTI, and the asst. prof. at MDT&M and RTS Chair. He is the Head and Treasurer of IEEE SibSUTI Student Branch and the Student Activities Coordinator of the IEEE Russia Siberia Section. His scientific interests include data security techniques in telecommunications systems.

Sergei N. Novikov (M’01-04, SM’05) was born in 1957. He has graduated from Novosibirsk electro-engineering institute of communications (NEIC) in 1979 and received the Ph.D. degree in 1986. He is an Asst. Prof. at the Radioengineering system chair, SibSUTI, an expert in the modern technologies of transfer and information protection in communication networks with guaranteed QoS. He is author more than 60 scientific papers in

telecommunications. Currently S.N. Novikov is the treasurer of IEEE Russia Siberia Section.

The Construction of Wireless Network Model with Security and Performance Criteria (Security Matrix Based)

Rodion Sutormin¹, Dmitry Pochufarov²

Katanov State University of Khakassia, Abakan, Khakassia, Russia, e-mail: napehb@khsu.ru¹, tel.: (39022) 7-42-45 e-mail: romantic@mail.ru²

Abstract — In the paper, the problems on security of a wireless 802.a/b/g standard network are considered.

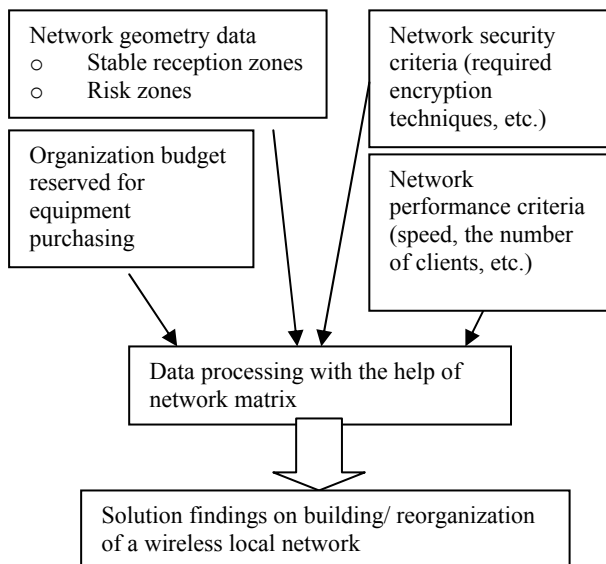
Index Terms — wireless 802.a/b/g network, security, Global Positioning System

INTRODUCTION

It is well known the current wireless networks built on the IEEE 802.11 a/b/g/ standard are not secured adequately. To be exact, the security implementation of the standard itself evidently needs completing, and this improvement can be made with the IEEE 802.11.i standard extension. However, one can be sure about it only after this extension being accepted. At present there are few manufactures who offer completed decisions on wireless local network security. Despite the insufficient, existing possibility of data transmission security, the administrators of wireless networks including the operators of quite large-scale organizations often do not care for it at all. Thus, human element, i.e. unqualified network administrators is considered to be the most vulnerable source in wireless data transmission networks built on the IEEE 802.11 a/b/g standard.

The objective of the given project is the creation of an application complex, designed to build new networks or to modernize already existing wireless access networks in order to organize enterprise security functionality with security and network performance being taken into account.

Overall Scheme of Application Complex Functionality



Network geometry data is the result of wireless network coverage zone testing made on the notebook with a client card and Global Positioning System (GPS) module. The program registers the signal level in the given point, and GPS defines its coordinates. According to the results, stable reception zones and risk zones are built up. Here geographic position (in town, in the country) and environment (other buildings, crowded streets), buildings, three-dimensional building layouts are to be considered.

Network security and performance criteria and organization budget, reserved for equipment purchasing are defined by the client.

Next, the found data is filled in security matrix for the analysis and decision-making.

MULTILEVEL SECURITY MATRIX, MLS

Many security policies are defined through informational streams. For example, all the system informational streams (some potential included) are divided into two disjoint subsets: legal and illegal streams. In this case the security system should support legal streams and prohibit illegal streams. Multilevel security policy (MLS) can be referred to policies of this kind. The SC value scale is the base of MLS policy. Linearly ordered multitude of secrecy signatures “not secret” < “secret” < “top secret” is the simplest example of such value scale. More

generally, subject category subsets can be added to secrecy signature from the specified category sets. As a result we also get a value scale where some elements are ordered.

FUTURE DEVELOPMENT PROSPECTS

At the following development stage, in addition to the enhancements of the already existing application complex, module integration is planned. That allows configuring different encryption types. For example, TCP-IP packet encryption made by the key received at biometric user passport scanning.

REFERENCES

- [1] J. Felling, “Wireless network technology: freedom of movement for the organization employees”. Windows 2000 Magazine/re, 2003, p.18-24.
- [2] J. Felling, “The configuration of basic 802.11b network security environment”. Windows 2000 Magazine/re, February 2003, p.30–34.
- [3] <http://stra.teg.ru/lenta/security/5151>
- [4] A.A. Vladimirov, K.V. Gavrilenko, A. V. Mikhailovsky, “Wi-fu: “fighting” positions for breaking and securing wireless networks’. Moscow: NT Press, 2005 – 463 p.

Rodion Sutormin, student of the Katanov State University of Khakassia, has been participated in different contests, for example, “Katanovskiye Chteniya”, All Russian Contest and Conference on the Information Security “SIBINFO-2005”.

Dmitry Pochufarov, student of the Katanov State University of Khakassia.

The Analysis of Probability-Time Characteristics of a Telecommunication Network

Sergey N. Novikov, *Member, IEEE*, Artyom A. Burov, *Student Member, IEEE*

Siberian State University of Telecommunications and Informatics, 86 Kirova str., 630102 Novosibirsk, Russia
E-mail: snovikov@nsk.ru, art@irs.ru, Tel.: +7-3832-66-14-78

Abstract — **The algorithm of modeling of the analysis of probability-time characteristics of a telecommunication network is proposed.**

Index Terms — **QoS, probability-time characteristics, route**

I. INTRODUCTION

Probability-time characteristics are fundamental to any telecommunication network. They allow estimating operate of a network, not being limited to any certain technology. They concern to reliability of connection between two users, and a waiting time of arrival of the next message package via network.

Modern lines of telecommunication systems development are directed on required quality of service QoS demanded by end users of system. The following parameters concern to the basic parameters of QoS: peak cell rate on a network, a cell delivery delay and probability of blocking of the user.

The first parameter is unequivocally provided with the equipment used on the communication network. Other two depend on such properties, as the method of routing used on the network, and topology. There is a necessity for development of the probability-time characteristics analysis, common for all communication networks as the given properties of the varying telecommunication networks.

II. THE INITIAL DATA

For the probability-time characteristics analysis, it is necessary to have a data on used method of routing and topology of the network. The requirements of the initial data are following.

- It is given directed graph, determining topology of a communication network, as set of nodes and edges: $G = \{A, L\}$;
- The weight matrix of the waiting time of cells on each of edges column $T = \{t_{i,j}\}_{S \times S}$, where S is number of nodes in the graph;
- A stream of cells acting in a communication network λ , and its distribution described by a matrix of gravitation

$$\Pi = \|\pi_{ij}\|_{S \times S}; \quad i, j = \overline{1, S}$$

- The routing method used on a communication network, and the tables of routing received with the given method.

III. THE ANALYSIS ALGORITHM

Assume all initial data determined in the previous section are given. One way to get the initial data is described in [1]. Let's divide initial graph on set of pairs nodes. For each pair nodes there is a set of the routes connecting the given nodes. For each edge from route the following characteristics are given:

- Probability of a choice of the given edge at a route formation P_{route} ;

- The waiting time of a package along the given edge t .

These sizes undertake from the initial data. Using the given sizes it is possible to calculate an average waiting time of cells between two pairs nodes i and j the following way:

- Along each of l routes the waiting time of cells as is calculated:

$$T^{ij}_l = \sum_k t_k$$

where t_k is the waiting time of cells along an edge k that are included in a route, T^{ij}_l is the waiting time of cells along route l .

• For each of l routes the probability of its choice is calculated. For calculation of probability of the choice it is possible to use the routing tables generated by one of methods.

- On each of routes we find:

$$T^{ij}_{route l} = T^{ij}_l \cdot P^{ij}_{route l}$$

As all routes form full group of events, i.e.:

$$\sum_i P^{ij}_{route i} = 1$$

Then, calculated the sum of all values $T_{route l}$ on all possible routes l , we shall receive an average waiting time of the message between two units i and j :

$$t_{ij} = \sum_l T_{ij}^{route l}$$

Having calculated an average waiting time between all pairs units i and j , we shall receive a matrix which elements characterize a communication network on each pair units separately. From the given matrix it is possible to proceed to a general characteristic of a communication network – to an average waiting time of cells between anyone two users of a network. For this purpose it is necessary to multiply elements of the received matrix by elements of a matrix of gravitation and calculate a sum:

$$T_{\Sigma} = \sum_i \sum_j t_{ij} \cdot \pi_{ij}$$

As the matrix of gravitations has the following property: the sum of all of its elements gives unit we shall receive a general characteristic of a waiting time for whole network as a whole. Knowing stream acting on a network, we find probability characteristics of a network: differential and integrated reliability of a network on a method described in [1].

Thus, characteristics of a network are received from us as a whole. Changing parameters of a stream of cells acting on a network it is possible to receive the following functional dependences:

- Dependence of reliability on a stream acting on a network;
- Dependence of a waiting time on an acting stream;
- Dependence of reliability on a waiting time.

Generally we have a functional dependence:

$$\{T, P\} = f(\lambda, M, G \{A, L\}),$$

where λ is a stream acting in a network; M is the method of routing used on a network; $G \{A, L\}$ is the graph, describing topology of a network.

REFERENCES

- [1] S.N. Novikov, A.A. Burov. “Modeling of the Routing Process Occurring in Communication Networks with Guaranteed Quality of Service”. The IEEE-Siberian Conference on Control and Communications SIBCON-2003. Tomsk, 2003, pp. 32–35.

Sergei N. Novikov (M’01-04, SM’05) was born in 1957. He has graduated from Novosibirsk electro-engineering institute of communications (NEIC) in 1979 and received the Ph.D. degree in 1986. He is an Asst. Prof. at the Radioengineering system chair, SibSUTI, an expert in the modern technologies of transfer and information protection in communication networks with

guaranteed QoS. He is author more than 60 scientific papers in telecommunications.

Artyom A. Burov (M'02) was born in 1983. He is the five year student of SibSUTI. He has a broad of scientific interests. He has received bachelor diploma in 2004.

Automatic Detection of Local and Global Software Failures

Peter Hazy, Rudolph E. Seviora

Department of Electrical and Computer Engineering, University of Waterloo, 200 University Avenue West, Waterloo, ON Canada N2L 3G1, Phone: +1-519-888-4567 ext 2850, fax +1-519-746-3077 {phazy|seviora}@swen.uwaterloo.ca

Abstract — The problem of automatic detection of failures of reactive, session-oriented software programs is described. Detection of failures is carried out by a separate unit, which observes the inputs and outputs of the target program and reports the failures detected.

Index Terms — software failures, automatic detection of software failures, specification-based failure detection, reactive systems, telecommunication software, software reliability, ITU-T SDL

1. INTRODUCTION

This paper considers the problem of automatic detection of failures (deviations of the actual from the specified behavior) of reactive, session-oriented software programs. An example is the control program of a telephone exchange. Detection of failures is carried out by a separate unit, the supervisor, which observes the inputs and outputs of the target program and reports the failures detected.

The specification of external behavior of the program at all of its interfaces is assumed to be available and expressed in a formalism based on communicating finite state machines. The ITU-T Specification Language SDL is an example of such formalism 0.

A principal challenge in specification-based detection of failures arises from the nondeterminism present in the specification. Nondeterminism facilitates the design of the program by allowing several distinct but legal outputs under the same set of inputs. However, it makes the task of failure detection much more difficult, since the supervisor must consider all legal behavioral alternatives in determining whether the observed output is correct.

Failures of the program class considered can be divided into two categories, namely locally-detectable and globally-detectable failures. The former can be identified from the behavior observed at a particular external interface of the target; the latter requires knowledge of behavior

at other interfaces. A telephony example of the former is the case when the keying of the first digit of the called number does not stop dial tone; the latter occurs when the caller hears busy tone when the called phone is actually idle.

For operational reasons, it is often sufficient to only detect local failures. However, under some circumstances, it is desirable to detect both kinds of failures.

The main objective of the research presented is the design of architecture and algorithms for a dual capability supervisor (local failures only, both local and global failures), for the case when the specification is expressed in SDL or similar language and exhibits SDL-style nondeterminism. The supervisor should have low run-time cost, with the target of $O(n)$, where n is the number of session initiations handled.

2. STATE OF THE ART

The research in specification-based detection of software failures can be categorized by the extent of the intrusiveness required.

The black-box research considers only the external behavior of the target. To deal with the specification nondeterminism, [2] proposed the belief-based method. In this method, the supervisor executes the specification for the inputs observed. When the execution encounters a nondeterministic construct, a separate ‘belief’ is created for every outcome. Consistent beliefs are combined into consistent belief sets (CBS). If the expected outputs from a particular CBS do not match the observed external outputs, the beliefs unique to the CBS are terminated. If there is no CBS left, there is no legal explanation for the observed behavior and a failure is reported. A major limitation of this method is its potentially high computational cost, which may reach factorial levels. To reduce computational cost, [3] first attempts to determine the alternative chosen by the target in its resolution of nondeterminism and then check the detailed behavior for this alternative. Experimental data indicate the running time of $O(n \log n)$ where n is the input event rate.

The white-box research, on the other hand, uses internal program information. It requires that the target be more extensively instrumented. It typically checks for satisfaction of certain property(s) of the program only. The Java Monitoring and Checking architecture (Java MaC, [4]) is an example. Probes are automatically inserted into the target program. During execution, probe outputs are processed by event recognizers and forwarded to a runtime checker. The checker determines whether the execution satisfies safety properties derived from design documentation

and expressed in a linear temporal logic form. The DynaMICs (dynamic monitoring with integrity constraints, [5]) approach also automatically instruments the program to collect events and conditions during execution, and check whether integrity constraints expressed in event-condition-action rules are satisfied. The constraints may apply to program behavior but also to assumptions and limitations imposed in design or implementation. A major limitation of these approaches is that only specific properties are checked and the program must be instrumented.

An intermediate line of research (gray-box) requires the availability of limited internal information. For example, with the Assume-Guarantee Monitor [6], the target must be instrumented to report its internal state, in specification terms, when the state becomes stable. This information is merged with the external behavior trace and used to reduce the number of nondeterministic alternatives considered.

The above only aim to determine whether a failure is present in the trace analyzed. They say nothing about failures in other executions of the programs. Such stronger claims are the goal of alternative approaches, such as model checking which aims to verify that certain specification properties would be satisfied in all possible executions [7]. However, such checking is done only on a model of the target, while this paper deals with the traces collected on implementations.

3. DESCRIPTION OF MAIN CONTRIBUTIONS

The main contribution of this research is in the architecture and set of novel algorithms for the operation of the dual-capability supervisor. The top level algorithm is in Figure 1. The parameter *localOnly* determines whether only local or both local and global failures are to be detected.

	Input: <i>systemTrace</i> , <i>CEFSM specification</i> , <i>Nu</i> =number of users, <i>tmax</i> =max chan delay, <i>seEvents</i> =set of session start/end events; <i>vusSet</i> =set of valid user sessions; <i>localOnly</i> = local analysis only Output: <i>failureFound</i> or <i>noFailureFound</i> report
1	//Local analysis - - -
2	for <i>U</i> =1, <i>Nu</i>
3	<i>tr</i> =removeIncomplSessions(getTrace(systemTrace, <i>U</i>), <i>seEvents</i> , <i>U</i>)
4	do localFailureDetection (<i>tr</i> , <i>U</i> , <i>vusSet</i> , <i>seEvents</i> , <i>tmax</i> , <i>traceOut</i>)
5	add <i>traceOut</i> to locallyAnalyzedTraceSet
6	endfor (<i>2</i>)

7	<i>if (localOnly) report noLocalFailureFound and exit</i>
8	<i>// Global analysis - - -</i>
9	<i>for U=1,Nu //preparatory step 1</i>
10	<i>foreach userSession in (getTrace(locallyAnalyzedTraceSet,U)</i>
11	<i>derive allSessionEvents from userSession, CEFSMu spec</i>
12	<i>append allSessionEvents to allEventsCEFSMu</i>
13	<i>endfor (10)</i>
14	<i>add allEventsCEFSMu to allEventSet</i>
15	<i>endfor (9)</i>
16	<i>propagateInternalEvents in allEventSet //preparatory step 2</i>
17	<i>for U=1,Nu</i>
18	<i>analyzeConsistencyWithUserCEFSMsSpec (allEventSet,U)t</i>
19	<i>endfor (17)</i>
20	<i>analyzeGlobalConsistency (allEventSet);</i>
21	<i>report noFailureFound and exit</i>

Fig. 1. Top level algorithm for the dual capability supervisor

The second main contribution of this work lies in an experimental evaluation of the detection capabilities and computational cost of the supervisor. The target program in the evaluation was the control program for a small telephone exchange. The evaluation results are summarized in the following section.

4. EXPERIMENTAL EVALUATION

In the evaluation methodology employed, traces of external behavior of the control program were collected under several different call load levels. Failures then were randomly seeded into the collected traces and the seeded traces processed by the supervisor. Two types of failures were seeded, event removal and event insertion. Each seeded trace contained one failure. If a seeded failure was not detected, the cause was determined manually. The CPU time of the supervisor was measured to determine its dependence on the number of calls handled.

The evaluation of failure detection capability showed that the supervisor detected 756 out of 760 event removal failures and 8572 out of 8580 event insertion failures, i.e. > 99.5% of all seeded failures.

The evaluation of computational cost showed that it was linear in the number of calls supervised, under Poisson distribution of call originations at the busy-season-busy-hour call levels.

5. FUTURE WORK

The follow-up research will involve several activities. The main one will attempt to augment the functionality of the supervisor to also detect *errors* (deviations of the actual from the specified state) in the internal state of the program before they manifest themselves as external failures. The detection of internal errors will give an early warning about impending problems. This effort will require that the target program be instrumented to supply information about internal state and events in the target.

REFERENCES

- [1] ITU-T, Recommendation Z.100, Specification and Description Language – SDL, International Telecommunication Union, Geneva, 2000.
- [2] M. Hlady et al., “An Approach to Automatic Detection of Software Failures”, Proc. 6th Int. Symp Software Reliab Eng, pp. 314–323, 1995.
- [3] T. Savor, R. Seviora, “Toward Automatic Detection of Software Failures,” IEEE Computer, vol. 21, no. 8, pp. 68–74, August 1998.
- [4] M. Kim et al., “Java-MaC: A Run-time Assurance Tool for Java Programs,” Proc. 1st Int Workshop on Runtime Verification, Electronics Notes in Comp Science, vol. 55, no. 2, pp. 115–132, Elsevier, July 2001.
- [5] A. Gates et al., “DynaMICs: Comprehensive Support for Run-time Monitoring”, Proc. 1st International Workshop on Run-time Verification, Electronic Notes in Comp Science, vol. 55, no. 2, pp. 61–77, July 2001.
- [6] M. Zulkernine and R. E. Seviora: "Towards Automatic Monitoring of Component-Based Software Systems," Journal of Systems and Software, Vol. 74, No. 1 , pp. 15–24, January 2004.
- [7] E. M. Clarke, O. Grumberg and D. A. Peled, “Model Checking”, MIT Press, 2000.

Design of the Steganography System Based on the Version 4 Internet Protocol

E.O. Savateev

Chelyabinsk State University, Faculty of the Computer Security and Applied Algebra

Abstract — A new steganography system has been considered. The stego-system program on ICMP has been developed.

Index Terms — steganography system, Internet protocol, stego-container, datagram

1. INTRODUCTION

At present, there are two general directions in the decision of a problem of the information protection from the unauthorized access: cryptography and steganography. The purpose of cryptography is hidden of contents of the message due to encryption. Unlike this, steganography is the science of hiding information such that its presence cannot be detected.

In connection with development of the computer hardware and enormous quantity of channels of the information transfer, the new steganographic methods have appeared, in which basis particularities of performance of the information in files, computer networks etc. are presented.

In the paper, the opportunities of steganography in the Internet Protocol versions 4 (hereinafter IP) and in Internet Control Message Protocol (ICMP), as part IP are considered. Search of these opportunities via analysis of the packet structure and content of corresponding protocols is carried out. On the base of the founded opportunities the means are described and the methods for formation of the hide channel of the information transfer are formulated.

2. BACKGROUND

The steganographic system or stegosystem is collection of means and methods which are used for formation of the hide channel of the information transmission [1]. Consider a generalized model of the steganographic system (Fig. 1).

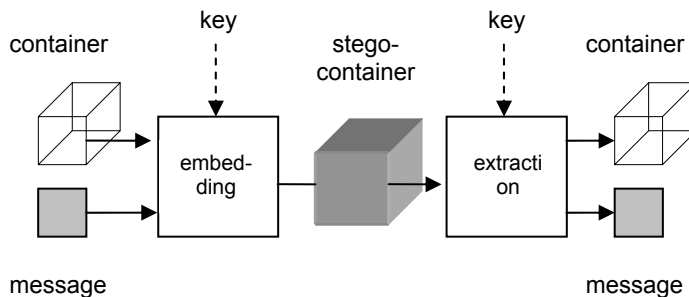


Fig. 1. Model of the steganographic system

Let us define the basic concepts.

Message is any kind of data.

Container is any information, suitable for hide of messages in it.

Stego-container is the container containing the hide message.

Key (stego-key) is the secret or open key required for encryption (decryption) of the message for strengthening protection.

Basing on the generalized model it is possible to construct the steganographic system on Internet protocol. As a container in such system the IP-datagram will be used. A key (secret or open) is chosen depending on algorithm of encryption. If the secret key is used, it should be determined before the beginning of the message exchange, or transferred on the protected channel. The open key may be sent via the unprotected channel.

2.1 The common methods, positions and requirements

Designing the stego-system it is necessary to take into account the following:

1) The potential adversary (the warden) has full performance to the

steganographic system and details of its realization. The unique information which remains unknown to the adversary is the key which help its owner may check the fact of presence of the hidden message and its contents.

- 2) If the adversary somehow finds out about existence of the hidden message it should not allow him to extract similar messages from other containers until the key is kept in the secret (it is ensured by cryptography means).

Besides the stego-system should answer a certain requirements:

- 1) Properties of the container should be modified so that the stego-container without hindrance passed on the communication channel without attention of the potential adversary.
- 2) Stego-system should be reliable, that is assume protection from loss, duplication and breaking sequence of stego-container's receiving, and to carry out the checking wholeness of message.

To take into account and to fulfill the requirements determined above, it is necessary to generate from the source message the sequence of the data blocks, available for embedding in the container (further M-blocks). Each such block should be encrypted, and besides the message fragment to contain the information, sufficient for ensuring of stego-system reliability. Also both M-block containing information of the message size, and M-block confirmed of the stego-container receiving should be determined.

Let us determine the common structure of the M-block and algorithms of sending and receiving of the stego-container. Another means and methods will be determined at the description of the stego-system basing specific protocol.

Common structure of the M-block

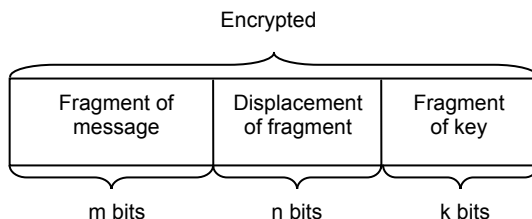


Fig. 2. Common structure of the M-block

Displacement of a fragment specifies where in the source message located given fragment.

The key fragment contains the elder k bit of the key.

The sequence of fields may be arbitrary, and for the strict description of the M-block structure it is necessary to define m , n , and k values only.

As M-blocks may be transferred on the communication channel in the free order, it is recommended to use the block cipher, working in Electronic Codebook (ECB) mode [2]. The block length, obviously, should comply with the M-block length.

Sending

1. Form a sequence of M-blocks.
2. Embed the M-block in the container.
3. Send the stego-container to the addressee.
4. Expect a confirmation of receiving from the addressee during certain time. If confirmation is not received, it is necessary to interrupt the sending process, or go to the step 5.
5. Execute steps 2-4 for each M-block of the formed sequence until end of this sequence.

Receiving

1. Define whether the received container contains the embedded message. If yes, go to the step 2, otherwise expect a receiving the following container.
2. Extract the fragment of message.
3. Confirm receiving of the stego-container.
4. Execute steps 1-3 until the fact of receiving of all messages will be ascertained. This fact can be ascertained by compare a size of the received message with its expected size transferred in the appropriate stego-container.

Removing the step 4 from algorithm of sending and the step 3 from algorithm of receiving, it is possible to increase transfer rate of the message, having lowered a reliability of stego-system.

2.2 Protocol IP

Internet Protocol provides transfer of the data blocks, co-called datagrams, from the sender to the addressee. If it is necessary, protocol IP provides also fragmentation and assembly of datagrams for the data transfer through networks with the small size of packages.

Table 1. IP-datagram header structure

Version	IHL	Type of Service	Total Length	
Identification			Flags	Fragment Offset
Time to Live	Protocol		Header Checksum	
Source Address				
Destination Address				
Options			Padding	

Version (4 bits) is protocol version; in this case version 4 is considered.

IHL (4 bits) is the header length.

Type of Service (8 bits) is type of service defined by means of certain abstract parameters.

Total Length (16 bits) is full datagram length.

Identification (16 bits) is identifier, is carried out by the sender for assembly of any datagram fragments.

Flags (3 bits) are control flags.

Fragment Offset (13 bits) is fragment offset.

Time to Live (8 bits) is maximum time allowed to datagram is in the Web.

Protocol (8 bits) is shows what protocol of following level uses a data from the Internet datagram.

Header Checksum (16 bits) is the control sum of header.

Source Address (32 bits) is address of sender.

Destination Address (32 bits) is address of addressee.

Options (variable length) are additional options.

Padding (variable length) is used to be convinced that the header finished on 32-bit boundary.

The Identification (ID) and Options fields is represented the most interest. Consider a purpose of these fields in detail.

According to the protocol specification IP [3], ID contains the unique packet identifier which is used for assembly scatter datagrams. Value of this field does not depend on values of other header fields and is saved at fragmentation.

Options should be supported by all Internet modules (hosts and gateways). Each datagram is not necessary carries options but it is may be. There are eighth various options from which only one is suitable for transfer of the secret message (it is possible to be convinced of it addressing to the specification [3]). It is option Internet Timestamp.

Table 2. The Internet Timestamp option structure (type 68)

Length (8 bits) is quantity of bytes in option, which include bytes of type, length, index and oflw/flag.

Pointer (8 bits) is quantity of bytes from begin of this option up to the end of time stamps, plus one.

Overflow (oflw, 4 bits) is quantity of the IP modules which are not able to provide registration of time stamps because of empty free place.

Flag (flag, 4 bits) is the flag, determines a way of registration of time stamps.

01000100	Length	Pointer	oflw	flag
Internet Address				
Timestamp				

Timestamp (32 bits) is a time stamp in milliseconds (for midnight in GMT). If time in milliseconds indeterminable or may not be counted from midnight in GMT, hence any time may be provided that eldest bit in the field of the time stamp will be installed in one (that specifies to use of non-standard value and gives some freedom in filling the given field).

Describe process of the sequence of M-blocks formation, structure of the M-block and embedding process. Also we shall define the M-block containing the information on the message size and the M-block that is a confirmation of stego-container receiving.

Structure of the M-block

The general structure of the M-block is determined on page 2. It is necessary to set variables m , n and k :

- $m = 24$
- $n = 16$
- $k = 24$

The message size

Information on the message size is carried the M-block, in which:

- field "Fragment of message" contains the message length;
- field "Displacement of fragment" contains quantity of M-blocks in the formed sequence including the fragment;
- field "Fragment of key" contains the bit sequence appropriate to line "siz".

Obviously that maximal length of the message is $3(2^{16} - 1)$ bytes (approximately 192 Kb).

Formation of the M-block sequence

1. Create from the source message the sequence of M-blocks, having added to it the block containing the information of the message size.
2. Order the received sequence on elder 16 bits by the algorithm, which gives a result, described in the following example.

Example (ordering a sequence)

Consider a sequence of decimal numbers, outlined the elder 16 bits of the M-blocks.

Source sequence: 3 1 2 1 3 3 4 5 1 4 2 5

Ordering sequence: 1 2 3 4 5 1 2 3 4 5 1 3

It is necessary to note that such ordering results that M-block containing the message size turns out to be in the any place of sequence.

Embedding

Embedding is carried out in field Identification of header of the IP-datagram and in the option of the Internet time stamp. Thus it is necessary to take into account the following.

- 1) Protocol specification IP [3] requires that identifier will be unique during Time To Live of datagram. In practice it is frequently realized by increase of the field ID value at one for each following datagram.
- 2) Despite possibility of using the non-standard time stamp, value of this field should be increased for each following datagram. The increase should takes place at least, for the certain number of datagrams going one to another.

Consider the embedded process in detail. The extraction process will become obvious after that and will not require an additional description.

1. Place eldest 16 bits of the embedded M-block in the ID field of the IP-datagram header. Ordering a sequence M-blocks are provided a partial performance of the first condition determined above. It is the partial condition, as far as ordering will only provide an increasing of the identifier greater or equal one, for the certain number of other IP-datagrams following one by one. Number of such datagrams either constantly or gradually decreases. In order to completely carrying out condition, assessed on changing a value of field ID, it is possible along with stego-containers to send the IP-datagrams do not containing the secret message, but providing increase of the identifier at one.

2. Create in header of the IP-datagram an option Internet Timestamp in 40 bytes length, containing two time stamps placed in the 32-bit words following one by one (the option fields are filled strictly according to the specification of protocol [3]). Bits 8-31 (numbering from zero, elder bit is zero) of each time stamp contains the 48 bits of the embedded M-block, the elder bit is installed in 1, and bits 1-7 provide of second condition described above. Thus for each following IP-datagram the time stamp bit 1-7 changes so as received 32-bit time stamp was more than the time stamp installed in the previous datagram. It is necessary to provide this condition for both time stamps inside one datagram, herewith both received values do not depend from each other. Obviously, increasing the time stamp is possible to carry out a minimum for 128 IP-datagrams following one by one.

3. Create the correct IP-datagram carrying in Data field any data, no causing suspicion at the potential adversary.

As far as registration of time stamps should be carried out on each router which IP-datagram is passed, the stego-container received as a result of embedding, may transferred maximum 23 routers then it will be destroyed owing to shortage of the registration place for the time stamp and overflow of the Overflow field of Internet Timestamp option.

Confirmation of receiving

The confirmation of receiving of the given stego-container is the M-block, in which values of fields "Fragment of message" and "Fragment of key" coincide with values of identical fields of M-block, extract from this stego-container, and the field "Displacement of fragment" is more at one.

As sending of confirmation of receiving should be carried out in view of the conditions stated in item "Embedding", it is reasonable confirm of receiving not only one stego-container. This number is chosen at random, for example, it may coincide with number of stego-containers in which value of field Identification is increased. Thus generalized algorithms of sending and receiving should be modified in parvo.

2.3 Protocol ICMP

Internet Control Message Protocol uses main IP properties, as if it was high-level protocol [4]. However in fact ICMP is a part of the Internet protocol.

As a rule, messages of the ICMP protocol notify on the mistakes arising at processing of datagrams, and are sent by the standard IP header. The structure of the message depends on its type. The most interest are presented the ICMP messages of type 8 (echo-request), as far as they are applied in the ping program – that is one of the main and useful tools of networks debugging.

Table 3. Structure of echo-message and response message to the echo

Type	Code	Checksum
Identifier		Sequence Number
Data		

Type (8 bits) is type of message: 8 for the echo-request and 0 for the echo-answer.

Code (8 bits) is a code that influences of fields Identifier and Sequence Number filling.

Checksum (16 bits) is the control sum.

Identifier (16 bits) is identifier for compliance of echo-messages and answers them.

Sequence Number (16 bits) is a queue number, the employee for compliance of echo-messages and answers them.

Data (variable length) is field for additional information.

The package send ping consists of IP-header of 20 bytes and, actually ICMP-messages of $8+n$ bytes (8 bytes for header and n byte for the additional information) [5]. Usually as value n the 56 (for UNIX) or 32 (for Windows) is chosen. As frequently the field of the additional information contains the certain data useful at the errors debugging, dependent from them, it is obviously possible to use it for the secret message transfer.

According to the specification of ICMP protocol [4], on each echo-request the echo-answer should be sent. Moreover if echo-message contained additional data, these data should contain in the message in response to the echo. Thus, the problem of the control of the message integrity and confirmation of receiving of the stego-container is already solved at the protocol level.

Let's pass to description of the steganography system based on the possibility discovered.

Structure of the M-block

- $m = 64$
- $n = k = 32$

The common length of the M-block thus is equal to 128 bits. Such value is chosen for the imitation of original program ping, allowing to fill in a field of the additional information by the given pattern with maximum length of 16 bytes. In the paper, the program ping included in UNIX-similar operating systems is considered.

The message size

- Field "Fragment of message" contains the message length.
- Field "Displacement of fragment" contains quantity of M-blocks in the formed sequence (including given).
- Field "Fragment of key" contains the bit sequence appropriate to a line "size".

Accordingly, the maximum length of the message is $2^3(2^{32} - 1)$ bytes (approximately 32 GB).

Formation of the M-block sequence

It is necessary to create only sequence of M-blocks from the initial message, having placed in its beginning the block contained information about the message size. Other restrictions on the element order of the given sequence are not present. Generally speaking, M-block containing information on the message size, can be located in any place of sequence. It is located in the beginning only that message size was known before the beginning of the secret information transfer.

Embedding

Embedding is carried out in a field of the ICMP echo-message additional information. We shall describe this process.

1. Creation the ICMP echo-message contained a field of the additional information of the certain length. The length is chosen from the interval from 24 up to 65507 bytes. It is calculated as a difference of the maximum IP-datagram length (65535 bytes) and sum of the minimum length of IP header (20 bytes) and ICMP header (8 bytes): $65535 - (20 + 8) = 65507$.

2. The time stamp is placed in the elder 8 bytes of the additional information. In the rest bytes the data appropriate to the embedded M-block is filled. Thus if the length of the additional information field exceed minimum, these data are filled in it cyclically. Therefore the original program ping is simulated.

3. The correct IP-datagram is formed with the created echo-message in the data field.

Sending

It is necessary to send each stego-container the certain times with the given time interval, simulating thus the ping program, in order to pay no attention of the potential adversary. Before sending of the new stego-container which is no duplicate previous, the time delay is necessary which should be sufficiently more and changeable.

3. PRACTICE

3.1 General questions of realization

First of all, the program realizing any of offered stego-systems, should be carried out on architecture client-server [5], however both the client and server may be equal in rights participants of exchange of the secret information.

Formation and sending of the stego-container (IP-datagram) may be carried out through the interface "raw" sockets [5], or using the library with required functions (for example, libnet). For receiving of the stego-container it is recommended to use the platform-independent library, allowing to intercept packages on a level of the operational system kernel. Libpcap may be such library [6].

3.2 Stego-system on ICMP base

The stego-system program on ICMP has been developed. In appendix some results of testing of this program are described.

4. CONCLUSION

4.1 The brief characteristic of the offered stego-systems

Table 4. The brief characteristic of the offered stego-systems

Protocol	IP	ICMP
Embedding	In the field Identification and option Internet Timestamp of the IP-datagram header the cipher is block (64 bits) in ECB mode	In field Data of ICMP-message of type 8 (echo-request)
Restrictions	Cipher is block (64 bits) in ECB mode; maximum length of the message is 192 KB; stego-container can transfer by 23 routers maximum	The cipher is block (128 bits) in ECB mode; maximum length of message is 32 GB
Advantages	Fact of the message is well hidden; It is possible to use the opportunities which have been found in higher-level protocols (including ICMP)	8 bytes of the message in the container; simplicity of realization

Disadvantages	Relatively hard restrictions; The 3 byte message in container; Difficulty of realization	embedding direct in the data field; Big time expenses
---------------	--	---

4.2 Further studies

In the future it is planned to realize stego-system basing on Internet Protocol, as well as to consider opportunities of formation of the hide channel of the information transfer in Internet Protocol ver. 6 and in Transmission Control Protocol.

REFERENCES

- [1] O.V. Genne, "The General Positions of Steganography". In *Zaschita Informatsii. Konfident.* 2000. No 3.
- [2] Bruce Schneier, "Applied Cryptography. Protocols, algorithms and Source Texts on C". Triumph, 2002. – 816 p.
- [3] Marina del Rey, Request for Comments 791, Internet Protocol, September 1981.
- [4] J. Postel, Request for Comments 792, Internet Control Message Protocol, September 1981.
- [5] Ion Sneider, "Efficient Programming TCP/IP". St.-Petersburg, Piter, 2001. – 320 p.
- [6] U.R. Stevens, "UNIX: Development of the Network Applications". St.-Petersburg, Piter, 2004. – 1086 p.

Cryptographic Data Security in Wireless Networks Based on Biometrical Passport

Denis V. Vishnyakov¹, Anton G. Serdyukov²

Katanov State University of Khakassia, Abakan, Khakassia, Russia, e-mail: denis_tmk@rambler.ru¹, antonserdyukov@yandex.ru²

Abstract — The use of a biometric passport for encoding data which are transmitted across open wireless 802.11g standard channels. The generation of encryption key is based on biometrical data.

Index Terms — biometrics, shorthand, packet encryption, network, biometrical passport

INTRODUCTION

The security status of wireless networks is unsatisfactory; that increases the possibility of breaking in, scanning and accessing a wireless 802.g network.

In the standard such cryptographic algorithms as WEP, TKIP, AES can be used; it makes no difficulty for a malicious user to break them in. That's why it is necessary to create a new security model.

A biometrical passport is suggested as one of the key moments of the new model. Its use is determined by the uniqueness of biometrical data of each human and by great selection difficulties in breaking this data. This allows generating encryption keys stable to cryptography.

The project objective is to create software designed for encoding data that are transmitted through open radio channels, where a biometrical user passport is used for key generation.

OVERALL SCHEME OF APPLICATION COMPLEX FUNCTIONING

The program complex functions including the following stages:

1) Fingerprint scanning

Fingerprint scanning is made with the help of the hardware BioLink U-Match scanner.

2) User authentication by fingerprinting.

3) Key generation by fingerprinting and a key word.

Generation is performed according to the mathematical fingerprint pattern and a key word entered by the user.

- 4) Data encryption with the help of generated keys.
- 5) Data transmission.
- 6) Data decoding on the base of the already given key.

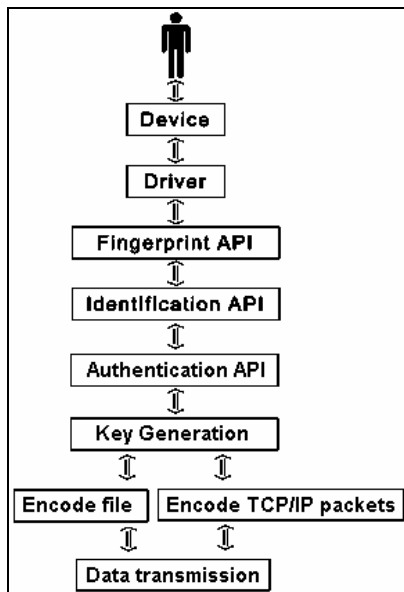


Fig.1. Overall Scheme of Program Complex Functioning

Note: The key transmission mechanism is not considered in the given paper, it means that key distribution has already occurred between clients.

PRACTICAL IMPLEMENTATION

There are two approaches:

- 1) a single file decryption.

It is performed by the application which uses a biometrical key. The file is transmitted across the network with the help of standard transmission protocols: FTP, HTTP, and SMTP.

- 2) TCP/IP packets encryption.

On interconnecting computers an extra service is set up, which works at the network TCP/IP level. Its task is transparent TCP/IP packets encryption. The work at TCP/IP network level is performed by means of NDIS (Network Device Interface Specification) driver.

- 3) Shorthand (data hiding) in the network traffic.

That is building data into transmitted TCP/IP packets without any damage to the integrity of information being transmitted.

At fingerprint scanning a 1.23 kb-sized pattern is created and stored for the following user authentication. It is impossible to get the image of the original fingerprint in order to provide security. After user identification is made it is necessary to enter a key word and then encryption key is generated on the base of fingerprint pattern and the entered word.

At the current stage of the development the following is made: fingerprint is taken, fingerprint pattern is stored in the database for further user identification, encryption key is generated according to fingerprint pattern a key word, a single file is encoded with the help of the given key. TCP/IP packets encryption is to be completed at the following stage.

Further practical usage of the development is for project security organizations dealing with wireless and heterogeneous networks.

REFERENCES

- [1] BioLink Fingerprint Software Development Kit. Developer's Guide.
- [2] MSDN April 2004 – NDIS driver.
- [3] C.H. Rowland. "Covert Channels in the TCP/IP Protocol Suite", Psionic Technologies Inc., 2002.

Denis V. Vishnyakov has participated in the international student programming contest (team championship) in the quarter-final and semi-final – ACM Programming Contest 2002, 2003.

Anton G. Serdyukov has participated in the 5th Student Paper Contest and Conference on the Information Security (SIBINFO-2005).

Tensors Analysis for Investigation Next Generation Network

Dmitriy U. Ponomarev

*Krasnoyarsk state technical university
26, Kirenskogo Street, Krasnoyarsk, 660074, Russia,
Tel: +7-3912-430875, E-mail: kafaes@krasmail.ru*

Abstract — Analyse multiservice networks characteristics is a complex and necessary task, because of that dependent quality of service in these networks. There is present tensor method for solving this problem.

Index Terms — multiservice networks, tensor analyse, queuing system, next generation network, queuing nets

Integrated services digital networks development result in appearance new technologies, networks and new properties information stream in this nets. The main technologies for building integrated services digital networks is asynchronous transfer mode (ATM) and technologies bases on Internet protocol (IP). However, because of technology development not stop, appear new standard for rendering multiservices. One of them is multiprotocol label switching (MPLS). Common methods to building this networks result in Next Generation Networks conception (NGN). This idea provide accordance practically unlimited set of services, flexible management system, allocation functions services accordance to nets point and interaction with classical networks. However, for providing given quality of service necessary define processing system characteristics.

There is present tensor approach to probability and time characteristics multiservice networks, as queuing nets models. Tensor methodology initiator is a famous American scientist and engineer G. Kron, which first use tensor analyze and topology for electrical nets theory. Further, tensor analyze ideas evolution for information system get in works Petrov A.E., Armenskiy A.E., Kuznetsov O.L. etc.

There is present utilization expression as invariant equation for engineering analyzes queuing nets characteristics (probability and time), which give connection between intensity arrival (λ) and mean service time (t_{serv}): $\rho = \lambda t_{serv}$. For applying tensor method to complicated queuing net, using concept of initial and primitive nets, necessary take expression for definition utilization in initial net, and set parameters for

primitive net. For example, in common form for queuing nets, consist from some single-channel queuing systems with unlimited buffer (this parameters is not method limitation) necessary define primitive net, consist from same number systems and present invariant equation $\bar{\rho}' = \bar{\lambda}' \bar{t}'_{serv}$. Further, find transfer matrix (\bar{C}) from one projection to other: $\bar{\lambda}' = \bar{C} \bar{\lambda}$, define components matrix equation: $\bar{C}^T \bar{\rho}' = (\bar{C}^T \bar{t}'_{serv} \bar{C}) \bar{\lambda}$. Solving this equation relatively λ , find utilization in initial net. This approach allow with minimal costs estimate systems loading in net, providing determination other queuing nets characteristics: probability distribution in different queuing systems: $p_n = f(\rho)$, as well as mean queue \bar{N} and mean service time \bar{T} .

For example, one of queuing nets present on fig. 1.

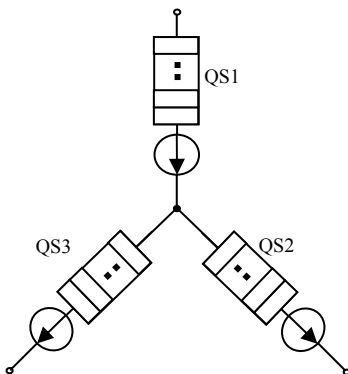


Fig. 1. Queuing net

For realization tensor analyze, turn from initial net to primitive: in this, add imaginary branches for constitution closed circuit with corresponding circuit intensity (fig. 2).

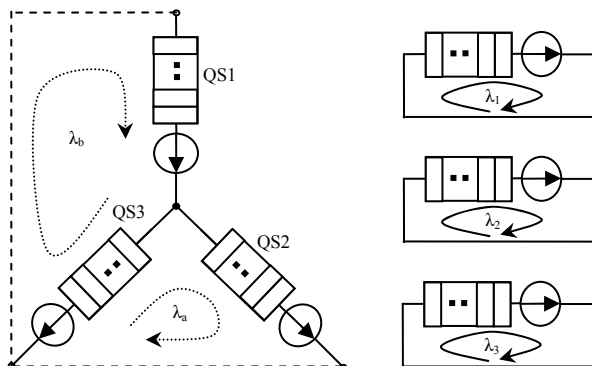


Figure 2. Initial and primitive queuing nets

For determination transfer matrix compose conformity table for initial and primitive nets circuit intensities:

	λ_a	λ_b
λ_1	0	1
λ_2	1	0
λ_3	1	1

Consequently, transfer matrix takes form as: $\bar{C} = \begin{pmatrix} 0 & 1 \\ 1 & 0 \\ -1 & 1 \end{pmatrix}$.

Set mean service time as: $\bar{t} = \begin{pmatrix} t_1 & 0 & 0 \\ 0 & t_2 & 0 \\ 0 & 0 & t_3 \end{pmatrix}$ and system utilization as:

$\begin{pmatrix} \rho_1 \\ \rho_2 \\ \rho_3 \end{pmatrix} = \begin{pmatrix} t_1 & 0 & 0 \\ 0 & t_2 & 0 \\ 0 & 0 & t_3 \end{pmatrix} (\lambda_1 \ \lambda_2 \ \lambda_3)$ for primitive net. For initial net, invariant

equation take form: $\begin{pmatrix} \rho_a \\ \rho_b \end{pmatrix} = \begin{pmatrix} t_a & 0 \\ 0 & t_b \end{pmatrix} (\lambda_a \ \lambda_b)$.

Consequently, cross from one net to other, for utilization initial net get next expression: $\begin{pmatrix} \rho_a \\ \rho_b \end{pmatrix} = \bar{C}^T \bar{\rho} = \begin{pmatrix} 0 & 1 & -1 \\ 1 & 0 & 1 \end{pmatrix} \begin{pmatrix} \rho_1 \\ \rho_2 \\ \rho_3 \end{pmatrix} = \begin{pmatrix} \rho_2 - \rho_3 \\ \rho_1 + \rho_3 \end{pmatrix}$, and for service time:

$$\begin{pmatrix} t_a & 0 \\ 0 & t_b \end{pmatrix} = \bar{C}^{-T} \bar{T} \bar{C} = \begin{pmatrix} 0 & 1 & -1 \\ 1 & 0 & 1 \end{pmatrix} \begin{pmatrix} t_1 & 0 & 0 \\ 0 & t_2 & 0 \\ 0 & 0 & t_3 \end{pmatrix} \begin{pmatrix} 0 & 1 \\ 1 & 0 \\ -1 & 1 \end{pmatrix} = \begin{pmatrix} t_2+t_3 & -t_3 \\ -t_3 & t_1+t_2 \end{pmatrix}.$$

Finally, may write: $\begin{pmatrix} \rho'_2 - \rho'_3 \\ \rho'_1 + \rho'_3 \end{pmatrix} = \begin{pmatrix} t_2+t_3 & -t_3 \\ -t_3 & t_1+t_2 \end{pmatrix} \begin{pmatrix} \lambda_a \\ \lambda_b \end{pmatrix}$. Solve this equation relatively λ_a and λ_b , may define intensity arrival in initial net system, as: $(\lambda_1 \ \lambda_2 \ \lambda_3) = \bar{\lambda}^T \bar{C}^T = (\lambda_a \ \lambda_b) \begin{pmatrix} 0 & 1 & -1 \\ 1 & 0 & 1 \end{pmatrix}$, and utilization every channel initial net find as:

$$(\rho_1 \ \rho_2 \ \rho_3) = \bar{\lambda}^T \bar{C}^T \bar{T} = (\lambda_a \ \lambda_b) \begin{pmatrix} 0 & 1 & -1 \\ 1 & 0 & 1 \end{pmatrix} \begin{pmatrix} t_1 & 0 & 0 \\ 0 & t_2 & 0 \\ 0 & 0 & t_3 \end{pmatrix}.$$

For example, consider net with given time matrix:

$$\begin{pmatrix} t_1 & 0 & 0 \\ 0 & t_2 & 0 \\ 0 & 0 & t_3 \end{pmatrix} = \begin{pmatrix} 0.3 & 0 & 0 \\ 0 & 0.2 & 0 \\ 0 & 0 & 0.85 \end{pmatrix}, \quad \text{and utilization present as:}$$

$$\begin{pmatrix} \rho'_1 \\ \rho'_2 \\ \rho'_3 \end{pmatrix} = \begin{pmatrix} 1/\mu_1 \\ 1/\mu_2 \\ 1/\mu_3 \end{pmatrix} = \begin{pmatrix} 0.3 \\ 0.2 \\ 0.85 \end{pmatrix}. \quad \text{Loading source is a Poisson arrival pass through}$$

queuing system 1 (QS1).

Computation result is intensities information stream in all queuing systems: $(\lambda_1 \ \lambda_2 \ \lambda_3) = (1.3505 \ 0.4742 \ 0.8763)$, and utilization value in all points: $(\rho_1 \ \rho_2 \ \rho_3) = (0.4052 \ 0.0949 \ 0.7449)$.

For confirmation theoretical estimation was realize model simulation in GPSS World. Simulation and theoretical results practically agree, that analyze values verify, which present in table 1.

Table 1

	ρ_1	ρ_2	ρ_3
Theory	0,4052	0,0949	0,7449
Simulation	0,405	0,095	0,744

This results let conclude about available tensor method application for analyze different queuing nets characteristics. Furthermore, as conclusion necessary note, that this method let enough fast and reliability give analyze essential queuing nets characteristics, as models

of multiservice networks, for providing necessary quality of service different classes of information streams.

Dmitriy U. Ponomarev was born in 1976. Candidate of science (2002), associate professor at the Communication nets and systems chair, Radioelectronics Institute, Krasnoyarsk State technical university. A scientific interest is queuing theory and its application in telecommunication. Author of more than 50 publications, including 2 monographs.

A Protection Profile and Its Content

Solonskaya Oksana

*86 Kirova st., Novosibirsk, 630102, Russia, Siberian State
University of Telecommunication and Informatics*

Abstract — The protection profile determined by Common Criteria is intended for certification of protection information means of IT products and IT systems and reception of comparable evolutions of their security. The protection profile can be generated by any user with the purpose of promotion of security requirements to an IT product or IT system.

Index Terms — Common Criteria, Information Technology, Security, Protection Profile, IT product, IT system, target of evaluation

BACKGROUND

In 1997 the "Common Criteria" (CC) versions 2.0 were accepted. In 2002 the Russian analogue of this document the standard GOST R ISO/IEC 15408-2002 "Information Technology – Methods and Means of a Security – Evaluation Criteria for IT Security" was issued. In the given standard the basic definitions concerning security of information technologies are described, including, three types of designs of requirements and their content are submitted: a protection profile (PP), a security target (ST) and a package. Now there is no standard on development and designing of protection profile.

STATEMENT OF THE PROBLEM AND THE PURPOSE

According to CC, security requirements of information technologies is intended for typical mechanisms, products and systems of information technologies should be made out as protection profile. The protection profile – is the normative document intended for a statement of security problems of certain set of IT products and IT systems and a formulation of security requirements for the decision of the given problem. It is necessary to note, that Protection Profile (PP) does not regulate, how the given requirements will be executed, providing, thus, independence of realization.

The protection profile is developed for definition of a typical set of security requirements with which should satisfy one or more products or

with which should satisfy IT systems intended for use in definite purposes.

Protection profile are used as standardized sets of requirements with the purpose of increase of validity of the task of requirements to security of IT products, evaluation of security and an opportunity of realization of the comparative analysis of a level of security of various IT products.

THE DESCRIPTION OF RESEARCHES SUBJECT AND ACHIEVED RESULTS

The GOST R ISO/IEC 15408-2002 determines a protection profile as set of IT requirements independent of concrete realization for some category of IT products which is intended for satisfaction of the common inquiries of users in security. In a role of users can act: consumers of products, developers and evaluator.

Consumers of IT products (for example, distributors or buyers) require the information, giving a common view about how the target of evaluation (TOE) solves problems of security. Developers require unequivocal understanding of security requirements to create appropriate IT products. Evaluators require the information which will motivate technical correctness and efficiency PP.

Any protection profile can be registered in the registry of protection profile. In authority of registration to it the appropriate registration label which is unique is given identifies PP in the registry. The registration label consists of the following parts shared by hyphens:

- type of an element of the registry;
- year of registration (year of entering PP in the registry – four figures);
- registration number (a serial number in the current year – three figures).

At performance of a protection profile on registration, its application should include the description of it. Into the content of a profile enters seven sections:

1. PP introduction.
 - 1.1. PP identification.
 - 1.2. PP overview.
2. TOE description.
3. TOE security environment.
 - 3.1. Assumptions.
 - 3.2. Threats.
 - 3.3. Organizational security policies.
4. Security objectives.

- 4.1. Security objectives for the TOE.
- 4.2. Security objectives for the environment.
5. IT security requirements.
 - 5.1. TOE security functional requirements.
 - 5.2. TOE security assurance requirements.
 - 5.3. Security requirements for the IT environment.
6. PP application notes.
7. Rationale.
 - 7.1. Security objectives rationale.
 - 7.2. Security requirements rationale.

The first section identifies PP and its overview in the form most suitable to inclusion in catalogues and registries PP is given.

The second section includes the information about IT product (or type of IT product), intended for the explanatory of its assignment and security requirements.

The section "TOE security environment" included the description of environment aspects of security IT product which should be taken into account for IT product.

The section of the "Security objectives" includes a summary of prospective reaction to aspects of the security environment, as from the point of view of the security objectives which should be satisfied with IT product, and from the point of view of the security objectives which should be satisfied with IT- and non-IT- security measures within the limits of IT product environment.

The section "IT security requirements" include the security functional requirements of IT product, requirements of security assurance, and also security requirements of software, hardware-software and hardware maintenance of the IT-environment of IT product.

The section "PP application notes" can include any additional information which developer PP counts useful.

Section "Rationale" shows, that PP specifies the full and interconnected set of IT product security requirements, and that appropriate IT product takes into account the identified aspects of the security environment.

Additional sections which can be necessary for granting the helpful information can be included in a profile.

The analysis of the contents of a profile shows, that its development is carried out in the following (descending) sequence:

- identification of aspects of the environment security;

- definition of the security objectives which are taking into account identified aspects of the environment security;
- formation of security requirements IT directed on satisfaction of the security objectives.

Thus, in view of the given sequence of actions, it is visible, that process of PP development has iterative character. For example, formation of security requirements can promote updating of the security objectives or even needs for security. In result, a lot of iterations for the fullest account of interrelations between threats, organizational security policies, the objectives and security requirements, and also security functions can be demanded.

Finally, when the protection profile is generated, registered, it is published in the official registry.

The analysis of an opportunity of use of criteria for technical realization of a structure in services of telecommunication systems is carried out.

REFERENCES

- [1] GOST R ISO/IEC 15408-1-2002 Information Technology – Approaches and Means of Security. – Evaluation Criteria for IT Security. Part 1: Introduction and general model.
- [2] GOST R ISO/IEC 15408-1-2002 Information Technology – Approaches and Means of Security. – Evaluation Criteria for IT Security. Part 2: Security functional requirements.
- [3] GOST R ISO/IEC 15408-1-2002 Information Technology – Approaches and Means of Security. – Evaluation Criteria for IT Security. Part 3: Security assurance requirements.
- [4] A. Burov, A. Kiselev, S. Novikov, E. Safonov, O. Solonskaya, "Routing and protection of the information on a network layer in multiservice communication network", deposited with VINITI, № 1732-V2004.
- [5] S. Novikov, O. Solonskaya "Protection of the information in networks with guaranteed quality of service," work in progress.

Solonskaya Oksana (M'03) has graduated from Siberian State University of Telecommunication and Informatics in 2000 on specialty "Communication networks and systems of switching". In 2004 she has the bachelor degree on "Development of methodology of an evaluation of the protection profile of the user information at a network level", and after that has arrived in a MS course on a direction "Telecommunication" with a topic of the MS dissertation "Research

and development of methods of the analysis and synthesis of a protection profile in communication networks with guaranteed quality of service".

Study Sensing Properties to CH₄ of Pt/SnO₂:Sb Thin Film Gas Sensor in Pulsing Mode

O.V. Anisimov*, N.K. Maksimova, S.S. Schogol, R.V. Chernykh,
E.V. Chernikov

*V.D. Kuznetov Siberian Physicotechnical Institute, Tomsk
State University, 1, Novosobornaya sq., Tomsk, 634050,
Russia*

**Oleg73@mail2000.ru*

Abstract — The resistance-time profiles of Pt/SnO₂:Sb thin films sensor of methane during cyclic variation of the working temperature have been studied. The time-period of one cycle was 10–12 min: 2 sec heating up to 400–570°C and 8–10 sec down-heating to 80–150°C. It was demonstrated the electrical and sensing properties of sensors as function of pulsing temperatures, methane concentration and humidity. It was shown that the using pulsing mode decreases the effect of humidity on the response to methane but does not provide the perfect stabilization of sensors parameters at humidity and environment temperatures variation.

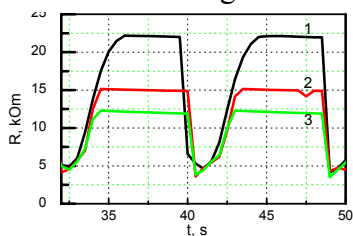
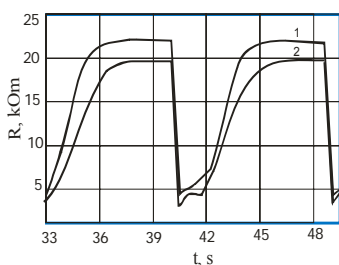
Index Terms — sensors of methane, thin films, tin oxide, humidity, working temperature

One of the major problems with tin oxide gas sensors is their lack of selectivity as well as their dependency on humidity causing more or less drastic changes in sensor properties. In recent years some researchers (for example [1]) have suggested a way to improve the capability of gas identification and concentration determination of the sensors when the operating temperatures are varied periodically in time while the conductance of the sensitive layer is sampled simultaneously. However the research on this direction is only starting, the experiments are to carry on TGS thick film sensor elements from Figaro Engineering mainly. The

conductance-time profile shapes represent the gas molecular specific temperature behavior of the conductance. It is interesting to study the thin film gas sensor in pulsing mode.

In this study we present the investigations of the resistance-time profiles (RTP) of created by us [2-5] Pt/SnO₂:Sb thin film (50–100 nm) methane sensors for variation of the working temperature with a time period of 10–12 sec. The problem of reduction of the humidity effect on the response to methane was examined.

The technology of the thin film sensors was reported in the papers [2–4]. The used elements were mounted onto TO-8 socket and placed in a testing chamber. The whole experimental system was connected to a PC for acquiring and plotting the resistance-time profiles in real time. The measurements were performed at room temperature in wet (RH=100%, the absolute humidity A=20–25 g/m³) and dry (A= 0.34 g/m³) air. The operating temperatures were evaluated by temperature coefficients of platinum heater and thermal resistance. It provided the stabilization of the sensor temperature both in heating cycle and in cooling cycle. The resistance was measured in pure air and after addition of mixture 85 % methane + air in a testing chamber by



determined volume syringe.

The response value is defined as R_s/R_0 , where R_s – the measured resistance of a sample in the air + gas from 0.5 up to 2% methane, $R_0=R_s$ in dry air in the case of 0.5% methane.

Fig. 1. The RTPs of Pt/SnO₂:Sb thin film in pulsing mode in pure dry air: a – T_h= 500 °C, T_l=80 °C (1), 120 °C (2), 150 °C. b – T_l=80 °C, T_h=450 °C (1), 500 °C (2)

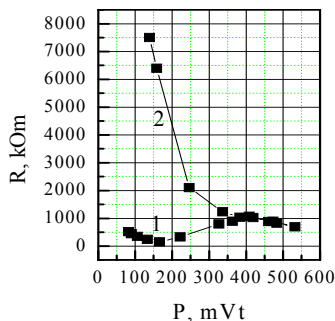


Fig. 2. The resistance of Pt/SnO₂:Sb as function of heating absorbed power: 1–increasing P, 2–decreasing P.

Typical resistance–time profiles (Fig. 1) are shown that the resistance in cooling cycle is above the resistance in heating cycle. When the working temperature is varied from 80 up to 150 °C in cooling cycle (T_l) and from 400 up to 570 °C in heating cycle (T_h), the corresponding sensor resistances are decreased. These regularities can be explained by hysteresis of the temperature dependence resistance of Pt/SnO₂:Sb thin films. As Fig. 2 is demonstrates, at increasing of heating absorbed power P the typical N- shaped dependence takes place (curve 1). At sufficiently fast (during 30 min) decreasing of heating absorbed power the sensor resistance increases sharp (curve 2). In the works [2-4] we have shown that at heating from room temperature up to 160-180 °C (P around 160–170 mVt) the resistance is decreased due to ionization of shallow and deep impurity centers in part of a film, not depletion by charge carriers. At temperatures above 160–180 °C, there is a growth of resistance, which is resulted to surface transformations providing increase of a negative charge and depletion layer thickness: at 160 °C the transitions O₂⁻ O⁻ are possible; at 230–300 °C - transitions O⁻ O²⁻; at 250-450 °C there is a desorption of water. Apparently at fast cooling the transition in molecular oxygen O₂⁻ and adsorption of water don't have time for realization on

semiconductor surface. It takes about two hours at low (80–100 mWt) heating absorbed power for a surface relaxation into equilibrium. We can assume that in pulsing mode at every temperature some quasi-equilibrium correlation between resistances in heating and cooling cycles according to Fig. 2 (curve 2) is realized.

In Fig. 3 the resistance pulses during one period of time in dry and wet pure air and in mixture gas + air are compared. The pulsing

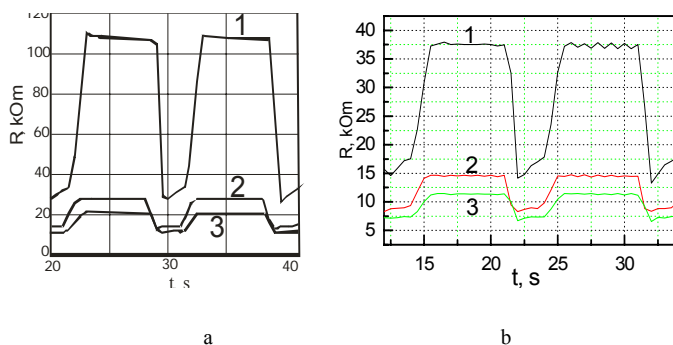
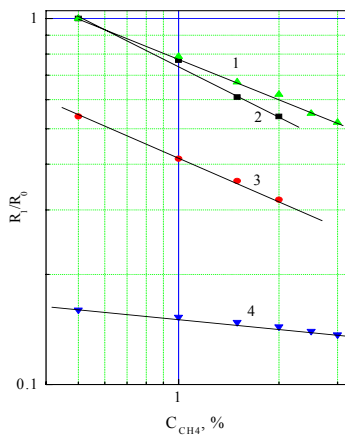


Fig. 3. RTPs of the sensor in pulsing mode from 100 up to 400 °C in dry (a) and wet (b) air: 1- pure air, 2- $C_{CH_4}=1\%$, 3- $C_{CH_4}=2\%$

temperature had been varying in interval 100–400°C. It is interesting that the higher response to methane is observed in cooling cycle. As was reported earlier [8], usually the response on methane is visible at 240 °C and amounts to maximum at 450–500°C. At low temperatures the processes



of methane dissociative adsorption and desorption of reaction products are difficult, above 500°C the response decreasing is due to methane desorption from overheating semiconductor surface. Apparently the period and

amplitude of temperature pulses used provide the conditions for methane dissociative adsorption and desorption of reaction products in heating cycle.

The evolving atomic hydrogen reacts with chemisorbed oxygen, which takes place on SnO₂ surface in cooling cycle

Fig. 4. The concentration dependencies of the response to methane in constant temperature mode (curve 1,4) and in pulsing mode (curve 2,3). Humidity value: 1–15 %, 2–dry air, 3–100 %, 4–90%

also. The overheating up to 570°C assists the response decreasing in heating cycle due to intensive desorption processes.

In wet air the sensor resistance is decreased both in pure air and in mixture methane + air (Fig. 3). In Fig. 4 the concentration dependencies of the response to methane (in cooling cycle) in dry and wet air in constant temperature and pulsing modes are compared. Moreover in experiments in pulsing mode the humidity values has been varying in larger limits. Apparently the using of pulsing mode decreases the humidity effect on the response to methane even in cooling mode. However the choused modes don't provide the total desorption of chemisorbed water.

REFERENCES

- [1] W.M. Sears, K. Colbow, F. Consadori. *Sens. Actuators* **19**, 333 (1989).
- [2] O.V. Anisimov, N.K. Maksimova, N.G. Filonov et al., *Sensor*, **7**, 35 (2003) (in Russian).
- [3] O.V. Anisimov, N.K. Maksimova et al., *Proc. of EUROSENSORS XVII*, Guimaraes, Portugal, Sept. 21–24, 2003. p. 890.
- [4] O.V. Anisimov, N.K. Maksimova, N.G. Filonov et al., *J. Phys.Chem.* **78**, 1907 (2004) (in Russian).
- [5] O.V. Anisimov, N.K. Maksimova et al., *Proc. of 10-th Intern. Meeting Chem. Sensors*, Tsukuba, Japan, July 11–14, 2004. p. 688.

Diffusion of Chromium into GaAs as a Way to Detector Material Making

M.V. Ardyshev*, I.A. Prudajev, S.S. Khludkov

*V.D. Kuznetov Siberian Physicotechnical Institute, Tomsk State
University, 1, Novosobornaya sq., Tomsk, 634050, Russia*

**ard.rff@elefot.tsu.ru*

Abstract — The diffusion of chromium that is deep impurity in GaAs has been investigated as a way to high-ohmic detector material making. The coefficient of diffusion and the limiting dissolubility of chromium have been estimated.

Index Terms — gallium arsenide, chromium, coefficient of diffusion

INTRODUCTION

Gallium arsenide doped with chromium has extremely high resistivity (up to 10^9 Ohm-cm [1]). In some cases, the doping is favourably to provide by diffusion. Such “diffusive” high-ohmic GaAs could be used as a material for making detectors of radiation in, for example, medical diagnostics using X-ray [2].

The chromium diffusion into GaAs was studied in earlier works [see 3-7]. In [3-5], the authors used direct methods of investigation. All of [3-7] experimental data were obtained for diffusion in vacuum. The Arrhenius' dependence from [3] has great inaccuracy of measurements that leads to the coefficient of diffusion spread up to two orders at the same temperature. Such result, evidently, is related with uncontrolled changes in experiment conditions. In [4], it was found out that chromium diffuses by dissociative mechanism, but the coefficient of diffusion was not estimated. In bulk, chromium moves on internodes. When meet with vacancy, chromium occupies it. At the same time, in gallium node, chromium displays as a deep acceptor.

Most complete investigation of the diffusion was done in [5]. However, presented data on the coefficient of diffusion were obtained under condition that the near-surface region (10-50 μm) of the diffusion profile could be approximated by erf-function that is uncorrected.

EXPERIMENTAL

LEC-grown n-type (Sn- or Te-doped) (100)-oriented GaAs samples with dislocation density $\sim 3 \cdot 10^4 \text{ cm}^{-2}$, free charge carriers concentration $10^{15} \text{--} 10^{18} \text{ cm}^{-3}$, thickness 400-700 μm , square $\sim (2\text{--}3) \text{ cm}^2$ were used. After chemical-dynamic polishing, the film of chromium was deposited on one of the sample sides using the thermal evaporation technique.

After the diffusion, a thickness of the high-ohmic layer was measured using the anodizing method (anodization voltage 130 V). An estimation of the coefficient of diffusion and the surface concentration of chromium were provided with the help of so-called “two samples” method with the assumption of erfc-profile [9]:

$$C_1 = C_S \cdot \text{erfc} (x_1 / 2\sqrt{Dt}); \quad C_2 = C_S \cdot \text{erfc} (x_2 / 2\sqrt{Dt}),$$

where C_S is the surface concentration of chromium, D is the coefficient of diffusion, t is the diffusion process duration, x_1 and x_2 are the thicknesses of the high-ohmic regions, C_1 and C_2 are the carrier concentrations in initial samples (before the diffusion).

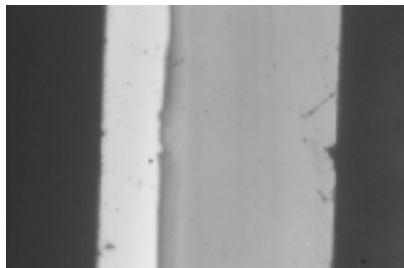
After solving for preexponential factor D_0 and activation energy Q from Arrhenius' dependence, the same dependence was used for finding the limiting dissolubility of chromium for other temperatures (the p-n junction method) with the assumption of erfc-chromium distribution in GaAs:

$$C_S = C_1 / \text{erfc} (x_1 / \sqrt{4 \cdot t \cdot D_0 \exp(-Q/kT)}),$$

where T is temperature, k is Boltzmann constant.

Owing to the fact that investigations were carried out by indirect method, systematic inaccuracy is great enough and estimate around 100%.

RESULTS



The typical image of anodizing chip is presented in fig.1. The light region corresponds to the high-ohmic layer. One can see that the high/low-ohmic interface is quite straight that means no dislocation influence on chromium diffusion.

The temperature

Fig. 1. The typical image of anodizing chip

dependences of chromium coefficient of diffusion is given in fig.2. One can see that four experimental points are well flattered in semilogarithmic coordinates. The coefficient of diffusion is described by Arrhenius':

$$D = D_0 \exp(-Q/kT),$$

where $D_0 = 1.7 \cdot 10^{-2} \text{ cm}^2/\text{s}$, $Q=1.43 \text{ eV}$.

The temperature dependences of chromium limiting dissolubility is given in fig.3. This dependence is also flattered in semilogarithmic coordinates and is described by:

$$C_S = C_0 \exp(-Q_{Cr}/kT),$$

where $C_0 = 8.9 \cdot 10^{21} \text{ cm}^{-3}$, $Q_{Cr} = 1.22 \text{ eV}$.

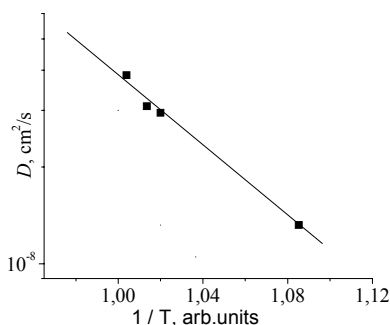


Fig.2. The temperature dependences of chromium coefficient of diffusion

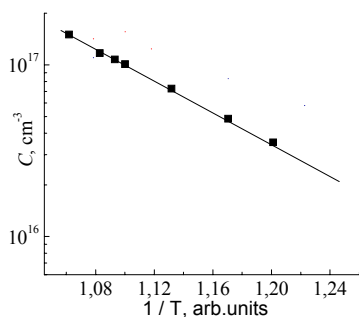


Fig.3. The temperature dependences of chromium limiting dissolubility

The above-mentioned data are in close (in order) agreement with data from [3, 4] ($D \sim 10^{-8} \text{ cm}^2/\text{s}$). However, the dissolubility is found to be higher almost by order. Such result can be related with the fact that, in our experiment, the diffusion of chromium goes on from sprayed coating in contrast to from pure chromium bits as in [3, 4]. This, seemingly, leads to an increase in chromium concentration (chromium in a phase that is source of diffusion).

The work was financially supported by RFBR Projects No. 04-02-17486.

REFERENCES

- [1] O.P.Tolbanov. In Proc. 8th Rus. Conf. «Gallium Arsenide and III-V Semiconductor Compounds». – Tomsk, 2002. – P. 26.

- [2] M.V. Ardyshev, I.A. Prudajev. In Mat. Internat. Conf. "Modern Problems in Physics and Hi-Tech." – Tomsk, 2003. – P. 154.
- [3] N.V. Gontar, L.B. Gorodnik et al. Diffusion and behavior of chromium in GaAs. In: Properties of doped semiconductors. – Moscow, Nauka, 1977. – P. 31.
- [4] Tuck B., Adegboyega A. In J. Phys. D: Appl. Phys. – 1979. – V.12. – No 11. – P.1895.
- [5] Deal M.D., Stevenson D.A. In J. Appl. Phys. – 1986. – V.59. – No 7. – P. 2398.
- [6] S.S. Khludkov et al. In Izv. AN SSSR. Ser.: Inorg. Mat. – 1972. – V.8. – No 6. – P. 1044.
- [7] S.S. Khludkov et al. In Fiz. i Teh. Polupr. – 2004. – V.38. – No 3. – P. 274.
- [8] E.V. Buts, L.N. Vozmilova. In Electr. Tehnika. Ser.2. Semicond. Devices. – 1979. – No 9. – P.86.
- [9] D. Shaw, Ed. "Atomic diffusion in semiconductors". Moscow, Mir, 1975. – 684 p.

Detectors for the X-Ray Testing Systems

G.I. Ayzenshtat¹, M.D. Vilisova², M.A. Lelekov¹,
A.I. Ivashchenko¹, D.Yu. Mokeev², L.P. Porokhovnichenko¹,
O.P. Tolbanov², L.G. Shapoval¹

¹*Scientific and Production State Enterprise "Semiconductor Devices Research Institute", Tomsk, 634034, Russia, e-mail: ayzen@tomsknet.ru*

²*Siberian Physics-Technical Institute, 1, Novo-Sobornaya Sq., Tomsk, 634050, Russia*

Abstract — The gallium arsenide detectors working in photovoltaical mode on epitaxial films compensated by chromium are developed. It is shown that in such detectors it is possible to essentially increase the efficiency of charge collection at inclined position of the detector relatively X-rays. The image with resolution 5 lp/mm is received by created coordinate detectors.

Index Terms — GaAs-detector, X-Ray detector

In the most modern digital systems of the X-Ray testing the silicon active elements matrixes covered with the scintillator layer as detectors are used [1]. There is a double transformation of the gamma quantum energy in known detectors: first of all, energy of quantum transformed in light, and then in a charge of the silicon photodetector. It results in loss of signal part, and consequently, leads to increase the dose loadings on research object. At the same time in medical examination systems the most important problem is the maximal decrease of dose loading on patients. Especially strongly this problem costs in mammography [2].

The purpose of the investigation was development of X-Ray detectors with direct transformation of quantum energy to a charge for digital systems. Attempts to create such detectors on monocrystal [3] or epitaxial gallium arsenide [4] were earlier undertaken. The main disadvantages of detectors from a monocrystal material were relatively high levels of the dark currents, creating serious problems for using of the specialized electronics that perfectly working with silicon detectors [3]. It was possible to remove the given disadvantage in detectors from epitaxial material, however these detectors till now are not used widely

because of basic difficulties of reproducible creation of layers with concentration equilibrium electrons about 10^{12} cm^{-3} in gallium arsenide.

In the investigation, detectors were created on a basis of epitaxial gallium arsenide, compensate by chromium. Specific resistivity of active layers of detectors was $\rho \sim 10^8 \text{ Ohm}\cdot\text{cm}$. Realization of such epitaxial layers guarantees high percent of suitable detectors, unlike technology of creation "clean" epitaxial gallium arsenide layers, which have $\rho \sim 10^3 \text{ Ohm}\cdot\text{cm}$.

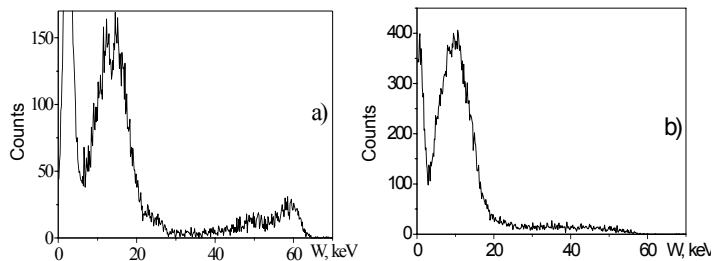


Fig. 1. Amplitude spectrums of detectors from «clean» (a) and compensated by chromium (b) layers epitaxial GaAs radiated by ^{241}Am gamma-quantums

In fig. 1, amplitude spectrums of detectors thickness $40 \mu\text{m}$ are submitted, made from epitaxial gallium arsenide layers for "clean" (a) and compensated (b) materials at impact on them of gamma-quantums from americium - ^{241}Am isotope. The comparative analysis of these spectrums shows the following. On amplitude spectrums of detectors based on $p^+ - n^- - n^+$ -structures, where n^- is "clean" epitaxial gallium arsenide layer, it is possible to select monolines of quantumms with energy 14, 17 and 59 keV (a). Efficiency of charge collection for such detector is close to 100%. It means that in the detector the full collection both nonequilibrium electrons and holes are carried out. At the same time, in the amplitude spectrums $p^+ - i - n^+$ -structures based on the i -layer compensated by chromium a line 59 keV is not present. Position of the peak, corresponding to 14 and 17 keV based on 10 keV vicinity. The spectrum is similar for detectors from gallium arsenide alloyed by chromium [3]. In such material the life time for holes has extremely low value. There are no collection of holes. It is visible also from results on the charge collection when detectors was irradiated by beta particles from ^{90}Sn isotope. Collection of charge in this case is only the half of calculated value. Particularity of the given detectors is that they work in photovoltaical mode. At zero displacement on detectors the amplitude

spectrum a little differs from the picture of spectrum submitted on fig. 1b.

Searching for a way of efficient using the detectors based on the epitaxial gallium arsenide compensated by chromium for mammography has shown that the kind of amplitude spectrum can be improved essentially if detector install under a corner to X-rays direction. On fig. 2 results of amplitude spectrum calculations are shown at impact of gamma-quantums on our detector depending on the corner of the detector inclination to the collimate photons stream direction.

Calculations were based on the modernized formula describing the amplitude spectrum form (1). We have changed the formula received earlier in [6] to take into account the inclined position of the detector concerning the radiation stream direction.

$$P(E) = \int_0^d \frac{\frac{k}{\sin \alpha} \exp\left(-\frac{k}{\sin \alpha} \cdot d\right)}{\sqrt{2\pi} \cdot \sigma(x) \cdot \left[1 - \exp\left(-\frac{k}{\sin \alpha} \cdot d\right)\right]} \cdot \exp\left(\frac{-(E - E_0 \cdot \eta(x))^2}{2 \cdot \sigma^2(x)}\right) dx \quad (1)$$

Here $P(E)$ is number of events with energy E , k is a factor of radiation absorption, d is distance between detector electrodes, E_0 is energy of falling radiation, $\eta(x)$ is Hecht function, $\sigma(x)$ is root-mean-square deviation by fluctuations of formed electron-hole pairs, α is the corner of radiation falling.

Calculation of amplitude spectrum of the target signal was carried out for the epitaxial detector located in relation to a radiation source under corners 90° , 6° and 2° . Thus energy of falling radiation $E_0=20$ keV, absorbing factor $k=175$, and electronics noise is $\sigma=\text{const}=4$ keV.

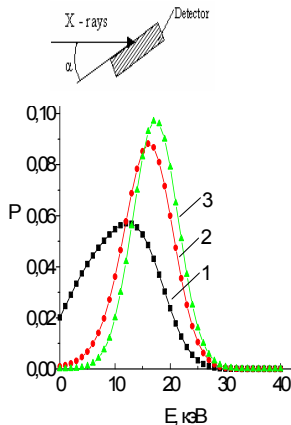
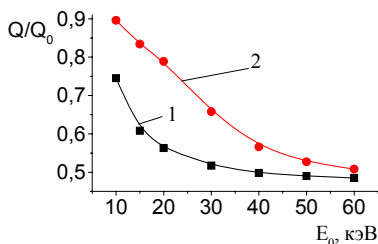


Fig. 2. Amplitude spectrum thickness $d = 0.10$ μm in photovoltaical mode under different corners of radiation fall. Curve 1 – $\alpha = 90^\circ$, 2 – $\alpha = 6^\circ$, 3 – $\alpha = 2^\circ$

In result, as can be seen from fig. 2, the signal spectrum from detector thickness 40 μm at reduction of fall the corner becomes less spread and it is displaced in 20 keV area of energy quantum. It results in increase of the collected charge from the detector. Hence on fig. 3 accounted efficiency of charge collection in the detector from the energy of X-Ray quantum is shown, for located under a corner 6° as well as for the detector with perpendicular frontal plane of flying quants. For quantum energy from 10 up to 30 keV the efficiency of charge collection is increased practically in 1,5 times.

The effect of spectrum improvement at inclined detector was observed experimentally. On fig. 4 the result of experiment confirming calculations are shown.

The coordinate detectors with number of channels 256 were created from epitaxial $p^+ - i - n^+$ -structures of gallium arsenide. The high resistance i -layers was carried out by alloying of the epitaxial layers by chromium atoms. The step of contacts in the detector was 110 μm . The narrow slots between contacts were created in detectors. The similar design for the first time is considered by us in work [4]. Testing of coordinate detectors were carried out in Institute of Nuclear Physics (Novosibirsk) on the low dose X-Ray device. The detectors joined with



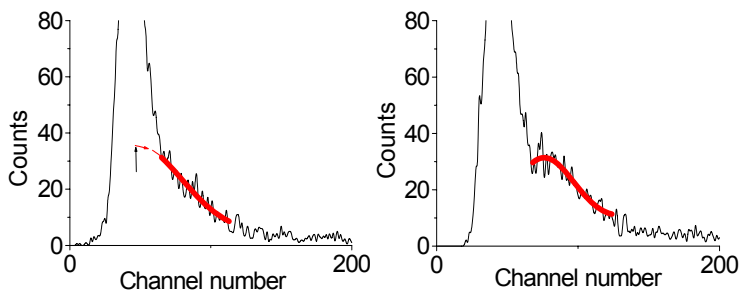
chips of specialized device of Perkin Elmer company, were installed under a corner of 6 degrees to the radiation source. It is proven from measurements that the given detectors satisfy all requirements for digital mammography detectors. The spatial resolution 5 lp/mm is received. Detectors are characterized by high linearity of a target signal from the X-Ray tube current at its change from 1 up to 90 mA.

Fig. 3. Efficiency of charge collection for different corners of detector inclination. Curve 1 – corner $\alpha = 90^\circ$, 2 – $\alpha = 6^\circ$

Fig. 4. Amplitude spectrums of detectors for different corners of inclination one: $\alpha = 90^\circ$ - (a), $\alpha = 18^\circ$

REFERENCES

- [1] E. Pisano, M. Jace, M. Bradley, et al. “Current status of full-field digital mammography”. *Acad. Radiol.*, 2000, V. 7, pp. 266–280.
- [2] R. Cahn, B. Cederstrom, M. Danielsson, A. Hall, M. Lundqvist and D. Nygren, “Detective quantum efficiency dependence on X-Ray energy weighting in mammography”, *Med. Phys.* 1999,26:(12), pp. 2680–2683.
- [3] G.I. Ayzenshtat, E.A Babichev, S.E., Baru et al., “GaAs detectors for medical imaging” *Nucl. Instr. and Meth.* – 2003. – Vol. A.509, pp. 268–273.
- [4] G.I. Ayzenshtat, V.G. Kanaev A.V. Khan et al., “GaAs X-Ray coordinate detectors”. *Nucl. Instr. and Meth.* – 2001. – A466, pp.162–167.
- [5] G.I. Ayzenshtat, D.L. Budnitsky, O.B. Koretskaya et al., “GaAs as a



material for particle detectors”. *Nucl. Instr. and Meth.* – 2002. – A494, pp.120-127.

- [6] R. Trammel, J.F. Walter, in *Nucl. Instr. and Meth.* 1969, 76, pp. 317.

Analysis of Free-Carrier Charges Distribution in the n-GaAs Monocrystals Used at Formation of the High-Resistance Material for the Ionizing Radiation Sensors

D.L. Budnitsky*, O.B. Koretskaya, V.A. Novikov,
O.P. Tolbanov

*Siberian Physics-Technical Institute, 1, Novo-Sobornaya Sq., Tomsk,
634050, Russia
kanc@spti.tsu.ru**

Abstract — In the paper, analysis of charge distribution in the gallium arsenide monocrystals are presented. The absorption spectrums are investigated. It is described that non-destroying testing of monocrystals before diffusion is possible.

Index Terms — gallium arsenide, absorbing spectrum, free-carrier charge

INTRODUCTION

Diffusion of chromium in *n*-GaAs allows to form high-resistance material with the properties required for detectors of ionizing radiating: long time life of the charge carriers and high resistivity. Therefore researches of *n*-type conductivity properties, initial for diffusion of chromium in gallium arsenide represents wide doubtless physical interest: in particular, research of absorption of IR radiation by free electrons and its distributions on diameter and length of monocrystals. The practical value of these researches is opportunity of non-destroying testing of plate properties before diffusion.

EXPERIMENTAL RESULTS

For researches the gallium arsenide of *n*-type conductivity with initial concentration of charge carriers (n_0) from $(2-3) \cdot 10^{15} \text{ cm}^{-3}$ up to $\sim 1 \cdot 10^{18} \text{ cm}^{-3}$ was used according to the manufacturer. Diffusion of chromium will be carried out into *n*-GaAs washers with thickness $d=(0.5-1.2) \text{ mm}$, and this condition defined thickness of samples for optical researches. It is known that for definition of the absorption factor (α) with the minimum error the following condition is required:

$$\alpha \cdot d \approx 1 \tag{1}$$

Therefore the absorption spectrum of GaAs washer of the given thickness was initially measured $\alpha(h\nu)$ and the energy of photons for which the condition (1) was carried out was defined by spectrum. Studies have shown that condition (1) at the sizes determined above n_0 and d is answered the absorption spectrums in the field of photon energy of $h\nu=(0.05\div 0.12)$ eV.

RESULTS

The typical absorption spectrum is given on fig. 1. In GaAs crystals investigated by us the absorption spectrum in the field of $h\nu < 0.07$ eV is characterized by smooth change of the absorption factor and the absorption level is much lower than it was possible to expect on the known data [1]. We did not analyze the reasons of such

behavior of α . The nonlinear change of the absorption factor in the chosen coordinates is more interested. According to theoretical representations, absorption on free charge carriers has a power-mode type, which parameter characterizes the mechanism of dispersion of the charge carrier [2]. In our opinion, observed deviation of spectral dependence of absorption factor from linear behavior aside excess α suggest about presence in this spectral interval of additional absorption stipulate by optical transition from the local level in conductivity zone. For clarity on the diagram dependence $\alpha \sim (h\nu)^{-2,55}$ is presented.

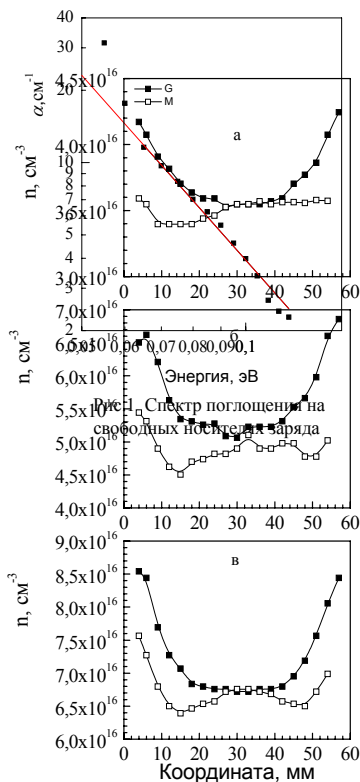


Рис.2. Распределение n_0 по сечению монокристалла диаметром 60 мм: а-начало; б-середина; в-конец монокристалла.

carriers in the investigated spectral area and having determined the certain spectral form, may result in the systematic uncertainty in definition of n_0 from absorption spectrum. However the use of caliber curves representing dependence

$$\alpha = f(n_0)$$

allows to reduce and even to avoid errors from additional absorption.

Using results of calibration on n -GaAs washers, prepared for the further technological operations, the measurement of concentration distribution of electrons on diameter in two mutually perpendicular directions were carried out. On fig. 2 the distributions $\alpha(d)$ are given for washers taken various parts of a monocrystal in diameter of 60 mm. There is no radial symmetry in distribution of n_0 for all three parts of monocrystal. Moreover, change of the distribution form is observed on a direction of measurements: in the parallel to a base cut direction (011) the distribution of $n_0(d)$ has the U-form, and in perpendicular – the W-form. Besides, the parallel direction is characterized by the greater scatter of values n_0 between the centre and steal of the plate. Taken as a measure of this scatter a value

$$P = \frac{n_{0_{\text{макс}}} - n_{0_{\text{мин}}}}{n_{0_{\text{мин}}}}$$

we have in the same plate (fig. 3, c) $P_{\text{пар}}=0,2$, but $P_{\text{сер}}=0,06$. From diagrams the increase of size P from the beginning to the end of a monocrystal from 0.2 up to 0.27 is evidently visible at measurements in parallel to the base cut, perpendicular from 0.06 up to 0.11. Changing of concentration n_0 on the monocrystal axis is submitted on fig. 3 and shows double increase n_0 on length. Applicable to technology of formation the high-resistance GaAs:Cr it means not only necessity of increase of diffusion temperature in process of monocrystal use, but also necessity of orientation to the maximum value of electron concentration in the section.

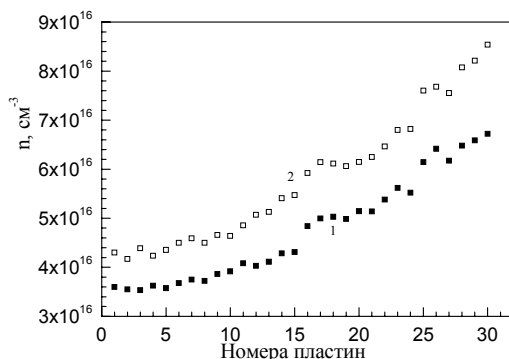


Рис.3. Распределение n_0 по длине монокристалла диаметром 60 мм: 1- на оси монокристалла; 2-на поверхности монокристалла

Trends of the electron concentration changing on diameter for monocrystal with 40 mm diameter have the same character, as in monocrystal of greater diameter. However value P is less and does not exceed ≈ 0.07 in second half of monocrystal. In this case monocrystals n -GaAs of 40 mm diameter are more acceptable for diffusion.

The concentration distribution on length of the monocrystal axis in 40 mm diameter is characterized by the same regularities, as for monocrystal of greater diameter.

CONCLUSIONS

1. Monocrystals n -GaAs of smaller diameter have the best distribution homogeneity of n_0 on diameter.
2. Monocrystals n -GaAs in diameter 60 mm are characterized by the orientation dependence and increasing of n_0 concentration scatter on diameter to the end of the crystal.
3. The use of monocrystal of smaller diameter is preferable to formation of high-resistance gallium arsenide by chromium diffusion because they allow to avoid overheat of gallium arsenide bring falling the life time of the charge carriers.
4. There is no absorption from the lattice fluctuations in the absorption spectrums of n -GaAs in the photon energy 0.055 eV– 0.12 eV.

The work has been supported by RFBR grants 04-02-17486, 05-02-98008.

REFERENCES

- [1] Gallium Arsenide. Reception, Properties and Application. Ed. F.P. Kesamanla and D.N. Nasledov. Moscow, Nauka. 1973. – 209 p.
- [2] E. Haga and H. Kimura. In Journal of the Phys. Soc. of Japan. – 1964. V. 19, No 4. P. 471-481.

Study of Particularities for Metal Contact Formation to the Semiconductor High-Resistance GaAs:Cr

D.L. Budnitsky, A.D. Lychagin, L.S. Okaevich*,
O.P. Tolbanov

*Siberian Physics-Technical Institute, 1, Novo-Sobornaya Sq.,
Tomsk, 634050, Russia, okaevich.rff@elefot.tsu.ru**

Abstract — In the paper, studies of volt-ampere and volt-luxing characteristics of the detector structures based on gallium arsenide, compensated by chromium are carried out. It is shown that metallic contacts to a structure are barrier for electrons. One of contacts is inject at any bias polarity.

Index Terms — gallium arsenide, the detector structure, ohmic contact

INTRODUCTION

High-resistance gallium arsenide, formed by chromium diffusion in n-GaAs is a basis of the broad circle of detectors of the ionizing radiation. A basis of devise is the high resistance GaAs:Cr. In this case it is possible to perform the big size of sensitive area that no achieved using of barrier structures. Therefore, increasing requirements are showed to linearity of contacts: they should be ohmic without injection. Methods of formation of the ohmic contacts to low resistance GaAs [1] may be applied and to high resistance monocrystal. However properties of such contacts required additional researches, as it was the purpose of this study.

EXPERIMENTAL RESULTS

In the present investigation, the studies of volt-ampere and volt-luxing characteristics typical for a detector of ionizing radiating, the resistive structures with are submitted "ohmic" contacts generated by various metal combinations. Characteristics of the investigated samples are given in table 1.

Table 1. Characteristics of resistive structures from GaAs:Cr

N	Contact	ρ on VAC, Ohm*cm	Barrier calc., ϕ_0 , eV	Barrier exper., $\Delta\phi$, eV
1	AuV	$1,2 \cdot 10^9$	1.14	1.1
2	Al	$1,1 \cdot 10^9$	1.20	1.18
4	NiCr	$1 \cdot 10^9$	1.12	1.04

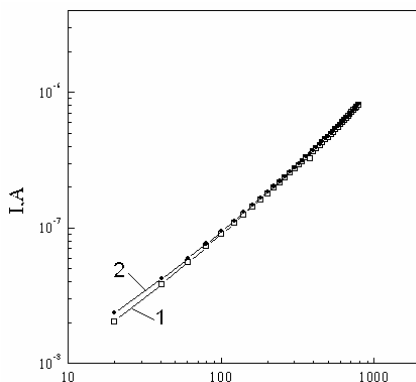


Fig. 1. Straight (1) and reverse VAC of the GaAs:Cr-metal structure

Typical for all structures volt-ampere characteristics are given on fig. 1. Super linear increase of the current is typically for them, a weak deforming VAC at small bias and becoming more appreciable at the high bias. Results of an estimation of specific high resistance GaAs: Cr on initial VAC are given in the table 1 (column 3). As would expect, ρ are close

to minimal that maximum for GaAs, at the account of rather low mobility (in comparison with grown GaAs:EL2), both electron ($\mu_n \approx 3000 \text{ cm}^2/\text{V}\cdot\text{sec}$), and holes ($\mu_p \approx 200 \text{ cm}^2/\text{V}\cdot\text{sec}$) in comparison with grown GaAs:EL2. The analysis of VAC with Origin software shows that it may be described analytically by dependence of a kind

$$J = A \cdot U + B \exp(C \cdot eU) \quad (1)$$

or

$$J = A \cdot U + B \cdot U^2 \quad (2)$$

Dependence of a kind (1) is represented more natural since specifies the effect, which may arise in contacts: injection of charge carriers. It is necessary to assume that contacts to high resistance GaAs:Cr have the inject properties. Therefore despite of technological conditions of ohmic contact formation, the Schottky barrier on border metal – high resistivity GaAs is arisen. Characteristics of this barrier should be considered below.

Square-law VAC might specify of the currents limited to a spatial charge. However the big concentration of traps for the charge carriers in

high resistance GaAs:Cr shifts the moment of occurrence the current limited to the spatial charge in area of the high bias and refuse this version of VAC explanation. Thus by results of the VAC analysis it is possible to assume an occurrence of a barrier on boundary metal- high resistance GaAs:Cr. Taking into account properties of the high resistance material – bipolar conductivity with close sizes of electronic and hole components, any zone bend (upwards or downwards) will result in injection one or another type of charge carrier.

For an estimation of zone bend the measurement of the volt-luxing characteristic were carried out. Radiation of the helium-neon laser was focused on the contact metal - semiconductor for achievement the high excitation ($h\nu \approx 2$ eV). Diameter of the stain contact was 50 microns. The density of radiation capacity was ≈ 10 Wt/cm². Focusing of radiation allowed not only to achieve increase of excitation capacity but also to investigate both contacts separately. The potential difference between the lighted and dark contacts after output on saturation comes nearer to size equal to a zone bend on surface GaAs:Cr with a small systematic uncertainty aside reduction by true of size ϕ_{kont} on (1-2) kT/e Volt. For definition of a direction of zone bend the sign of the potential difference was defined. In all cases the potential of lighted metal contact was higher than dark, i.e. in volume of the semiconductor. Dependence of the potential difference vs capacity density is submitted on fig. 2.

This difference, as well as both its change and existence with the excitation level shows that on border metal - semiconductor of the zone bend a barrier for electron is arisen. Value of the zone bend is rather insignificant, it does not exceed (0.4-0.5) eV. Hence efficient resistance of arising zone is insignificant also. It was earlier shown [2] that at $\phi_{\text{kont}} \approx 0.6$ eV the volume resistance and efficiency resistance of contact are comparable, especially it is justified for linear smaller values ϕ_{kont} .

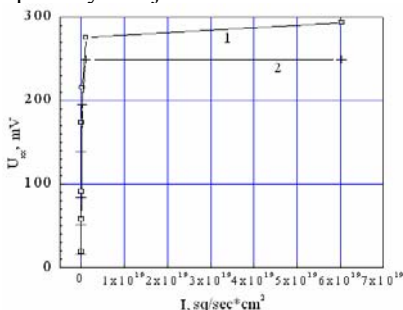


Fig. 2. Potential difference vs capacity density. (1)- light on the upper contact, (2) – on the bottom

Evaluations of barrier size ϕ_0 on the metal-semiconductor border are carried out using of known formula for photodiode in a valve mode [1].

Calculated values ϕ_0 with Fermi level positions in the high resistance GaAs:Cr ($F \approx E_g/2$ eV) practically coincide with value

$$\Delta\phi = \phi_{\text{kont}} + F/e.$$

The corresponding values are presented in the table (columns 4 and 5).

On fig. 3 the zoned diagram of the detector with two "Ohmic" contacts is plotted. The current injection component depends on direction of device bias follows from it. Besides, it is possible to expect an appearance of the inverse layers on surface GaAs:Cr which properties, most probably, define by characteristics of transitions metal-

semiconductor, used as ohmic contacts to high-resistance GaAs:Cr.

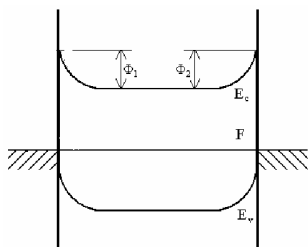


Fig. 3. The energetic diagram of the structure

CONCLUSIONS

Thus, despite of special actions on ohmic contacts formation to high resistance GaAs:Cr this problem did not solved. It results in appearance of surplus dark current worsening the detector characteristics. In connection that properties of the high resistance GaAs:Cr do not allow to form barrier structures, it is necessary to continue studies for properties of the contacts formed using other, nonconventional metals, as well as physical properties of the semiconductor surface under contacts.

The work was financially supported by RFBR Projects No 04-02-17486, 05-02-98008.

REFERENCES

- [1] Gallium Arsenide. Reception, Properties and Application. Ed. F.P. Kesamanla and D.N. Nasledov. Moscow, Nauka. 1973. – 209 p.
- [2] D.L. Budnitski, A.I. Gossen, "An Estimation of Effective Resistance OPZ of Contact High- and Low Resistance of Semiconductor".

Proceedings of the International Conference "Actual Problems of Electronic Instrument Making". Novosibirsk, 2000. Vol. 2. Pp. 117-118.

The Influence of Thermal Annealing on Sensitivity of Silicon MOS-Diodes to Reducing Gases

V.I. Baljuba, V.Y. Grisyk, T.A. Davidova, V.M. Kalygina,
S.S. Nazarov, A.V. Panin*, L.S. Khludkova

Tomsk State University, Russia. E-mail: vmk@elefot.tsu.ru

**Institute of Strength Physics and Materials Science, Siberian Division,
Russian Academy of Science, Russia. E-mail: pav@ispms.tsu.ru*

Abstract — The influence of the thermal annealing in the range of $T_{an}=(200-610)^{\circ}\text{C}$ on sensitivity and transient response characteristics of Pd-SiO₂-Si MOS-diodes upon exposure to hydrogen and ammonia was studied. It is shown that after annealing at 200°C during 10 minutes the capacitance response to H₂ is higher than NH₃ response. After annealing at $T_{an} \geq 300^{\circ}\text{C}$ the MOS diode sensitivity to H₂ practically disappears while the NH₃ response is enough high still though it decreases gradually as T_{an} increases. The Pd surface relief was investigated with AFM after annealing of diodes at (200–610)°C.

Index Terms — MOS-diodes; Ammonia; Hydrogen; Annealing temperature

INTRODUCTION

It is known that electrical characteristics of MOS- structures depend on the value and sign of surface potential ϕ_s . If by some reason ϕ_s changes therefore direct and reverse currents of MOS-diode, its capacitance and conductance increase or decrease depending on semiconductor conduction type. Just this effect is foundation for using MOS-diodes as gas-sensing elements. Pd-SiO₂-Si-diodes with tunnel thin dielectric show high sensitivity to H₂ [1, 2], but at definite conditions their response to NH₃ became much higher than to H₂ [3]. NH₃ sensors operating at (20–30)°C and biases (0.2–0.6) V can be work out on the base of Pd-SiO₂-Si-diodes. At the present time uncontestable model of NH₃ effect on MOS-diodes is absent. Lack of such model hinders development of technology of sensors selective to NH₃. The analysis of publication of experimental results shows that high changes of flat band voltage ($U_{f.b.}$) of MOS structures are observed if barrier electrode is penetrable for NH₃ molecules [4]. In this paper the thermal

annealing was proposed as a method of modification of Pd-SiO₂-Si-diodes properties.

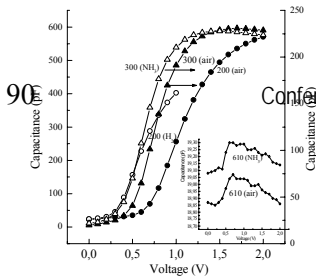
2. EXPERIMENTAL

The samples were based on n⁺-n Si wafers with $\rho = (5-7) \Omega\cdot\text{cm}$ of n-layer. SiO₂ film 0.3 μm thick on n Si was formed. Al was evaporated on n⁺-Si to create ohmic contact. On the top of SiO₂ layer a Pt film was deposited and the heater and contact strip to Pd electrode were formed by integrated technology. The windows in SiO₂ film were opened and Pd film 25 nm thick was evaporated. Palladium electrode with $2.4 \times 10^{-3} \text{ cm}^2$ area was formed by lift-off method. In such diodes Pd contact is separated from n-Si by (3-4 nm) native oxide. The Si wafers were annealed at 200°C during 10 minutes in air and scribed into individual chips. A part of samples was annealed at 300°C, 400°C, 500°C and 610°C during 10 minutes in air. High frequency capacitance-voltage characteristics (CVC) of the samples exposed to gas mixture of H₂/air and NH₃/air were measured. The time dependences of capacitance at a fixed bias were studied as diodes were exposed to H₂ and NH₃.

Fig. 1

3. RESULTS

After exposing to 350 ppm H₂ and 350 ppm NH₃ in air the CVC of diodes with $T_{\text{an}}=200^\circ\text{C}$ and 300°C shift along voltage axis. Flat band voltage of diode measured in air is equal 1.05 V and decreases to 0.75 V in hydrogen ambient (Fig. 1). It was found that change of capacitance response at fixed diode bias and also change of U_{fb} are proportion to H₂ concentration as $(N_{\text{H}_2})^{1/2}$. The diodes annealed at 200°C show response to NH₃ but ammonia response is lower than hydrogen. The capacitance response to H₂ and NH₃ defined as the ratio C_g/C is a function of diode voltage and is presented by curve with maximum (C_g is capacitance in gas (H₂ or NH₃), C is capacitance in air). Maximum response to 350 ppm H₂ in air of the diode annealed at 200°C is equal 5 at voltage $V_{\text{max}}=0.5$ V. Maximum response of the same diode to 350 ppm NH₃ in air is equal 2.7. Thus the diodes annealed at 200°C have sensitivity to NH₃ as well as to hydrogen. Maximum response to 350 ppm H₂ of the diode annealed at 300°C reduces till $C_g/C=1.05$ while the response to 350 ppm NH₃ is equal 1.7. As T_{an} increases to (400-610)°C ammonia response of Pd-SiO₂-Si-diodes gradually vanishes but H₂ that disappears practically. As operating temperature (T_{op}) changes over (35-90)°C capacitance



response to 350 ppm NH₃ in air elevates till $C_g/C=2,0$ at first and than it diminishes.

Fig. 2 shows time dependences of capacitance of diodes annealed at 200°C and 300°C during exposure to 350 ppm H₂ in air and 350 ppm NH₃ in air. The hydrogen response time (τ_r) defined at 0.9 level is about 500 s at $T_{op}=20^\circ\text{C}$ and decreases as T_{op} rises. Approximately such values of τ_r were received for diodes with $T_{an}=200^\circ\text{C}$ during exposure to NH₃ ambient. Hydrogen and ammonia τ_r of diodes annealed at 200°C are high. After annealing of diodes at (300-610)°C τ_r and recovery time (τ_f) of diodes exposed to NH₃ vanishes sharp but hydrogen τ_r and τ_f do not change practically (Fig. 2). For diodes with $T_{an}=300^\circ\text{C}$ response time during exposure to 350 ppm NH₃ reduces about ten times and is equal 20–40 sec. Ammonia response times of such diodes decrease with NH₃ concentration rising and become

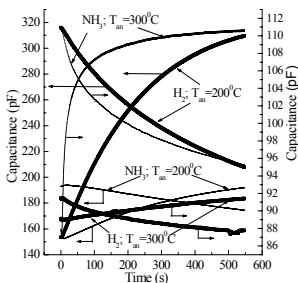
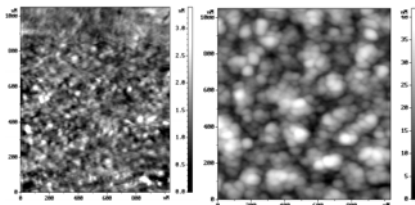


Fig.2

shorter as T_{op} increases.

4. DISCUSSION

The influence of hydrogen on $U_{f,b}$ of MOS diodes can be described as the following model. During the dissociative adsorption of H₂ a part of hydrogen atoms dissolves in the Pd film. Hydrogen atoms reach the Pd-SiO₂ interface by diffusion, adsorb on it and form dipoles. The electric field of these dipoles decreases the work function of



a) $T_{an}=200^\circ\text{C}$ b) $T_{an}=610^\circ\text{C}$

the electrons from Pd. The contact potential difference (U_c) and hence flat band voltage decrease [2]:

$$U_{fb} = - \frac{Q_s(\varphi_s = 0) + Q_d}{C_d/s} - U_c,$$

where $Q_s(\varphi_s=0)<0$ is density of surface state charge at the SiO_2 -n-Si interface when $\varphi_s=0$; Q_d is density of charge in dielectric; C_d is dielectric capacitance; s is barrier contact area. Hydrogen atoms that remain free reach the SiO_2 -n-Si interface by diffusion through the SiO_2 film [1]. A part of atoms forms neutral complexes with acceptor surface states and other atoms give their electrons to the n-Si conduction band and are adsorbed on SiO_2 -n-Si interface as protons. These effects must decrease U_{fb} [1, 2].

Fig. 3 shows the AFM images of morphological aspects of Pd surface. After annealing at 200°C electrode surface relief is smooth enough, its inhomogeneity does not exceed (0.4–0.8) nm (Fig. 3, a). The relief of Pd film becomes brightly expressed when T_{an} rises. Narrow cracks in thin (25 nm) Pd film after annealing at 200°C become wider as T_{an} rises to 610°C (Fig.3, b). During annealing Pd reacts with Si that results in formation of palladium silicides. Mechanical strains are developed in Pd electrode. Silicides of Pd have metallic conductivity but do not exhibit catalytic properties. This fact explains the decrease of sensitivity to H_2 of diodes annealed at $T_{an}\geq 300^\circ\text{C}$.

The drop of diode sensitivity to NH_3 after annealing at $T_{an}\geq 300^\circ\text{C}$ is caused by worsening of diode electrical characteristics. Fig. 2 shows different kinetic of response and recovery forming of diodes exposed to H_2/air and NH_3/air . At equal concentrations H_2 and NH_3 in gas mixtures τ_r of diode annealed at 300°C and exposed to NH_3 ambient is much lower than hydrogen τ_r . In our opinion NH_3 molecules diffused through the pores and cracks in Pd film achieve SiO_2 and locate on it. The nitrogen atom of each NH_3 molecule orients to the underlying SiO_2 surface and hydrogen atoms away from that. It results in rising of the positive charge on the surface of dielectric and causes the change of bandbending ($e\varphi_s$) on the Si surface. Very likely that electron transfer takes place from NH_3 molecule to some SiO_2 states. As a result negative surface potential of Si decreases and CVC shifts to lower biases. More dense Pd electrode of diodes annealed at 200°C hinders NH_3 molecules to reach SiO_2 surface quickly. This fact explains long response times of diodes exposed to NH_3 . The appearance of new pores and cracks in Pd film after diode annealing at $T_{an}>200^\circ\text{C}$ promotes diffusion of NH_3 molecules to SiO_2 surface and NH_3 τ_r decreases till 20-30 sec.

5. CONCLUSIONS

Using the thermal annealing it can be changed purposely the electrical and gas-sensitive properties of Pd-SiO₂-Si diodes. Silicon MOS-diodes with annealed at 200°C possess sensitivity to H₂ and NH₃. Response values to these gases are about the same although H₂ response of such diodes is larger than NH₃ that. After annealing at 300°C and above NH₃ response decreases somewhat but simultaneously diode H₂ sensitivity disappears because of change of structure and chemical composition of Pd electrode. Thus using the thermal annealing it can be formed silicon MOS diodes selective to NH₃.

REFERENCES

- [1] V.I. Gaman, M.O. Duchenko, V.M. Kalygina, Influence of hydrogen on voltage-current and voltage-capacitance characteristics of MIS silicon tunnel diodes, *Russian Physics J.* 42 (1999) 777–785.
- [2] V.I. Gaman, V.M. Kalygina, Time dependence of the capacitance of f MOS under the influence of hydrogen, *Russian Phys. J.* 46 (2003) 329–341.
- [3] V.I. Balyuba, V.Y. Grisyk, T.A. Davydova, V.M. Kalygina, S.S. Nazarov, L.S. Khludkova, Ammonia sensors based on Pd-n-Si Diodes, *Phys. Tech. Semicon.* 39 (2005) 285-288.
- [4] M. Löfdahl, C. Utaiwasin, A. Carlsson, I. Lundström, M. Erikson, Gas response dependence on gate metal morphology of field effect devises, *Sens. Actuators B* 80 (2001) 183–192.

New Photovoltaic Gamma and X-Ray Detector

G.I. Ayzenshtat¹, M.D. Vilisova¹, E.P. Drugova¹, D.Y. Mokeev^{2*},
L.P. Porokhovnichenko¹, V.A. Chubirko¹

¹*JSC Scientific Research Institution of Semiconductor Devices,
634034 Tomsk, Russia*

²*Siberian Physico-Technical Institute, 634050 Tomsk, Russia,
mkl@pochta.ru

Abstract — Detectors based on epitaxial gallium arsenide grown from the gas phase are investigated. Two types of structures are studied: 1 - with a not doped active layer ($n \leq 10^{13} \text{ cm}^{-3}$), 2 - with the active layer compensated by chromium. It is shown that both types of structures operates in photovoltaical mode that allows to remove the drain current. Structures may be used as detectors of gamma radiation. Detectors have 100 % efficiency of charge collection.

Index Terms — VPE GaAs; photovoltaic; X-Ray; radiation detector

1. INTRODUCTION

The problem of creation of solid-state detectors with most high efficiency of ionizing particles registration is especially actual for digital X-Ray devices with small radiation doses of patients. In many papers it is shown that detectors based on gallium arsenide have high efficiency of the gamma quantum registration [1]. The main restriction factor for a wide introduction of the gallium arsenide detectors is relatively high density of dark current in the coordinate detector channels. For design of coordinate detectors based on the gallium arsenide, in paper [2] it is offered to use the photovoltaical mode, when transformation of charge formed by gamma quanta into electrical signal carried out at zero bias (thus a zero current also).

The purpose of the present investigation is study of different types of the instrument structures for possibility of their use as the detectors working in photovoltaical mode.

The present paper is limited by measurement of the amplitude spectrum of detector which uniquely characterizes parameters of detector, and allows to estimate its most important characteristics.

2. STRUCTURES

Two p-i-n-structure detectors were investigated:

1. Structure on the epitaxial no doped layer of gallium arsenide with extreme low concentration of equilibrium electrons as an active i-layer;
2. Structure on the epitaxial doped layer of gallium arsenide, compensated by chromium during high-temperature diffusion as an active i-layer.

Both detector structures were grown by the gas epitaxy method in chloride system. Structures of the first type were not doped specially. Concentration of the free electrons in active area, measured by C-V-method consists of 10^{12} cm^{-3} , and thickness of the active area was 40 microns.

Structures with half-insulating active area, compensated during high-temperature diffusion originally also were grown by the gas epitaxy method and doped by sulfur. Resisitivity of such structures was about 10^9 Ohm*cm .

3. EXPERIMENTAL RESULTS

For revealing differences between structures 1 and 2 as detectors of the low-energy X-Ray radiation we shall consider their amplitude spectrum received from a source ^{241}Am .

On fig. 1 the amplitude spectrum for structure 1 are shown. Analysis of these spectrums shows the following.

1. The detectors based on the "clean" layers are efficient in photovoltaical mode as we see signal 13.9 keV and 59.5 keV gamma quanta different from zero.
2. The spectrum form and position of characteristic peaks at $U_{\text{bias}}=0\text{V}$ testify collection only one components of a charge – electrons.
3. At inverse bias the contribution of hole components grows, and efficiency of the charge collection becomes equal 100%, and at $U_{\text{bias}}=-20 \text{ V}$ the detector shows spectrometer properties (there are peaks appropriate various γ -lines). Spectrum of structures 2 are submitted on fig. 2.

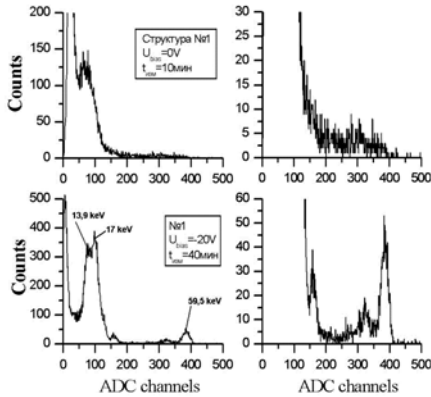


Fig 1. Amplitude spectrum received with ^{241}Am source for structure № 1

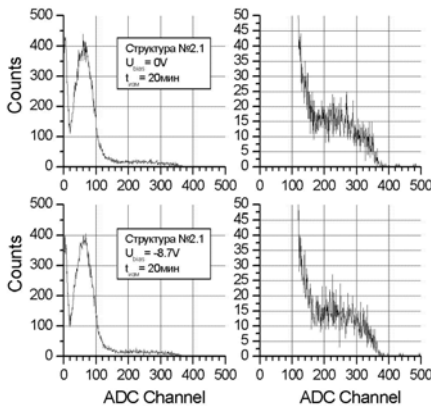


Fig 2. Amplitude spectrum received with ^{241}Am source for structure №2

From fig. 2, amplitude spectrum of epitaxial structures compensated by chromium is practically indiscernible in processes of diffusion and epitaxial growth. Both structures perfectly work in photovoltaical mode. Distinctive particularity of spectrum is that they are not deformed with increase of electrical field intensity. This fact is consequence of two circumstances.

1. In the structures compensated by chromium electrons are collected only [3].

2. Even at zero bias electrons have the life time exceeded drift time. Comparing spectrums of three types of structures it is possible to see that at zero bias they are extremely close on parameters. It means that clean material may be practically replaced to the compensated material

(it is known that growing of material with concentration less 10^{12} cm^{-3} is the difficult technological problem).

4. CONCLUSIONS

1. It is shown that "clean" epitaxial structures of thickness 40 nm at zero displacement effectively collect only electron charge.

2. Detectors from "clean" gallium arsenide, working in photovoltaical mode may be successfully replaced to detectors from epitaxial material compensated by chromium.

3. The detector structures received at introduction chromium in the epitaxy process or diffusions are practically indistinguishable by the amplitude spectrum form. Note that the possibility of working of such structures in photovoltaical mode is shown in the present paper for the first time.

ACKNOWLEDGEMENTS

This work was financially supported by the Russian Federation Ministry of Education, Project No. 63382.

REFERENCES

- [1] D.S. McGregor, H. Hermon, "Room-temperature compound semiconductor radiation detectors" Nucl. Instr. and Meth. A 395 (1997) 101.
- [2] R.A. Akhmadulin, V.F. Dvorjankin, G.G. Dvorjankina et al. –Letters in JTF. 2002. Vol. 26, no. 1, pp. 34-38.
- [3] G.I. Ayzenshtat et al. GaAs as a material for particle detectors. – Nucl. Instr. and Meth. A 494 (2002) 199.

The Detected Block for Systems of Nondestroying Testing Based on the GaAs Detectors

I.I. Nadreev¹, S.V. Kasyanov², S.A. Ryabkov¹,
O.P. Tolbanov³, A.V. Tyazhev³

¹RID Ltd, Studencheskaya St. 10b-1, 634034, Tomsk, Russia

²Introscope Institute at TPU, 3, Savinikh St., 634028, Tomsk, Russia

³Siberian Physics-Technical Institute, 1, Novo-Sobornaya Sq., Tomsk,
634050, Russia

Abstract — In the paper, results of development and preliminary tests of the detector block on the basis of microstrip GaAs detectors for nondestroying testing systems are submitted. The detecting block has the module design with possibility of expansion to 2560 channels at the scanning frequency 200 Hz. The special software is developed, allowing to carry out both the visual testing in real time, and adjustment of brightness and contrast of X-Ray images.

Index Terms — nondestroying testing, detector block, gallium arsenide

INTRODUCTION

In papers [1, 2] it was shown that high resistance GaAs is one of the perspective material for manufacture of semiconductor detectors of X-ray radiation for modern X-Ray diagnostic systems. However, the use of these detectors in the applied purposes requires additional studies in the field of development of constructive-technological requirements to design of the detector block and structure of multichannel systems of data mining.

The purpose of this study was development of the nondestroying testing system prototype based on GaAs detectors of X-Ray radiation and realization of preliminary tests for determination of the technical characteristics of similar systems.

RESULTS

The block diagram of the device is given on fig. 1. The detectors device consists of 7th detector modules (DM). The DM consists of GaAs microstrip detectors device on 64 channels and the specialized microcircuit (integrator - multiplexer). This microcircuit integrates a charge collected on each of 64 channels of the detector and multiplexing signal on the data mining card. From the card the digital signal with collected information transfer to the interface card. In turn, the interface card controls the data mining card, preliminary accumulation and formation of packages, as well as connection with computer with specialized interface PCI card.

GaAs detectors with common length of 54 cm is the basis of the developed device. A step of detector channels is 1.2 mm. Thickness of the sensitive detector layer is 0.5 mm. Detectors are located that the radiation direction coincided with a plane of detectors. The use of GaAs-detectors permits to carry out direct transformation of energy of X-Ray

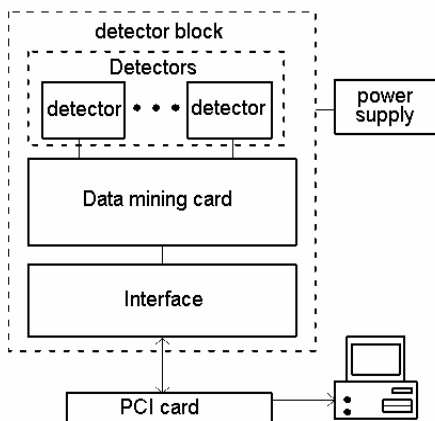
quanta to a charge what increases efficiency of charge collection in comparison with solid-state detectors of kind "scintillator - photodiode".

For minimization of influence of slowly varying detector parameters (the dark current) and other external factors the following technical decisions are realized: multiplexers with double correlated sample and pulsed radiator are used, the detector

thermostabilization system on the basis of elements Peltier is designed. Besides, for dark current influence reduction, the synchronous operation of radiator and receiver is realized.

The digital part of the device consists of two parts: one is based on DB together with detectors, second - is direct in the computer (PCI-adapter). Between them the consecutive synchronous interface is designed, with confirmation of data delivery what provides the data transmission via "twisted pair" cable on distance up to 100 m. The developed device provides the information collection and transfer to

Fig 1. The detector block



computer from the detector 448 channels from γ -radiation in real time that allows to carrying out the continuous control of objects.

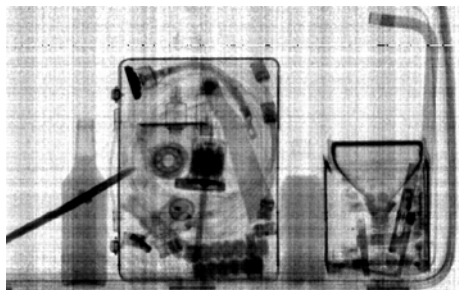


Fig 2. X-Ray image of the test objects

Tests of system with use of a pulse X-Ray source were carried out. Frequency was 200 Hz, the pulse duration was 5 mks, energy was 7.5 MeV, power of expositional dose in a plane of front DB wall was 280 mP/min). On fig. 2 the initial image (without preprocessing) the test objects, received with DB is submitted.

CONCLUSIONS

Thereby, the prototype of the modular detecting block with possibility of expansion up to 2560 channels (3 m) at frequency of scanning 200 Hz was developed. The device may be used for nondestroying testing of various objects with the spatial permit up to 1 mm. The special software has been developed, allowing to carry out both the visual testing in the real time, and adjustment of brightness and contrast of X-Ray images.

REFERENCES

- [1] G.I. Ayzenshtat, M.V. Ardyshev, D.L. Budnitsky, S.S. Khludkov, O.B. Koretskaya, V.A. Novikov, L.S. Okaevich, A.I. Potapov, O.P. Tolbanov, A.V. Tyazhev, A.P. Vorobiev. "Gallium arsenide structures for ionizing particles detectors". Proceedings of the 3rd Int. Workshop on Radiation Imaging Detectors (Orosei, Sardinia, Italy, September 23-27, 2001). Nuclear Instruments and Methods in Physics Research, Section A 487 (2001), pp. 96-101.
- [2] G.I. Ayzenshtat, M.V. Ardyshev, D.L. Budnitsky, S.S. Khludkov, O.B. Koretskaya, V.A. Novikov, L.S. Okaevich, A.I. Potapov, O.P. Tolbanov, A.V. Tyazhev, A.P. Vorobiev. "GaAs detectors for medical imaging". Proceedings of the 4nd Int. Workshop on Radiation Imaging Detectors (NIKHEF, Amsterdam, September 18-

12, 2002). Nuclear Instruments and Methods in Physics Research, Section A 509 (2003), pp. 268–273.

Estimation of GaAs Detector System Characteristics for Low Dose Mammography

M. V. Bimatov¹, I. Ph. Nam², A.V. Tyazhev³

¹*Tomsk State University*

²*Tomsk Polytechnic University*

³*Siberian Physicotechnical University*

Abstract — A digital detecting module for mammography system based on GaAs strip detectors is being developed. The high atomic number makes the GaAs a very efficient material for low energy X-rays detection (10–30 keV is the typical energy range used in mammography). Low contrast details can be detected with a significant dose reduction to the patient. The detecting module parameters have been calculated by using the characteristics of standard mammographic tube. The results will be presented and compared with radiographs obtained with traditional film/screen systems. The results of the modeling will be shown.

Index Terms — mammography, digital detector, GaAs

INTRODUCTION

Breast cancer is a major problem in disease prevention. It is foreseen that the yearly increment of cases since year 2000 will be around one million [1]. Mammographic screening programs rely consequently on an efficient early diagnosis. It is expected that such a diagnosis can reduce mortality by 30-40% for ages above 50. The research in mammography aims at an improvement of image quality, which brings over higher sensitivity and specificity in the diagnosis, together with a sensible reduction of the dose, which will favour the extension of the screening to ages below 50.

One of the most promising approaches to this problem is a mammographic imaging system based on GaAs detectors [2]. This detector features high detection efficiency, namely 98% compared to 60% of the conventional film (at the typical 20 keV mammography X-ray energy). It allows the detection of very low contrast ($\leq 3\%$) details with a high precision. The detection of such low contrast structures is the sole weapon to spot early tumoral mass formation, before they evolve in denser cancerous calcifications.

RESULTS

In Fig.1 the efficiencies for 300 μm of Si, CdZnTe and GaAs are plotted. The efficiency for silicon drops fast and is low already at 20 keV, but for high-Z materials the drop is less. To obtain high detection efficiency it is necessary to use GaAs, CdZnTe or another high-Z material.

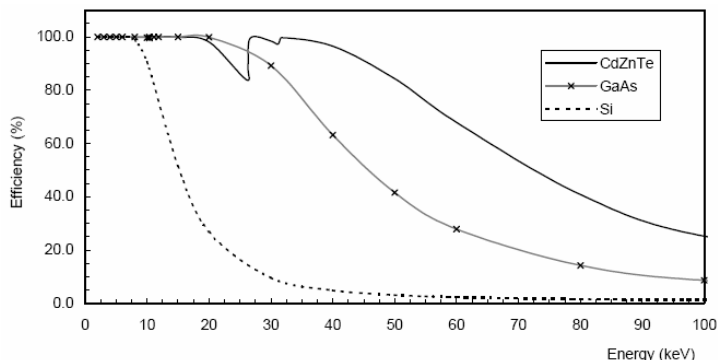


Fig. 1. The photon detection efficiency for 300 μm of Si, GaAs and CdZnTe plotted for the energy range from 2 to 100 keV. Data on linear attenuation coefficients comes from NIST[4]

For photons of a specific energy E , the Beer-Lambertian law (derived in any standard textbook describing interactions of radiation with matter) allows us to calculate the expected number of photons transmitted through different materials I , given I_0 incident photons. It says that the intensity of photons with a given energy decays exponentially into a material, and provides in our case:

$$I = I_0 \cdot \exp(\mu(E) \cdot x), \quad (1)$$

where $\mu(E)$ is the material dependent linear attenuation coefficient (proportional to the interaction cross-section) and x is the material thickness which was taken according to Fig2. The linear mass attenuation coefficients were obtained from a photon cross section database (XCOM) provided by the US National Institute of Standards and Technology [4] (NIST). From the equation (1) we obtained that even 30 keV photons are absorbed in 1.5 mm detector length as shown in Fig.3.

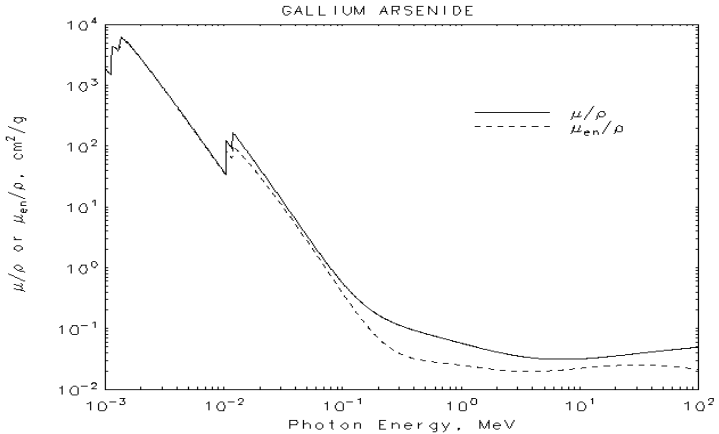


Fig. 2. X-Ray Mass Attenuation Coefficients for GaAs

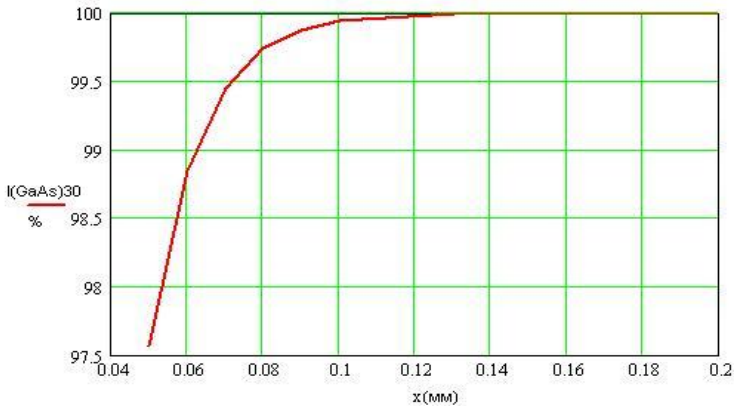


Fig.3. The photon detection efficiency for GaAs for the detector length range from 0.5 to 0.2 mm

The spatial resolution is in the scan direction limited by the detector pitch in the perpendicular direction. Suitable dimension is $100 \mu\text{m}$. GaAs line detector array has a pitch – $110 \mu\text{m}$. Each detector channel is decided to have cross section equal to $(40 \times 100) \mu\text{m}^2$, length – 1.5 mm .

The dynamic range (DR) and minimal patient dose (D) was also calculated for bulk and epitaxial GaAs detectors according to Blinov's methods. [5] It should be noted that standard parameters of x-ray tube and an integral mode of readout electronic were taken during calculations.

The minimal dose is dose when digital diagnostic system can identify in the image details with 1% contrast.

Contrast (C) is:

$$C = \frac{I_{background} - I_{spot}}{I_{background}} \cdot 100\%, \quad (2)$$

where $I_{background}$ and I_{spot} are intensities of radiation, transmitted through background area and spot area relatively.

The dynamic range is the ratio of maximum detector input radiation intensity to minimum detector input radiation intensity and digital diagnostic system must recognize test-objects with 5% contrast [5].

The criterion of recognition is:

$$(\langle \text{output signal of background} \rangle - \langle \text{output signal of spot} \rangle) > 2\Delta 90\% \quad (3)$$

i.e., the mean levels difference of output signals must be bigger than noise. It was obtained that the dose for bulk detectors is equal to 17 μGr and DR = 86 dB. For epitaxial detectors D=28 μGr , DR=90 dB.

CONCLUSION

In this paper, we obtained suitable dimension and material of detectors for mammography based on mathematical calculations. Moreover, we have got a minimal patient dose and dynamic range of digital diagnostic system operating in an integral mode. This data shows that it would be better to use epitaxial GaAs detectors for mammography applications due to a wide dynamic range and patient dose approximately 100 times lower than in other modern apparatus. The future experiments can prove or define our calculations more accurately.

The work was financially supported by RFBR Projects No. 04-02-17486.

REFERENCES

- [1] American Cancer Society, "Cancer Facts and Figures 1994", American Cancer Society, Atlanta, GA, 1994.
- [2] S.R. Amendolia, M.G. Bisogni, M. Campbell, A. Cola, S. D'Auria, C. Da Vi'a, E.H.M. Heijne, M.E. Fantacci, V. O'Shea, V. Rosso, K. Smith, L. Vasanelli, "Experimental Study of LEC GaAs Detectors for X-ray Digital Radiography". Nucl. Instr. and Meth, A380, 1996, pp. 410-413.

- [3] Akhmadullin et al., "Photovoltaic X-ray Detectors Based on Epitaxial GaAs Structures". *Pisma v GTF*. 2002. V. 28, I.1. pp. 34–37 (in Russian).
- [4] J. H. Siewersen, L.E. Antonuk, Y. Yorkston et al., "Signal, noise power spectrum, and detective quantum efficiency of indirect-detection flat – panel imagers for diagnostic radiology". *Med. Phys.*, 1998, vol. 25, no. 5, pp. 614–628.
- [5] N.N. Blinov, B.I. Leonova. "X-ray Diagnostic Apparatus". V. 1. Moscow, VNIIMT, NPO «Ekran», 2001. – 220 p.

Detector Structures Based on Epitaxial Gallium Arsenide Compensated by Chromium

M.D. Vilisova¹, O.P. Tolbanov¹, D.Y. Mokeev¹, E.P. Drugova²,
V.A. Chubirko², L.P. Porokhovnichenko², I.V. Ponomarev^{3*}

¹*Siberian Physicotechnical Institute, Tomsk, Russia*

²*Scientific and Production State Interprize "Semiconductor Devices Research Institute", Tomsk, Russia*

³*Tomsk State University, Tomsk, Russia*

*spti@pochta.ru

Abstract — Detector structures based on VPE GaAs layers, compensated by Cr at diffusion process, have been studied at present article. Detectors were with active region both n-type and π -type. It was shown, that at structures based on n-type layers width of space charge region depends on applied reverse bias. And charge collection efficiency from α -particles increased with bias. In structures based on π -type layers such dependence is particularly absent and charge collection efficiency is not changed. Both types of structures has high charge collection efficiency from γ -irradiation. At applied bias in structures based on n-type layers at the process of charge collection takes part not only electrons but also holes.

Index Terms — GaAs, detector, charge collection efficiency

1. INTRODUCTION

As was shown earlier, detectors prepared on pure (undoped) epitaxial layers of GaAs have high charge collection efficiency and can operate in photovoltaical conditions [1-3]. Low repeatability in producing of epitaxial layers with low free carrier concentration ($n < 10^{13} \text{ cm}^{-3}$) is the main difficulty of using undoped epitaxial GaAs for detectors. At this article we have investigated detector structures based on GaAs, compensated by chromium.

2. EXPERIMENTS AND RESULTS

Epitaxial GaAs structures were grown on high doped n^+ -substrates in Ga-AsCl₃-H₂ system and consisted of n^+ -buffer layer, active n-layer, doped by S ($n=5 \cdot 10^{14} - 10^{16} \text{ cm}^{-3}$) and front p^+ -layer. Active n-layer was

doped by chromium at the diffusion process and diffusion regime (temperature, time of diffusion) was varied at wide range. Ohmic contact was made by evaporating of thin Ni-Cr films upon rear p^+ -layer and substrate. Electrophysical parameters were measured by means of electrolytic profiler, spreading resistance technique and volt-capacitance (C-V) characteristics. C-V measurements were carried out on different frequencies (10^2 – 10^6 Hz).

Carried out investigations has shown that, resistivity of active layer and profile of free carrier concentration on it could be varied at wide-ranging by changing of diffusion parameters. As a result we obtained a layers both n-type with low free carrier concentration ($n \leq 10^{12} \text{ cm}^{-3}$) – I type structures, and high resistive π -layers with resistance $\rho \approx (3 \cdot 10^7 - 2 \cdot 10^8) \text{ cm}^{-3}$ – II type structures. Capacitance, width of space-charge region (SCR) and amplitude spectra of detectors was changed correspondingly.

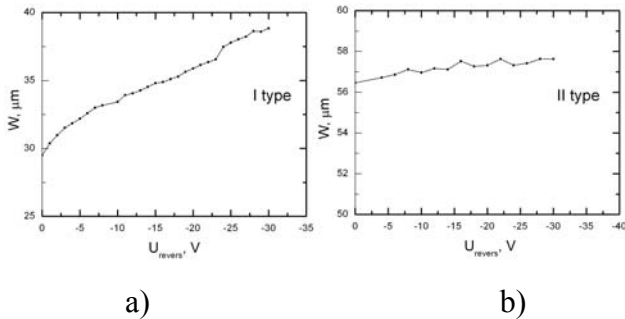


Fig. 1. Dependences of width of SCR (W) from applied reverse bias (U_{reverse})

It was obtained dependence of capacitance from frequency and applied reverse bias for structures of I type. Width of SCR also depended on applied bias and expanded with increasing bias (fig. 1a). However, capacitance of structures of II type were small depended on applied bias as well as width of SCR and equaled width of active layer (fig 1b).

The width of SCR was estimated from C-V-measurements by using following equation:

$$W = \frac{\varepsilon_a \cdot \varepsilon_0 \cdot S}{C},$$

where ϵ_a is permittivity of GaAs, ϵ is permittivity, S is detector area and C is capacitance of detector.

Dependences of charge collection efficiency after α -particles irradiation from ^{241}Am source (CCE_α) and width of active region (d_{active}) on applied reverse bias is represented in fig. 2. The width of active layer was estimated from amplitude spectra obtained after influence β radiation from ^{90}Sn source.

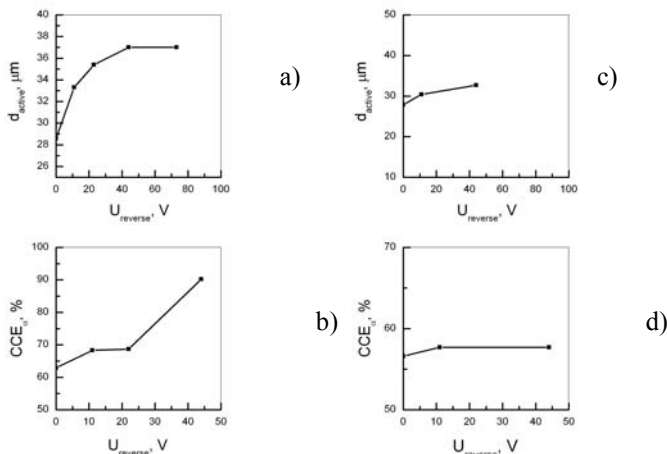
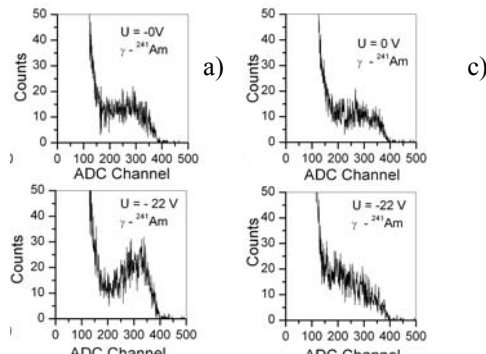


Fig. 2. Dependences of d_{active} and CCE_α from applied bias

In structures of I type CCE_α and d_{active} (fig. 2a,b) distinctly increases in accordance to applied reverse bias unlike for structures of II type. Where this parameters as a width of SCR (fig. 2c,d) is low depended on bias.

Measurements of amplitude spectrums after influence γ -radiation from ^{241}Am -source have shown that structures of both type, have high charge collection efficiency ($\sim 90\%$) at zero bias (fig.3a,c). But differences between amplitude spectrums at applied bias (-22 V) consists in peaks about 300 channel for structures of I type (fig.3b,d). It is usually observed in “pure” (undoped) GaAs layers and means what holes participated in charge collection.



b)

d)

Fig. 3. Amplitude spectrums after influence γ -radiation

It is follows from obtained results, what detectors based on compensated by chromium epitaxial layers operates with high charge collection efficiency without applied bias. And detectors characteristics can be changed by varying of compensation level.

REFERENCES

- [1] R.A Ahmadyllin, V.F Dvoriankin, G.G. Dvoriankina et al “Photovoltaical X-ray detectors based on epitaxial gallium arsenide”. TPL, 2002. V. 28, P. 34–37.
- [2] G.I. Ayzenshtat, M.D. Vilisova, D.Y. Mokeev et al. “Investigation of detectors of ionization irradiation based on gallium arsenide”. V Workshop of young scientists “Modern problems in physics, technology and innovation evolution”. Tomsk 2004, pp. 100–102.
- [3] Ayzenshtat G.I., Vilisova M.D., Drugova E.P. et al. “X-ray detectors based on epitaxial gallium arsenide” TPL (to be published).

Gamma Quantum and Alpha Particle Counters Based on GaAs Detectors

M.A. Rozhnev, S.A. Ryabkov, D.Yu. Mokeev, A.V. Tyazhev,
A.N. Zarubin

*Siberian Physics-Technical Institute,
1, Novo-Sobornaya Sq., Tomsk, 634050, Russia*

Abstract — In the paper, results of development and preliminary tests for counters of the gamma quantum and α -particles using the detectors on GaAs, compensated by Cr are presented. It is shown that GaAs detectors allows to create high-speed and selective ionizing radiation counters. It is founded that radiating stability of GaAs detectors exceeds 5 MRad and 50 MRad at irradiation by protons ($E_p = 1\text{GeV}$) and gamma quanta ($E_\gamma = 1\text{MeV}$), accordingly.

Index Terms — gamma quantum, alpha particle, GaAs, detector, counter.

STATE-OF-ART

High-resistance GaAs compensated by Cr, is one of the most perspective material for production of the semiconductor X-Ray detector for design of monitoring systems of ionizing radiation testing [1,2]. However, use of these detectors in the applied purposes requires an additional studying of such questions as: radiating stability of devices, speed, and ability to work in the background radiating fields.

STATEMENT OF THE PROBLEM AND PURPOSE

The purpose of paper is creation and study of characteristics of the pilot models for counters of the gamma of quantum and α -particles using the GaAs detectors for testing the technological processes of nucleus fuel conversion.

The main problems were following.

- To carry out measurement of pulse characteristics from the bias voltage at the impact on the detector structures the α -particles (5.5 MeV, ^{241}Am).

- To carry out estimation for parameters of gamma radiation detectors from viewpoint of optimum selectivity of the quantum account with energy (60-100) keV in relation to quanta with the energy 1 MeV.
- To develop the pilot models of counters and to investigate a study their technical characteristics.

DESCRIPTION OF RESEARCH OBJECT

As experimental samples the pad GaAs detectors with the sizes $3 \times 3 \text{ mm}^2$ and $10 \times 10 \text{ mm}^2$ with thickness of sensitive area (d) 40 mkm and 300 mkm accordingly were used. Irradiation of the detector by α -particles was carried out through the metallic contact. Polarity of the bias voltage on the detector was corresponded to drift only electronic components of a charge. The signal from the detector was amplified by amplifier with passband $F=1 \text{ GHz}$, gain $K=21 \text{ dB}$ and recorded by a digital oscillograph Tektronix 3552 with passband $F=500 \text{ MHz}$. The experiment circuit is submitted on fig. 1.

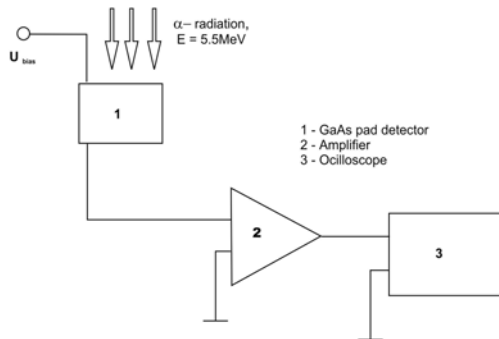


Fig 1. The experiment diagram

RESULTS AND THEIR USE

On fig. 2 the pulse characteristics are submitted vs bias voltage on the detector with thickness of sensitive area $d=300 \text{ mkm}$.

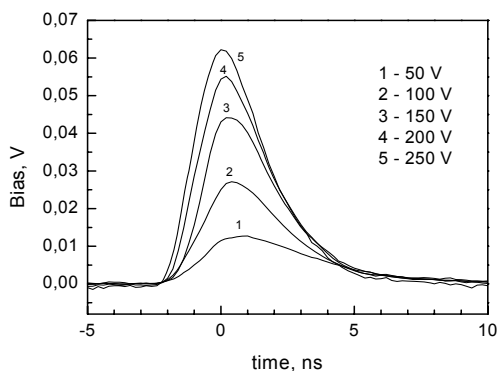


Fig 2. The pulse characteristics vs bias on detector

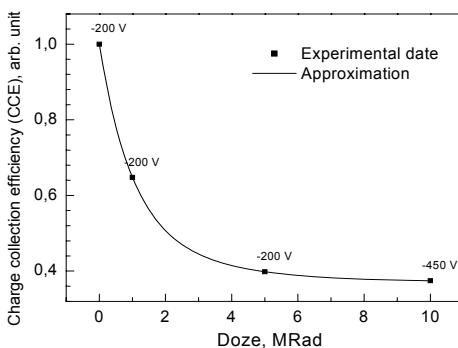


Fig 3. Radiating stability of the GaAs detectors at the proton impact

Analysis of the pulse current form (fig. 2) allows to draw a conclusion that at use of the detector with $d = 40$ mkm and area 0.01 cm², the design of the counter of α -particles is possible with speed not worse than 10^8 pulse/sec.

Studies of radiating stability of GaAs detectors at protons impact ($E_p = 1$ GeV) and gamma quanta ($E_\gamma = 1$ MeV) were carried out in IFVE, Protvino. Results are submitted on fig. 3. Analysis of fig. 3 shows that radiation stability of GaAs detectors is 5 Mrad. At impact of gamma quanta ($E_\gamma = 1$ MeV) the radiating stability exceeds 50 Mrad.

On the basis of the received results the pilot models of counters of the α -particles and gamma quanta within the energy range (40 – 120) keV were developed. One of application requirements of the gamma quantum counters is selectivity in relation to background radiation with energy 1 MeV. Given selectivity (K) was provided by a choice of the appropriate thickness and sensitive area of the GaAs detector. The carried out calculations have shown that for ensuring of selectivity $K \geq 10$ and stable work of the device it is necessary to use detectors with parameters: $d = (250-300)$ mkm, $S \leq 2$ cm². The laboratory tests were carried out for checking of counters. The testing technique of the α -counter consist in comparison of results of measurements of the α -particles quantity registered by the counter, with quantity of the particles registered by a etalon spectrometer complex "Kamak" on an equal conditions. The pulse quantity for 300 sec is:

α -counter: 14172 +/-2616;

"Kamak": 12842 +/-2911;

It is visible that quantity of the alpha particles measured by a dosimeter and the etalon "Kamak" are in same range.

The testing technique of the gamma quantum counter consist in measurement and comparison of absorption factors (k) of gamma radiation ($E_\gamma = 122$ KeV) of GaAs plates with use both complex "Kamak" and gamma counter. Results of test are:

α -counter: $k = 1,083\text{cm}^{-1}$;

"Kamak": $k = 2,344\text{cm}^{-1}$;

Divergences in absorption factor, probably, are caused by difference in minimum energy of quanta, under which account is begun. For Kamak complex this value is 5 keV, and for the α -counter – 30keV.

Thereby, it is shown that use of GaAs detectors allows to create the ionizing radiation counters with the account speed up to 10^8 pulse/sec and the radiating stability to the gamma radiation, exceeding 50 MRad.

REFERENCES

- [1] G.I. Ayzenshtat, M.V. Ardyshev, D.L. Budnitsky, S.S. Khludkov, O.B. Koretskaya, V.A. Novikov, L.S. Okaevich, A.I. Potapov, O.P. Tolbanov, A.V. Tyazhev, A.P. Vorobiev. "Gallium arsenide structures for ionizing particles detectors". Proceedings of the 3rd Int. Workshop on Radiation Imaging Detectors (Orsei, Sardinia, Italy, September 23-27, 2001). Nuclear Instruments & Methods in Physics Research, Section A 487 (2001), pp. 96–101.
- [2] G.I. Ayzenshtat, M.V. Ardyshev, D.L. Budnitsky, S.S. Khludkov, O.B. Koretskaya, V.A. Novikov, L.S. Okaevich, A.I. Potapov,

O.P. Tolbanov, A.V. Tyazhev, A.P. Vorobiev, "GaAs detectors for medical imaging". Proceedings of the 4nd Int. Workshop on Radiation Imaging Detectors (NIKHEF, Amsterdam, September 18-12, 2002). Nuclear Instruments & Methods in Physics Research, Section A 509 (2003), pp. 268-273.

Impulse Response of GaAs Radiation Imaging Detectors

A.V. Tyazhev, R.A. Ryzhov

*Siberian Physics-Technical Institute, 1, Novo-Sobornaya Sq., Tomsk,
634050, Russia*

Abstract — In the paper, the pulse characteristics of the detector structures based on GaAs, compensated by Cr are submitted at impact of alpha particles with energy 5.5 MeV from a source ^{241}Am . Based on analysis of experimental data it is established that under condition of homogeneous distribution of electric field intensity (E) in the detector and value $E \leq 3$ kV/cm, the pulse characteristic may be described within the framework of the PNTNOZ theory. It is shown that the offered technique can be used for evaluation of distribution uniformity of electric field intensity on the detector thickness and in some cases, for determination of electrophysical parameters of the detector material.

Index Terms — ionizing radiation, GaAs, imaging detector, pulse response

BACKGROUND

High-resistance GaAs is the most perspective material for production of semiconductor detectors of X-Ray used at creation the low dose X-Ray diagnostic systems. In works [1,2] it was shown that GaAs compensated by Cr, has higher efficiency of the charge collection, in comparison with LEC SI GaAs. However, there are no data on model of nonequilibrium charge carriers in the detector structures based on GaAs, compensated by Cr, as cause statement of the given study.

PROBLEM AND PURPOSE

The purpose of this study is a substantiation of applicability of PNTNOZ theory to the description of pulse characteristics of the detector structures based on GaAs compensated by Cr. There are following problems in this study.

- To carry out measurements of pulse characteristics from the bias voltage at impact of alpha particles (5.5 MeV, ^{241}Am) on detector structures.

- To carry out a qualitative and quantitative evaluation of the experimental data within the framework of PTNOZ and PTOOZ theories.

THE RESEARCH OBJECT

As experimental samples the pad GaAs detectors with the sizes $3 \times 3 \text{ mm}^2$ and thickness of sensitive area $d=400 \text{ nm}$ were used. Detectors had structure M-i-M where i-as area served high-resistance GaAs, compensated by Cr and metallic contact were made by the thermal evaporation in vacuum. Irradiation of the detector by α -particles was carried out through metallic contact. Polarity of the detector bias voltage corresponded to drift only electronic components of a charge. Amplifier with passband $F = 1 \text{ GHz}$ and gain $K=21 \text{ dB}$ was amplified a signal from the detector, which follows to the digital oscillograph Tektronix 3552 with passband $F = 500 \text{ MHz}$. The experiment circuit is submitted on fig. 1.

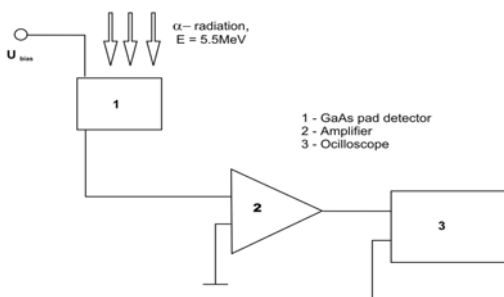


Fig 1. Experiment diagram

RESULTS AND THEIR APPLICATION

On fig. 2 the pulse characteristics are submitted on the detector bias voltage. According to [3], realization of mode PTNOZ or PTOOZ cause the following dependences:

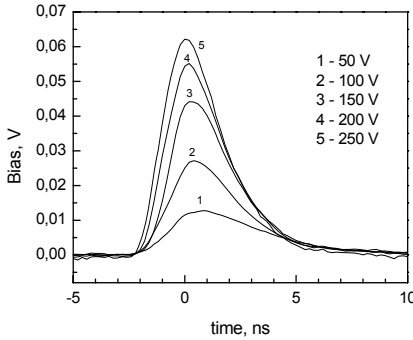


Fig 2. The pulse characteristics vs the detector bias voltage

- TNOOZ ("small signal" mode)
 - $Q \ll C \cdot U_{bias}$,

where Q is the nonequilibrium carrier charge generated by α -particle, C is capacity of the detector at U_{bias} voltage.

- $I(0) \sim U_{bias}$, where $I(0)$ is the current amplitude at the initial time, at electrical field intensity in the detector $E \leq 3$ kV/cm.
- $t_{dr} \sim 1/U_{bias}$, where t_{dr} is drift time of the charge carriers, in this case electrons through i-an detector area.
- TOOZ ("big signal" mode)
 - $Q \gg C \cdot U_{bias}$, where Q is the nonequilibrium carrier charge generated by α -particle, C is capacity of the detector at U_{bias} voltage.
 - $I(t_1) = I_{max} \sim U_{bias}^2$, where $I(t_1)$ is the current amplitude at the time t_1 , at electrical field intensity in the detector $E \leq 3$ kV/cm.
 - $t_1 \approx 0.8 \cdot t_{dr} \sim 1/U_{bias}$, where t_1 is drift time of the charge carriers, in this case electrons through i-an detector area.

Analysis of the pulse current form (fig. 2) and dependence of maximum current vs bias voltage presented on fig. 3, allows to draw a conclusion on TNOOZ mode realization. Comparison of the experimental data with the accounted maximum current (table 1) serves additional confirmation.

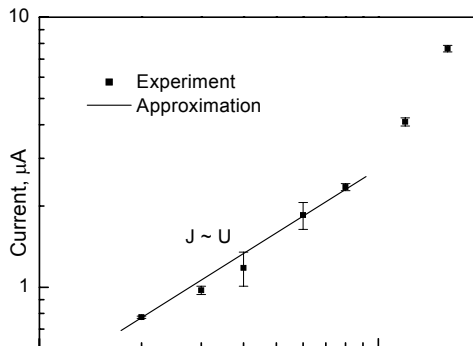


Fig 3. Maximum current in pulse mode vs bias voltage

Table 1. Comparison of the maximal current in pulse

Intensity of electric field E, kV/cm	Experimental values J(0), mkA	Counted values (TNOOZ) J (0), mkA	Counted values (TOOZ) J (t _i), mkA
0.75	1	0.3	2.4*10 ⁻⁴
1	1.3	0.4	3*10 ⁻⁴
1.5	2	0.8	5*10 ⁻⁴
2	2.3	1.3	6.3*10 ⁻⁴

According to TNOOZ model [3], drift time t_{dr} through the detector i-area is expressed by:

$$t_{dr} = \frac{d^2}{\mu_n \cdot U_{bias}}, \quad (1)$$

where μ_n is the electron mobility.

Estimations of size μ_n at $E \approx 2$ kV/cm, carried out in conformity with the formula (1) give value $\mu_n \approx 2000$ cm²/V·s, that is closed to values μ_n for these detectors, received from Holl measurements and the amplitude spectrum analysis.

Thus, it is established that the pulse characteristics of the detector structures correspond to PNT0Z at the electric field intensity in detector $E \leq 4$ kV/cm. It is shown that pulse characteristics may be used for evaluation of the nonequilibrium charge carriers mobility in the detector structures based on GaAs, compensated by Cr.

REFERENCES

- [1] G.I. Ayzenshtat, M.V. Ardyshev, D.L. Budnitsky, S.S. Khludkov, O.B. Koretskaya, V.A. Novikov, L.S. Okaevich, A.I. Potapov, O.P. Tolbanov, A.V. Tyazhev, A.P. Vorobiev. "Gallium arsenide structures for ionizing particles detectors". Proceedings of the 3rd Int. Workshop on Radiation Imaging Detectors (Orosei, Sardinia, Italy, September 23-27, 2001). Nuclear Instruments & Methods in Physics Research, Section A 487 (2001), pp. 96-101.

- [2] G.I. Ayzenshtat, M.V. Ardyshev, D.L. Budnitsky, S.S. Khludkov, O.B. Koretskaya, V.A. Novikov, L.S. Okaevich, A.I. Potapov, O.P. Tolbanov, A.V. Tyazhev, A.P. Vorobiev. "GaAs detectors for medical imaging". Proceedings of the 4nd Int. Workshop on Radiation Imaging Detectors (NIKHEF, Amsterdam, September 18-12, 2002). Nuclear Instruments & Methods in Physics Research, Section A 509 (2003), pp. 268-273.
- [3] A. Many, G. Rakavy, "Theory of transient space-charge limited current in solids in presence of trapping", Phys. Rev., 126, 1980–8 (1962).

Methods of Design Improvement of Balun Transformer with Additional Balancing Lines Using Microstrip Lines with Front Coupling

Sergey A. Goncharov, Valiriy I. Sedinin

*Siberia State University of Telecommunications and Informatics
86 Kirova St., Russia, Novosibirsk
Tel. (383-2) 66-02-86, E-mail sadfanat@ngs.ru*

Abstract — Methods of design improvement of balun transformer with additional balancing lines are considered in this paper. Calculation techniques for main characteristics of such devices are presented.

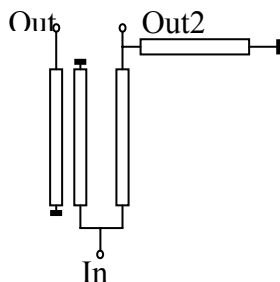
Index Terms — balun transformer, microstrip line, coupling

I. INTRODUCTION

While implementing multiplication schemes for extraction of even harmonics it is necessary to imply broadband balancing devices which makes changing symmetrical diode loads to asymmetrical load possible.

II. THEORY BACKGROUND

A balun transformer structure achieving the balance by using the additional balancing lines, given in [1], is presented in Fig.1. The balance is conditioned by the equality of characteristic impedance of additional balancing lines and coupling resistance of coupled strip lines. Such equality is hard to achieve in practice. A simulation has been conducted using MicroWave Office 2002 which showed that to achieve



such equality it is necessary to implement the 50 nm-gap between strips thus hardening development of such devices very much.

For achieving the balance of impedances (increasing coupled line characteristic impedance values) one

Fig.1. Balun transformer with additional balancing lines

can use microstrip lines with front coupling. Design of lines with front coupling is presented in Fig.2.

Processes in coupled microstrip line can be described by the following system of differential equations:

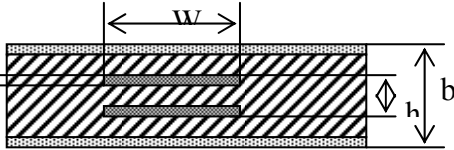


Fig.2. Strip lines with front coupling

$$\frac{\partial v_1}{\partial x} = -L \frac{\partial i_1}{\partial t} - M \frac{\partial i_2}{\partial t}; \quad \frac{\partial v_2}{\partial x} = -L \frac{\partial i_2}{\partial t} - M \frac{\partial i_1}{\partial t};$$

$$\frac{\partial i_1}{\partial x} = -C \frac{\partial v_1}{\partial t} + D \frac{\partial v_2}{\partial t}; \quad \frac{\partial i_2}{\partial x} = -C \frac{\partial v_2}{\partial t} + D \frac{\partial v_1}{\partial t}.$$

Introduced coefficients of linear inductance L and mutual inductance M , linear capacitance C and linear mutual capacitance D can be obtained using the presented above equations by calculations from [2]:

$$(L - M)l = \frac{La}{2}, \quad (L + M)l = 2L_s, \quad (C - D)l = 2Ca, \quad ,$$

$$(C + D)l = \frac{C_s}{2}, \quad L_s = C_s \frac{\rho_s^2}{4}, \quad L_a = C_a \frac{\rho_a^2}{4},$$

$$C_a = 0.4413 - H, \quad C_s = H \frac{W}{h},$$

where \mathcal{E} is dielectric constant of substrate, and H can be calculated as

$$H = \frac{\left(1 - \frac{h}{w}\right)lh \left(\frac{h}{w}\right) + \left(\frac{h}{w}\right) + lh \left(\frac{h}{w}\right)}{\pi \left(1 - \frac{h}{w}\right)}.$$

Solution of the presented above system is given below

$$\begin{aligned}
 u1 &= A_s e^{-i\beta_s x} + B_s e^{i\beta_s x} + A_a e^{-i\beta_a x} + B_a e^{i\beta_a x} \\
 u2 &= A_s \cdot e^{-i\beta_s x} + B_s \cdot e^{i\beta_s x} - A_a \cdot e^{-i\beta_a x} - B_a \cdot e^{i\beta_a x} \\
 i1 &= \frac{A_s}{\rho_s} e^{-i\beta_s x} - \frac{B_s}{\rho_s} e^{i\beta_s x} + \frac{A_a}{\rho_a} e^{-i\beta_a x} - \frac{B_a}{\rho_a} e^{i\beta_a x} \\
 i2 &= \frac{A_s}{\rho_s} e^{-i\beta_s x} - \frac{B_s}{\rho_s} e^{i\beta_s x} - \frac{A_a}{\rho_a} e^{-i\beta_a x} + \frac{B_a}{\rho_a} e^{i\beta_a x}, \text{ where}
 \end{aligned}$$

$$\beta_s = \varpi \sqrt{(C+D)(L+M)} = \frac{\varpi}{e} \sqrt{L_s C_s},$$

$$\beta_a = \varpi \sqrt{(C+D)(L-M)} = \frac{\varpi}{e} \sqrt{L_a C_a},$$

$$\rho_a = 59.952 \frac{\pi}{\frac{b\sqrt{\varepsilon}}{w} + C_a}, \quad \rho_s = 59.952 \frac{\pi}{\left[\frac{b}{w} \right] + \left[\frac{w}{h} \right] + C_s}.$$

In the latter expressions factor $\exp(i\varpi t)$ is omitted for simplicity.

Amplitudes of presented earlier current and voltage waves can be obtained from initial conditions at the line edges. For simplification of calculations let us present given section of transformer by quadruple with weight coefficients being known [3]. Balancing lines in their turn can be presented by cascaded quadruples with known A-parameters [4]

$$A = \begin{matrix} \cos \Theta & j\rho \sin \Theta \\ j\frac{1}{\rho} \sin \Theta & \cos \Theta \end{matrix}$$

It is known that cascaded connection of two quadruples gives multiplication of their A-matrices. Hence the resulting A-matrix is

$$A = \begin{matrix} \cos^2 \Theta & -\rho^2 \sin^2 \Theta \\ -\frac{1}{\rho^2} \sin \Theta & \cos^2 \Theta \end{matrix}$$

Additional lines have sequentially connected coupled line quadruples.

It is known that sequential connection of two quadruples gives addition of their Z-matrices. Let us convert A-matrices and Y-matrices of different quadruples into Z-matrices using the following formulas [3]. After addition of two Z-matrices we receive the overall Z-matrix. The

most important characteristic of transformer is the voltage standing wave ratio

$$VSWR = \frac{1 + |\Gamma|}{1 - |\Gamma|},$$

where Γ is reflection coefficient, can be found as

$$\Gamma = S_{21} = \frac{-2Y_{21}}{(1 + Y_{11})(1 - Y_{22}) + Y_{12}Y_{21}}.$$

For obtaining the overall Y-parameters let us use the following transition expressions

$$Y = \begin{array}{cc} \frac{Z_{22}}{\Delta Z} & \frac{-Z_{12}}{\Delta Z} \\ \frac{-Z_{12}}{\Delta Z} & \frac{Z_{11}}{\Delta Z} \end{array}$$

Frequency dependence of VSWR for such transformer is shown in Fig.3.

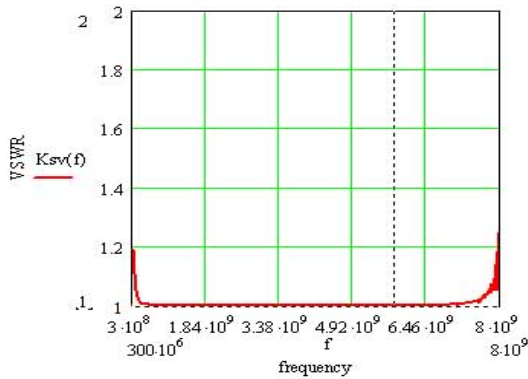


Fig.3. Frequency dependence of VSWR

III. CONCLUSION

In this paper, methods of improvement of design of balanced transformer with additional balancing lines are presented. Techniques for calculation of the main characteristics of such device are given.

REFERENCES

- [1] Avtorskoye svidetelstvo URSS №1729824/26-9
- [2] Ganston M.A.R. “Spravochnik po volnovym soprotivleniyam fidernykh liniy SVCh”. – Moscow: Svyaz, 1976. (In Russian).
- [3] Goncharov. “Analysis Balun transformer in UHF range”. Proceeding of IEEE-Siberian Workshop on Electron Devices and Materials EDM 2003.
- [4] Zelyakh E.V., Feldshtein A.L., Yavich L.R. i dr. “Minityurniye ustroystva UVCh i OVCh diapazonov na otrezkakh liniy”. Moscow: Radio I Svyaz, 1989. (In Russian).

Advanced Large Distance Optical Free-Space Link on the Infrared Diode in Nanosecond Pulsed Mode

Evgeniy D. Golovin and Oleg V. Stukach

*Tomsk Polytechnic University,
30 Lenin Avenue, Tomsk, 634050, Russia
E-mail: ieee@main.tusur.ru*

Abstract — In the paper, the brief performances of wireless communication systems are represented and their disadvantages are considered. The infrared diode in nanosecond pulsed mode was investigated. The new multipurpose circuit of infrared transmitter block for wireless free-space communication systems is offered. Using modification of infrared diode and enhanced method of radiation, up to 100 Mbps transfer rate can be achieved.

Index Terms — infrared transmitter, last mile, low cost, communication purposes

I. INTRODUCTION

Now all over the world there is a large amount of wireless networks for the various purposes. Certainly, wireless solution basing of various equipment (radio-modems, radio-relay lines, microwave digital transmitters etc.) is common knowledge. But the number of complexities does not decrease yet. Frequency band is oversaturated and it is rather difficult to receive allowing for use of radio equipment. And the capacity of this equipment essentially depends on cost.

Certainly, a laser as a radiate element is possible to use for increase of distance. Some enterprises developed such equipment, herewith distance of connection up to 5 kms is provided at rate 2 Mbt/sec. Unfortunately, the use of lasers in such devices makes an equipment rather expensive, comparable with the cost of a good laser.

In the paper, a light-emitting diode, as an electron device, capable to replace a laser is investigated. As far as the radiation power of the light-emitting diode in a continuous mode is small – about ~0.5 Wt, and in this case the distance of guaranteed connection does not exceed of hundred meters, the use of the light-emitting diode in nano-second

pulsed mode with large signal repetition were offered by us. In this case the radiation power is increased in value, multiplied on repetition, that is up to 5–50 Wt and it will be comparable to laser power. The cost of light-emitting diode is thus essentially less.

II. INFRARED SYSTEMS

Nowadays laser infrared (IR) link more and more are used. The laser link has a clear advantage of radio communication, when the matter concerns of organization of wireless bridges ("point to point") on 1-2 km distance. It has higher transfer rate (up to 155 Mbps and above), has a greater noise protection, a high secrecy, and does not require obtaining allowing for frequency band using. At the same time prices for equipment of laser link are quite comparable to the prices on a radio ones [1].

For maintenance of compatibility of infrared devices the association "Infrared Data Association" (IrDA) was established in 1993. The purpose of its creation was consolidation of efforts on development of the mobile communication market by means of infrared data transfer on small distances. Nowadays the systems on the IrDA standard provide data transfer with rate up to 4 Mb/sec, however the guaranteed by manufacturer distance of connection is very small.

Thus, laser link can be used for:

- creation of main and/or backup data link;
- several local networks joining up;
- solution of "last mile" problem [1];
- video observation systems and security television;
- service of mini-cellular link;
- an emergency communication, when the fast development is necessary.

Nowadays laser technology is developing in a way of transfer factor and distance raising that makes it especially perspective for application in high-speed communication systems. However common imperfection for the majority of modern systems is restricted operation conditions at a poor weather.

III. PROBLEMS AND SOLUTIONS

The commercial models of existent IR-systems under the price characteristics are oriented for business class and western customer. The minimum price of such systems is approximately \$3000...\$10000, that makes their inaccessible to majority of individual customers. Problem

of the IR-system creation with transfer rate up to 10 Mbps on distance from 300 up to 1000 meters at cost of components up to \$100 is intensive considered on the Web. Hence, there is a need for such devices, which radio amateurs are ready to assemble by they own means and paying \$100 for components!

Basic parameters of modern commercial laser links, influential to connection distance are following:

- average output power - 20...200 mW;
- transmit beam divergence - 0,5...10 mrad;
- receiver lens diameter - 100 mm;
- minimum received power - 0,1...2 mkW;
- communication range 1...2 km at a signal fading 6...10 dB.

At such characteristics the distance of link makes on average 1...2 km.

However, for an average device (fig. 1, dash line) at a small fog, meteorological optical range (MOR) is not less than 1 km, the connection will be steady on the distance not more then 1 km. But if the fog becomes denser the obtained signal will be lower than a threshold of sensitivity of the receiver (fig. 1, the dotted line with a point) and connection will become unstable or will be stopped. At MOR=0.5 km the signal level will make -14 dB relative to sensitivity. Such operation conditions are unacceptable for a reserve channel or emergency communication. In such cases it is necessary essentially to reduce distance of connection that is not always possible.

Expensive laser emitter, complex optical focus system and also the precision automatic mechanism of pointing and tuning at small beam divergence make expensive cost of devices.

Ways of operating distance increasing are following:

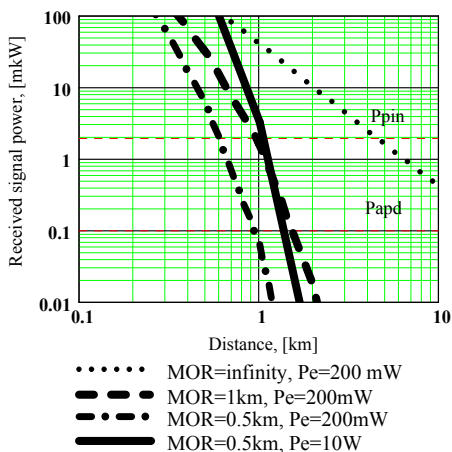


Fig. 1. Received signal power at receiver lens of the operation distance depending of fog density at: output power 200 mW, transmit beam divergence 10 mrad, receiver lens diameter 100 mm, sensitivity 2 mkW

1. The decrease of transmitter beam divergence allows to reduce losses of signal energy by transmission. But because of weather situation, natural conditions in atmosphere, the hunt effects of buildings etc. the beam divergence usually has limited to value 0.5 mrad, thus special tools of pointing (weapon sights) and device of automatic tuning already are required, that essentially has an effect to the price. At angle 10 mrad the special optical devices of pointing and automatic systems of tuning are not required, that essentially makes cheaper the system and installation time.

2. The increase of the reception lens diameter proportionally influences on mass and dimensions of the system, therefore the sizes are usual no more than 100...150 mm.

3. The increase of sensitivity of the receiver is limited to noise and hindrances.

4. But what about increase of output power of a signal? The use of more powerful laser emitters reduces also to essential high price of the system. So, for example, the laser diode with output power 4 W costs about \$600.

IV. HIGH POWER INFRARED TRANSMITTER

The calculations were carried out and the conclusion was made from this. Cost of components can be essentially reduced if instead of

the laser diode the infrared diode is used, which cost is lower 10...100 times, and also to simplify an optical part.

Transmitter and receiver of infrared pulses were developed. The general description looks as follows. On system source the information sequence of pulses is entered. Through matching device, necessary for agreeing of cable or communication link with transceiver input, the signal enters on pulse shaper. It creates the rectangular pulse of certain length and amplitude with steep-sided less than 10 ns front regardless of the form of source signal. Further the pulses gained by means of current generator and enter on infrared light-emitting diode. The optical system in a kind of assembling lens focuses the beam light radiated in the space. There is the similar optical system on the receiving target, focusing flow on photodiode. The photodiode current gains up to necessary level and acquires the necessary form on a pulse shaper.

The diode power in continuous mode is insignificant and makes 100...200 mW approximately. Using the IR-diode in the nanosecond pulsed mode with large porosity of signal, it is possible essentially increase of the emitted power, and consequently also operating distance. The advantage of such solution is universality of the system at switching modes of its operation on maximum distance or maximum transfer rate and also at a control of power in various meteorological conditions. So, for example, at short-term strong deterioration of visibility (strong fog or dense snow) the power of radiation can be increased (that is impossible for laser diode because of an optical strength of an output mirror is limited) unless the visibility will not be restored.

The IR-diode AL148A is offered to use as emitter. This diode has the following characteristics:

- constant direct current – 1 A;
- continuous emitted power – 200 mW;
- risetime of pulse – 30 ns.

As the optical system it is taken simple one-lens objective with 100 mm diameter of lens. The calculated and experimental data of the system shows that the operating distance of such system will make 1 km at 10 Mbps transfer rate and reserve 20 dB of the emitted power for fading in atmosphere (rain, snow, mist etc). Approximate cost of the system will make up to \$30...\$100. For example, an analog of such system WOCC-10MPD has the power reserve only 6 dB and price \$3500 with the same other characteristics.

V. ADVANCED FEATURES

The potential characteristics of the diode AL148A are quite a bit. The maximum pulse current of the diode can achieve to 300 A, at that the output pulse power will make about 50 W. Thus it is possible to essentially increase of operating distance of the IR-system.

For confirmation of theoretical accounts the mockup of the system was developed. The diode was used in pulsed mode with a large duty ratio of signal, so it emitted power has made 1 Wt. But because using of cheaper bad quality optical lenses with 50 mm diameter the beam divergence has made 40 mrad, as well at the receiver. Advantages of the mockup are direct corollary of it disadvantages: a large beam divergence. A disadvantage is large losses and therefore – decrease of distance, advantage – is simplicity of pointing and low requirement to the mount of devices. The operating distance of the system has made 0,5 km at good visibility, what has exactly coincided with calculation. Cost of half-package on components has made only \$12.

Practice and the calculations show that at small additional expenditures with better lenses will essentially rise of efficiency of the given system in many times. It is caused by decrease of a beam divergence up to 10 mrad and increase of reception lens diameter up to 100 mm.

As a result of researches the following characteristics of transmitter were achieved:

- pulse length – 100 ns;
- output-pulse frequency – 500 kHz;
- risetime of pulse – not more than 40 ns;
- falltime of pulse – not more than 40 ns;
- pulsed current of diode – 10 A;
- pulsed power of radiation – 5 Wt.

Main characteristics of receiver are following:

- risetime of pulse front – 5 ns;
- upper border of passband – 200 MHz;
- target voltage – 3 V.

Prospective distance of this device at rate 500 kbits/sec is near 1 km in conditions of bad visibility.

The main restriction on distance and rate of transfer information is introduced the characteristics of infrared light-emitting diode - risetime and maximum average diffuse power. Communication distance is connected with the radiation power, which is a direct proportional average diffuse power as follows:

$$R = k \cdot a \sqrt{P_{out} \cdot Q}, \quad (1)$$

where k is a factor, take into account of receiver sensitivity and additional losses; a takes into account a spreading of light in the space, $a=2...3$; Q is signal repetition.

From (1) it is visible that for increasing of distance it is necessary to increase the signal repetition Q :

$$Q = \frac{1}{\tau \cdot f_T}, \quad (2)$$

where τ is a length of radiate pulse; f_T is output-pulse frequency (equivalent of transfer rate).

To increase of pulse repetition (2) it is necessary to reduce f_T , that will be equivalent of rate reduction, or reduce of the radiate pulse length, which is limited of the diode characteristics: it is necessary that the radiation time will be in several times more than risetime. Thus, the main system characteristics are determined by diode parameters basically. It is necessary to use of light-emitting diodes with the maximum ratio risetime – radiation power.

Advanced circuit of transmitter lets easily to vary of its parameters such as operating distance and transfer rate at various meteorological conditions (table 1).

Usage of the diode in the transmitter scheme with accumulative capacity [2] allows effectively to regulate the emitted power controlling a supply voltage at the last cascade from 5 up to 40 V (fig. 2). Thus, at a strong fog (MOR=0.5 km and less), using the given solution, it is possible to boost the emitted signal power up to 10 Watts, that will provide an indispensable signal level on the receiver (fig. 1, solid line). However at increasing the pulse power it is necessary to increase a porosity of the signal that entails data rate reduction.

TABLE I
PARAMETERS OF INFRARED LINK

Maximum transfer rate (kbps)	Operating distance (km)		Maximum theoretical distance (km)
	fading 20 dB	fading 6 dB	
10000	1	5	10
640	2	10*	20
64	3.5	17*	35

For example, system installed on 3.5 km distance with reserve of the emitted power 20 dB for fading in atmosphere (such as strong rain,

snow or fog), at good weather can be fluently turned in fast transfer rate mode – 10000 kbps and 6 dB fading – by decreasing supply voltage of driver and increasing of signal duty ratio and vice versa.

So, using given high power transmitter with cheap IR-diode AL148A (it cost about \$2), price of infrared system is only about \$100. The calculations and experimental data of the system shows that the operating distance of such system will make 1 km at data rate up to 10 Mbps and reserve of the emitted power up to 35 dB for fading in atmosphere (rain, snow, fog etc).

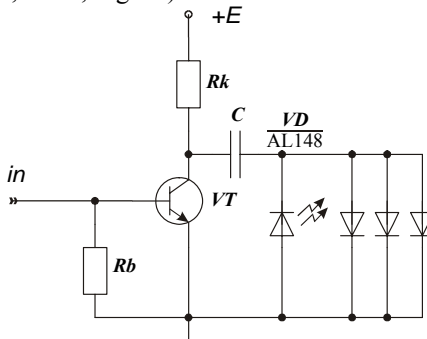


Fig.2. The last cascade of the high power transmitter

VI. CONCLUSION

Usage of the IR-diode AL148A in the offered scheme is an effective solution of the last mile problem. Basic merits of a designed system are its cheapness, simplicity of installation, which is not requiring special tools for development.

The developed circuit of infrared transmitter is universal block both for various types of communication as for Ethernet interface, and analog phone lines, at much less cost in comparison with its analog.

Using modification of diode AL148A and enhanced method of radiation, 100 Mbps and above transfer rate can be achieved and also longer distance.

REFERENCES

- [1] M. Fuller, "Free-space optics available for the last mile". *Lightwave*, Vol. 17, pp. 39-42, July (2000).
- [2] E.D. Golovin, O.V. Stoukatch, "The wireless Optical Home Link" in "PIERS – Progress in Electromagnetics Research Symposium", July 18-22, Osaka, Japan, p. 687, (2001).

Evgeniy D. Golovin (S'00, M'04), received the M.S. and the Ph.D. degrees in radio engineering from Tomsk State University of Control Systems and Radioelectronics in 2000 and 2004, respectively. His current research interests include differential transformations in electronics and wireless communication systems.

Oleg V. Stukach (M'97, SM'01), received the Candidate of Technical Sciences (Ph.D) degree in radio engineering in 1993. In 1988, he joined Picosecond Technique Labs, Tomsk, Russia. Currently, he is Associate Professor of the Tomsk Polytechnic University, Russia. He has published more than 120 technical papers and patents in the fields of picosecond pulse technique and theory of control. He is organizer and active participant of international scientific conferences, winner of the Tomsk Region Prize in science and education.

Inductive Voltage Divider Simulation in MATLAB

V.L. Kim, R.G. Dulbinov

*Tomsk Polytechnic University,
30 Lenin Avenue, Tomsk, 634050, Russia
Tel.: 8-3822-417527, e-mail: sov@camsam.tpu.ru*

Abstract — The single-harness decade inductive voltage divider model was made with the MATLAB/Simulink. The transfer function algorithm was given. The mathematical model accuracy was estimated with the comparing with the Pspice-model. The calculation results of amplitude error differ no more than 20%.

Index Terms — Decade inductive voltage divider, simulink-model, transfer function, mathematical model accuracy

BACKGROUND

It is necessary to have transfer function blocks of the structure scheme for the functional simulation of the measurement systems, control systems having the inductive voltage divider. The *IVD* transfer function may be obtain with the equivalent scheme. In work [1] the *IVD* linear electric model was offered. This model has twenty five reactive elements. The analytic method of the model calculation is not available. So the computer design methods give a chance to research the complicated processes of the *IVD*.

MATLAB with Simulink is the suitable software. The software tools of MATLAB allow to obtain the analytical formulas of the main dynamical characteristics of the electrical model.

The main gain of the article is to design the *simulink-model* of the decade *IVD* and the algorithm of the transfer function taking. The research object is the decade *IVD*. The full and simplified models of

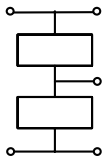
this *IVD* were offered in [1]. The *IVD* analysis in the frequency band is available with the simplified model (so called macromodel). In the table 1 the *IVD* macromodel parameters with the different gains, the identical section parameters $e_j = e_0$, $r_j = r_0$, $l_{sj} = l_{s0}$ and the equivalent capacities C_0 .

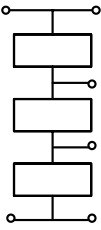
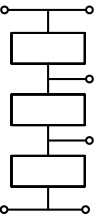
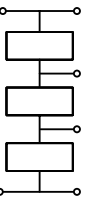
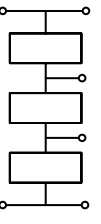
Then the algorithm of the decade *IVD* mathematical model design as the transfer function will be considered.

1. MAKING THE SINGLE-DECADE SIMULINK MODEL

The *simulink-model* of the *IVD* decade is given in the figure. The values of the input network elements are $R1 = R2 = 0.01$ Ohm; $R3 = 10$ kOhm; $L1 = L2 = 0.01$ μ H; $L3 = 4$ H; $C1 = 500$ pF. The values of the output network elements are $r_0 = 0.12$ Ohm; $l_{s0} = 1.1$ μ H; $C0 = 300$ pF from the table 1. For example, for gain $K_j = 0.1$ we have $R4 = 0.96$ Ohm; $L4 = 8.8$ μ H; $C2 = 693$ pF; $R5 = R6 = 0.12$ Ohm; $L5 = L6 = 1.1$ μ H; $C3 = 3.75$ nF; $C4 = 1.35$ nF; $R7 = R8 = R9 = 10^{-5}$ Ohm. The last elements $R7$ – $R9$ that are not in the basic models MT_{15} , MT_{j+1} , MT_{16} , are necessary to start the *simulink-model* simulation. As the computer experiment results such small values of resistance do not influence the simulation results. Besides R , L , C elements the *simulink-model* have the following blocks: controlled voltage source (*CVS0*–*CVS6*), voltage measurement (*VM0*–*VM2*), multipliers (*Gain*) $G1$ with a multiplier 0.8, $G2$ and $G3$ with a multiplier 0.1.

Table 1. The average values of elements of *IVD* macromodel

Gain, K_j	Parameters of equivalent basic model			Output network of macromodel
	MT_{15}	MT_{j+1}	MT_{16}	
0,0 (0,9)	$e_{1,10} = 9e_0$ $r_{1,10} = 9r_0$ $l_{s1,10} = 9l_{s0}$ $c_{1,10} = 1,98C_0$		$e_{0,1} = e_0$ $r_{0,1} = r_0$ $l_{s0,1} = l_{s0}$ $c_{0,1} = 4,5C_0$	

<p>0,1 (0,8)</p>	$e_{2,10} = 8 e_0$ $r_{2,10} = 8 r_0$ $l_{s2,10} = 8 l_{s0}$ $c_{2,10} = 2,31C_0$	$e_{1,2} = e_0$ $r_{1,2} = r_0$ $l_{s1,2} = l_{s0}$ $c_{1,2} = 12,5 C_0$	$e_{0,1} = e_0$ $r_{0,1} = r_0$ $l_{s0,1} = l_{s0}$ $c_{0,1} = 4,5C_0$	
<p>0,2 (0,7)</p>	$e_{3,10} = 7 e_0$ $r_{3,10} = 7 r_0$ $l_{s3,10} = 7 l_{s0}$ $c_{3,10} = 2,64C_0$	$e_{2,3} = e_0$ $r_{2,3} = r_0$ $l_{s2,3} = l_{s0}$ $c_{2,3} = 18,5 C_0$	$e_{0,2} = 2 e_0$ $r_{0,2} = 2 r_0$ $l_{s0,2} = 2 l_{s0}$ $c_{0,2} = 4,25C_0$	
<p>0,3 (0,6)</p>	$e_{4,10} = 6 e_0$ $r_{4,10} = 6 r_0$ $l_{s4,10} = 6 l_{s0}$ $c_{4,10} = 2,97C_0$	$e_{3,4} = e_0$ $r_{3,4} = r_0$ $l_{s3,4} = l_{s0}$ $c_{3,4} = 22,5 C_0$	$e_{0,3} = 3 e_0$ $r_{0,3} = 3 r_0$ $l_{s0,3} = 3 l_{s0}$ $c_{0,3} = 3,94C_0$	
<p>0,4 (0,5)</p>	$e_{5,10} = 5 e_0$ $r_{5,10} = 5 r_0$ $l_{s5,10} = 5 l_{s0}$ $c_{5,10} = 3,3C_0$	$e_{4,5} = e_0$ $r_{4,5} = r_0$ $l_{s4,5} = l_{s0}$ $c_{4,5} = 24,5 C_0$	$e_{0,4} = 4e_0$ $r_{0,4} = 4 r_0$ $l_{s0,4} = 4 l_{s0}$ $c_{0,4} = 3,63C_0$	

For the work capacity test of the model the sinusoidal sources SW0 and SW1 connect to the *Input point 0* and the *Input point 1*, imitating the output voltage of the previous decade. If the first one is simulated, then it is necessary the amplitude value of voltage, equivalent to zero, in the block adjustment window. *VM3*, *VM4* and *Scope* help to watch the output signals. The block parameter adjustment is done standantly. The

simulink-model is saved as *ivd01.mdl* and set the parameters of simulation. In menu **Simulation/Simulation parameters/Solvers** the following data are set: **Start time - 0.0; Stop time - 1.0; Type - Variable-step, ode 23 tb [stiff/TR-BDF2]**. Pay attention to last option (the solve method of the differential equations). As the computer experiments have shown only **ode 23 tb** allows to simulate the design *IVD simulink-model*. After the button *Start Simulation* is realized, you can watch the results in the scope window.

2. CHOISE OF TRANSFER FUNCTION

The transfer function is taken with the **LTI-Viewer** of *Control System Toolbox*. It is necessary to do the following:

- open the file *ivd01* and in menu **Tools** do **Linear analysis**. As the result start **LTI-Viewer**;
- in open **LTI-Viewer** window to choose **Simulink** menu and do **Get Linearized model**.
- in the **LTI-Viewer** window do **File/Export/Export to Workspace**. In the workspace of MATLAB the *ivd01_1* structure will be done with the *A, B, C, D* matrices of the state space equations.

Matrices may get the following way:

» **[A, B, C, D] = ssdata (ivd01_1);**

- get the transfer function writing in the command window
- » **ivd01t = tf (ss (A, B, C, D)).**
- decrease the model order (get the reduced *rtf-model*).

Use the following functions:

» **ivd01m = minreal (ivd01t),**

» **[ivd01b, g] = balreal (ivd01m).**

As the result get **g** vector of the resulting gramian

g = 25,9492; 25,8508; 20,9581; 20,8583; 0,2527; 0,2509; 0,2000; 0.

Now decrease the model order removing zero states of gramian with the function **modred**

» **ivd01rt = modred (ivd01b, [8], 'del').**

Call **tf**-function

» **ivd01rtf = tf (ivd01rt).**

The transfer functions expression of the first tapping is appeared in the command window

$$K_{0,1} = \frac{0,5s^7 + 7,091e5 + 3,061e16 + 7,089e21 + 1,234e31 + 1,413e36 + 1,202e45}{s^7 + 1,419e6 + 1,008e17 + 2,281e22 + 7,545e31 + 8,356e36 + 1,202e46}$$
 For

the second tapping

$$K_{0,2} = \frac{0,5s^7 + 7,094e5 + 4,149e16 + 9,466e21 + 2,146e31 + 2,406e36 + 2,403e45}{s^7 + 1,419e6 + 1,008e17 + 2,281e22 + 7,545e31 + 8,356e36 + 1,202e46}$$

3. MODEL QUALITY ESTIMATION

The model error may be estimated with the real *IVD* gain-frequency characteristic and the *IVD* model gain-frequency characteristic. But this method is not available, because the hard natural experiments must be done.

The model accuracy was estimated comparing the *PSpice-model* (as a standard model), created the OrCAD 9.2 [1]. The compare criteria is the maximum of the relative deviation of amplitude errors in the work frequency range

$$\varepsilon = \max \left| \frac{\gamma_p - \gamma_r}{\gamma_p} \right| \cdot 100\%,$$

where γ_p , γ_r is the relative gain errors of *PSpice* and *rtf-models*.

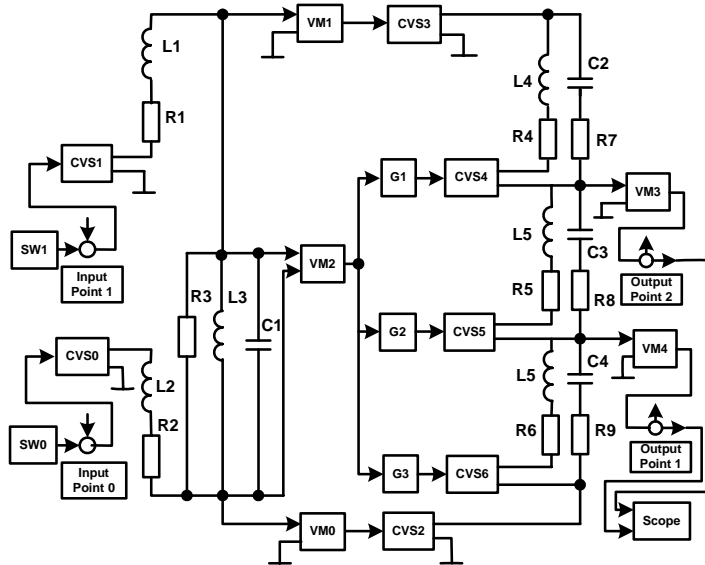
The experiment results are shown in table 2 (the work frequency is 200 kHz).

Table 2. The amplitude error of decade *IVD* γ_j , %

Gain K_j	Type of the model		Criteria of quality ε_j
	<i>rtf</i>	<i>PSpice</i>	
0,1	-0,640	-0,630	2
0,2	-0,440	-0,400	10
0,3	-0,220	-0,240	8
0,4	-0,120	-0,110	9
0,5	0,001	0,001	0
0,6	0,075	0,070	7
0,7	0,115	0,110	5
0,8	0,120	0,110	9
0,9	0,060	0,070	14

So we have the *IVD* $\varepsilon_{j\max} = 14$ %. Such value ε_j is got, because we did the reducing of model, the transformation of *ss-models* into *tf-form* and inverse and so on. The maximum error of the reduced model is $\varepsilon_{\max} = \varepsilon_{j\max} + \varepsilon_e \approx 20$ %.

Such model accuracy is enough for the practical calculations. So this *simulink-model* allows to do researches of the frequency characteristics and calculations of the *IVD* metrological characteristics.



REFERENCES

- [1] V.L. Kim, S.V. Silushkin, A.N. Plotnikov, "Mathematical Models and Methods of Multidecade Inductive Voltage Divider Calculation" The IEEE-Siberian Conference on Control and Communications (SIBCON-2003). Proceedings. Tomsk, October 1-2, 2003. – P. 98 – 101.

The Electric Circuit Property for Use in Blocks of Data Mining and Processing

G.I. Peredelsky, A.C. Romanchenko, U.V. Didenko

Kursk State Technical University, ul. 50 let Oktyabria, 94, Kursk, 305040, Russia

Abstract — It is substantiated the property of two-port networks of definite structures in their new particular implementations. The use of these two-port networks in multiarm bridge circuits for control systems is presented.

Index Terms — two-port networks, increasing circuits, voltage pulses, bridge circuits, conditions of balancing

Electric bridge circuits [1, 2] as input units are used in control systems, automation control and their blocks of collection and primary information treatment. Modulating transducers or objects examined control, automatization, including those have multielement equivalent circuits are included into these circuits. A number of claims are laid to the bridge circuits, including such important claims as separate balancing and balancing by adjustable model resistors only. The latter, are generally known, as excel adjustable model capacitors and inductors in a number of parameters and characteristics.

Multiarm bridge circuits meet the abovementioned requirements. They are energized by impulses with change of voltage during their duration in accordance with the law of power functions [3]. There is a group of particular solutions in this field (for example [4]). Generalization is published in [5], it is connected with a new capacity of two-port networks of definite structures. Further research have led to doubling of the number of two-port networks, which provide separate balancing only by adjustable resistors of bridge circuits for determining the parameters of multielement one-port networks.

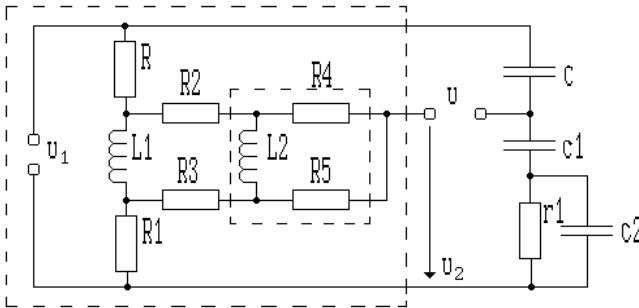
New variants of two-port networks of definite structures are given in the paper. Substantiation of their ability is adduced. The results of the analysis of the multiarm bridge circuits with the use of these two-port networks and their use in devices of gathering and primary data processing are also given.

As a particular example a new version of two-port network as a part of a multiarm bridge circuit is shown in figure. The main two-port network is given in dotted line. The increasing circuit which is in main two-port network and which is repeated a required number of times, depending on the number of elements (or parameters) in the object of control, is also presented in dotted line.

Voltage pulses affect the main two-port network. Their form is described by an expression

$$u_1 = U_1(t/t_u)^h, \tag{1}$$

where U_1 is pulse amplitude; t_u is its duration; t is current time; $h=0,1,2,\dots$



Output voltage of the main two-port network is determined in general by a known formula [6]

$$u_2 = \frac{U_1 h!}{t_u^h} \left[\frac{\Psi(0)}{\psi(0)} \frac{t^h}{h!} - \frac{t^{h-1}}{(h-1)!} \sum_{i=1}^k \frac{\Psi(p_i)}{p_i^2 \psi'(p_i)} - \frac{t^{h-2}}{(h-2)!} \sum_{i=1}^k \frac{\Psi(p_i)}{p_i^3 \psi'(p_i)} - \dots - t \sum_{i=1}^k \frac{\Psi(p_i)}{p_i^h \psi'(p_i)} - \sum_{i=1}^k \frac{\Psi(p_i)}{p_i^{h+1} \psi'(p_i)} (1 - e^{p_i t}) \right], \tag{2}$$

where

$$\Psi(p) = D_0 + D_1 p + D_2 p^2 + \dots; \tag{3}$$

$$\psi(p) = d_0 + d_1 p + d_2 p^2 + \dots + d_k p^k; \tag{4}$$

p_i is roots of an equation $\psi(p)=0$; k is number of these roots; $d_0, d_1, d_2, \dots, D_0, D_1, D_2, \dots$ are generalized quantities, which are determined by parameters of the elements, which are a part of the main two-port network.

Equations of high powers turn out when a number of elements in the main two-port network is big, especially reactive ones. Complexity

of their solution grows fast with the growth of their power. In order to avoid solving equation of high powers when back manipulation of functions in the operated form to the original equations, which are received for the main two-port network, are not solved, but fragments of a formula are isolated for back conversion which contain roots and are changed into equivalent formulas which do not contain these roots as shown in [7].

For this each item of numerators in (2) is divided by a corresponding denominator. As a result there are fragments of a formula, which has a structure

$$\sum_m = \sum_{i=1}^k \frac{p_i^m}{\psi'(p_i)}, \quad (5)$$

where m is whole numbers of positive and negative signs. According to [7] they are equal to zero or changed into equivalent formulas, which have only an absolute term and coefficients of an equation, depending on the sign m and correlation between the meanings of k and m. For example, when pulse of line changed voltage acts output voltage of the main two-port network is defined by the expression

$$u_2 = \left[U_1 / t_u (R + R_1)^2 (R_2 + R_3) \right] \left\{ t R_1 (R + R_1) (R_2 + R_3) + L_1 (R R_3 + R_1 R_2) + (R + R_1)^2 (R_2 + R_3) \sum_{i=1}^3 \left[e^{p_i t} \Psi(p_i) / p_i^2 \psi'(p_i) \right] \right\}. \quad (6)$$

After the transient process has faded out exponential components are attenuated until zero and output voltage depends on meanings of parameters of elements L1, R, R1, R2, R3, and does not depend on the other parameters of the circuit.

The ability of the main two-port networks examined in the report consists of the following: when pulses with the voltage changing in accordance with the law of power functions affect them, output voltage after fading the transient process in the chosen period of time does not depend on the meanings of parameters of a whole complex of elements, with the increase of power in mathematical description of a pulse per unit the number of parameters, output voltage does not depend on, is diminishing 3-4 units among which one is a reactive parameter, the rest are parameters of resistance.

On the basis of the main two-port networks shown in the report one can build many bridge circuits with complex pulses and with separate balancing regulated only by resistors. They relate to multiarm

bridge circuits, contain different number of increasing circuits useful for determining parameters of one-port networks of different complexity with homogeneous reactive elements. The bridge circuit shown in figure allows to determine parameters of three elements c_1 , c_2 , r_1 , which are a part of a multielement one-port network in accordance with the following conditions of balancing:

$$A_1 = c_1 R_1 - c_2 R_2;$$

$$A_2 = c_1 L_1 R_3 - c_2 L_2 R_2 - c_1 r_1 R_1 (R_2 + R_3);$$

$$A_3 = c_1 L_1 [L_2 R_5 + c_2 r_1 R_3 (R_4 + R_5)] - c_2 L_2 [L_2 R_4 + c_2 r_1 R_2 (R_4 + R_5)] - c_1 r_1 (R_4 + R_5) [L_1 (R + R_2) + L_2 R].$$

As it is seen from the conditions of balancing, the first balancing is made by adjustment of resistors R or R_1 or by sequential adjustment of both resistors, the second – R_2 , R_3 , the third – R_4 , R_5 .

REFERENCES

- [1] Тензоизмерительная система для прочностных испытаний / М.П. Цапенко, Я.М. Диковский, Б.В. Карпюк и др. // Приборы и системы управления. 1976. № 1. С. 31-33.
- [2] Кнеллер В.Ю. Автоматическое измерение составляющих комплексного сопротивления. М.-Л.: Энергия, 1967. 368 с.
- [3] Передельский Г.И. Мостовые цепи с импульсным питанием. М.: Энергоатомиздат, 1988. 192 с.
- [4] Передельский Г.И., Романченко А.С. Мостовые цепи для измерения параметров многоэлементных двухполюсников // Известия вузов. Приборостроение. 1995. Т. 38. № 5–6. С. 49–51.
- [5] Передельский Г.И. Многоплечие мостовые цепи с уравновешиванием регулируемые резисторами // Измерительная техника. 1999. № 6. С. 50-54.
- [6] Передельский Г.И. О теории построения мостовых цепей для определения параметров четырехэлементных двухполюсников // Измерительная техника. 1987. № 2. С. 45–47.
- [7] Передельский Г.И., Нечаев И.А., Нечаева Н.В. Упрощение анализа измерительных цепей с многоэлементными двухполюсниками // Измерительная техника. 1995. № 10. С. 48–50.

Gennady I. Peredelsky graduated from radio engineering faculty of Tomsk polytechnic institute. In 1989 he defended a doctor's thesis in Moscow

energy institute concerning theory of bridge circuits in problems of measuring parameters of one-port networks. Now he is Professor of Kursk State Technical University.

Alexander S. Romanchenko graduated from instrument-making faculty of Kursk polytechnic institute State Technical University in 1979. In 1996 he defended a master's thesis in Kursk State Technical University concerning theory of bridge circuits in devices of gathering and data processing for control systems. He is an assistant professor of Kursk State Technical University.

Uri V. Didenko graduated from computer engineering and automation faculty of Kursk polytechnic institute in 1990. In 2000 he finished post-graduate studies in Kursk State Technical University. He is an engineer in a joint-stock company «Kurskenergo».

Digital Calculation of Frequency of Periodical Signal (Sinusoidal and Triangular)

T. Benslimane, B. Chetate

*Research Laboratory of Electrification in Industrial Enterprises
Independance avenue, Boumerdes (35000), Algeria
Phone/Fax : +213 24 8170 50, Fax : +213 24 81 91 72
bens082002@yahoo.fr*

Abstract — In this paper, a method of digital calculation of frequency of periodical signal (sinusoidal and triangular signals) is proposed. This method is based on calculation of time between two successive peaks of the rectified signal which constitutes its half period. This method allows the measurement of AC current and voltage of AC electrical network. To apply this method, it is necessary to have current and voltage sensors, analogue/digital converter (ADC) and a processor. A software C++ based program is developed which can be implemented using appropriate processor. In the end are presented the digital simulation results.

Index Terms — Frequency measurement, Sinusoidal signal, Triangular signal, Data type, Digital measurement, Peak value, AC voltage and current.

I. INTRODUCTION

AC systems (AC network, induction motor) need to be controlled continuously to avoid damages caused by faults. This control may cover peak values (or RMS values), frequency values, phase values, etc. In this paper, a digital frequency measurement method is proposed. This method based on calculation of time between two successive peaks of rectified voltage or current then doubling this value to get the period of the signal. The frequency is deduced by inverting the period value. A software C++ based program is developed which can be implemented using appropriate processor. In the end are presented the digital simulation results.

II. PRINCIPLE OF PROPOSED DIGITAL FREQUENCY MEASUREMENT METHOD

This method based on calculation of time between two successive peaks of rectified signal then doubling this value to get the period of the signal. The frequency is deduced by inverting the period value (fig. 1).

A. Rectification of sinusoidal and triangular signals

This rectification is ensured by simple software program in C++. This former algorithm is like follow:

$$\begin{aligned} \text{If } (V_a \geq 0) \quad V_a \text{ rectified} &= V_a. \\ \text{If } (V_a < 0) \quad V_a \text{ rectified} &= -V_a. \end{aligned}$$

Rectified signal result is presented in fig. 1.

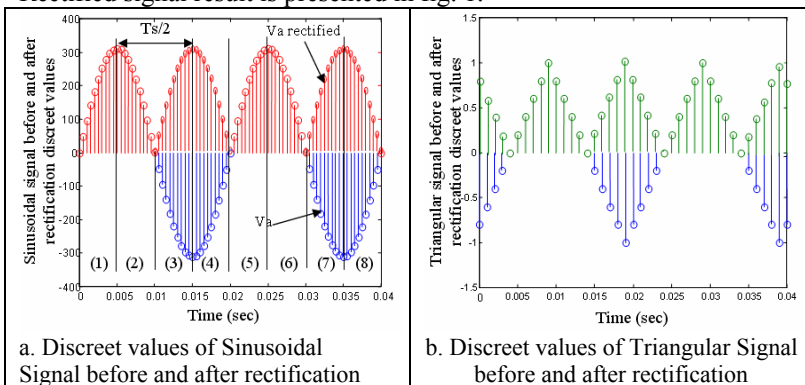


Fig. 1. Discret values of Sinusoidal and Triangular Signal before and after rectification

B. DIGITAL CALCULATION OF PEAK VALUE OF SINUSOIDAL AND TRIANGULAR SIGNALS

The calculation of signal peak value is ensured by software C++ program respecting the algorithm of fig. 2. The first part of this algorithm constitutes software rectifying of the signal. The calculation of peak value ($V_{apmaxdef}(n)$), that is initially nil, is based on calculation of temporary maximal value of the signal ($V_{apmaxpro}(k)$). Voltage $V_a(k)$ is acquisitioned and rectified to get $V_{ap}(k)$. Then, it will be compared to $V_{apmaxpro}(k)$ that is initially nil. If $V_{ap}(k)$ is greater than $V_{apmaxpro}(k)$ then there will be new temporary maximal value of this signal which is $V_{ap}(k)$ else $V_{apmaxpro}(k)$ stays the same.

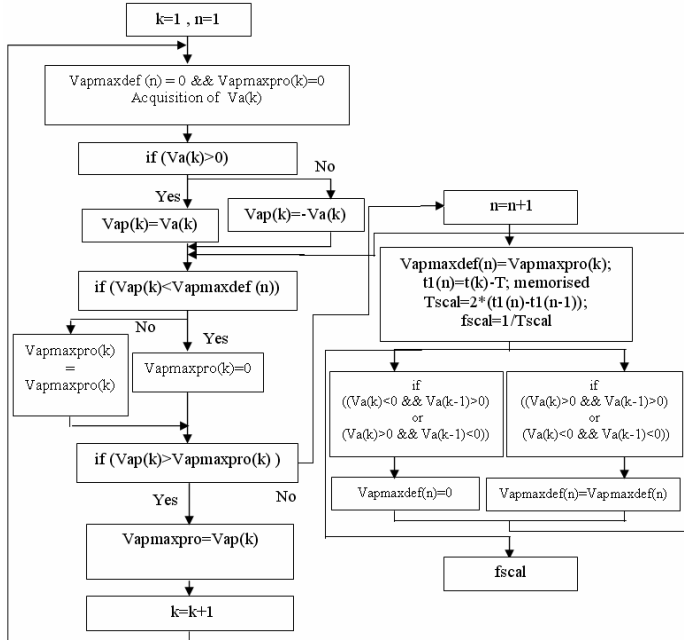


Fig. 2. Algorithm of the proposed method of the signal frequency calculation

The peak value ($Vapmaxdef(n)$) will be got when the acquired value of the rectified signal $Vap(k)$ becomes less than temporary maximal value of the signal $Vapmaxpro(k)$. In this case we will have a new peak value ($Vapmaxdef(n) = Vapmaxpro(k)$). Time corresponding to this peak value is being ($t1(n)=t(k)-T$ with T as sampling time). The difference between two successive peaks corresponding times ($t1(n)-t1(n-1)$) constitutes the half period of the sinusoidal signal. Then the period will be the double of this difference:

$$Tscal=2(t1(n)-t1(n-1)) \quad (2)$$

The frequency will be finally deduced by taking the inverse of the calculated period:

$$fscal=1/Tscal \quad (3)$$

Its remarkable that there is an over flow of frequency at the beginning of the signal (fig. 8). This is due in fact, to the initial value of $t(n)$ which was taken nil. The frequency in this case is wrongly calculated by $fscal=1/Tscal=1/(2(t1(1)-0))$ and will be very high. Therefore, we can limit this value to pre defined maximal value $fsmx$ by using simple software program:

$$\begin{aligned} \text{If } (f_{scal} \geq f_{smax}) \quad f_{scal} &= f_{smax}. \\ \text{If } (f_{scal} < f_{smax}) \quad f_{scal} &= f_{scal}. \end{aligned} \quad (4)$$

When time belongs to the intervals (3), (5) and (7) $V_{apmaxdef}(n)$ will be taken as nil to allow the calculation of next temporary peak value $V_{apmaxpro}(k)$ and then next $V_{apmaxdef}$. The transfer from of Interval (2) to (3), from (4) to (5) and from (6) to (7) is detected like indicated on the (fig. 2.) by defining the signs of signal values $V_a(k)$ and $V_a(k-1)$ for example transfer from interval (2) to (3) is characterized by $(V_a(k) < 0)$ and $(V_a(k-1) \geq 0)$ (fig. 1). Along the intervals (2), (4) and (6) $V_{apmaxdef}(n)$ will stay invariable because there is no peak values to be calculated in these intervals (fig. 1).

III. RESULTS OF DIGITAL SIMULATION

The simulation is done by using the software language C++ with following parameters:

For sinusoidal signal: $V_{rms} = 220$, (25 Hz, 40 Hz, 50 Hz and 60 Hz),

For triangular signal: $V_{max} = 1$, (25 Hz, 40 Hz, 50 Hz and 60 Hz),

Sample time $T=0.0001$ seconds.

IV. CONCLUSION

In this paper, a digital new method to calculate the frequency of periodical signal (sinusoidal and triangular signals) is proposed. This method based on determination of times corresponding to two successive peak values of the signal then getting the frequency from the difference between these two times. This method can easily be implemented by using signal sensors, analogue/digital converter and processor. Simulation results confirm the high precision of this method in sinusoidal signals frequency calculation.

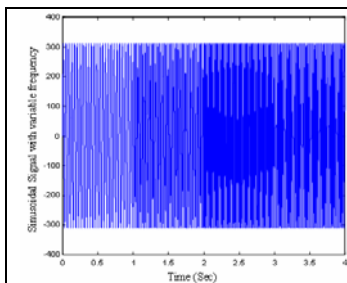


Fig. 3. Simulation result of Sinusoidal Signal with variable frequency (25 Hz, 40 Hz, 60 Hz and

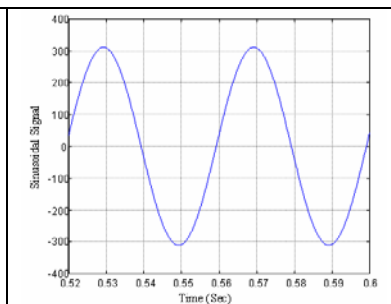


Fig. 4. Simulation result of Sinusoidal Signal (25 Hz)

50 Hz)

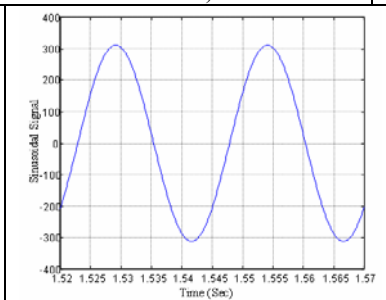


Fig. 5. Simulation result of Sinusoidal Signal (40 Hz)

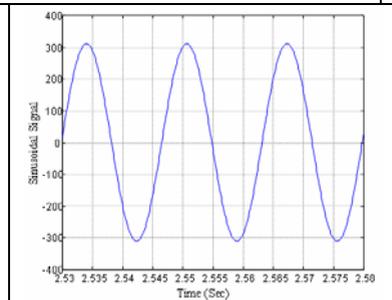


Fig. 6. Simulation result of Sinusoidal Signal (60 Hz)

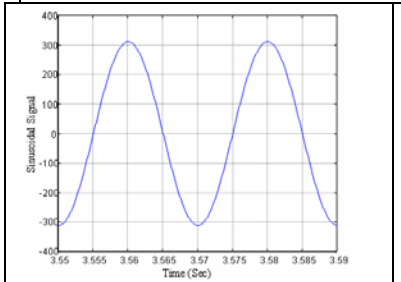


Fig. 7. Simulation result of Sinusoidal Signal (50 Hz)

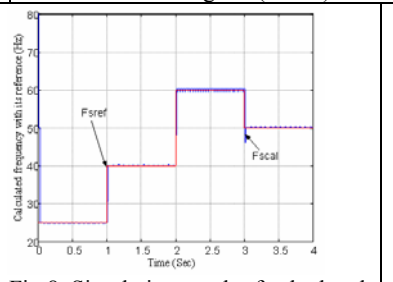


Fig. 8. Simulation result of calculated frequency of Sinusoidal Signal with its reference

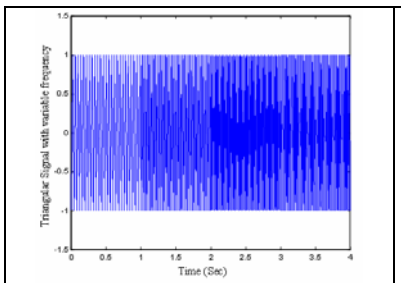


Fig. 9. Simulation result of Triangular Signal with variable frequency (25 Hz, 40 Hz, 60 Hz and 50 Hz)

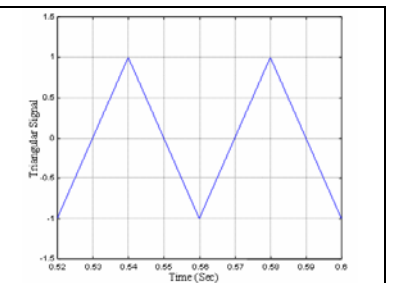


Fig. 10. Simulation result of Triangular Signal (25 Hz)

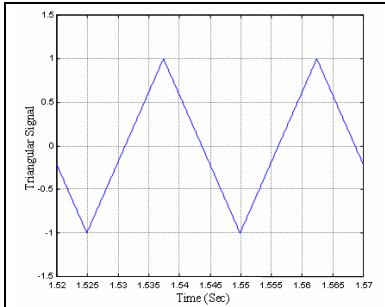


Fig. 11. Simulation result of Triangular Signal (40 Hz)

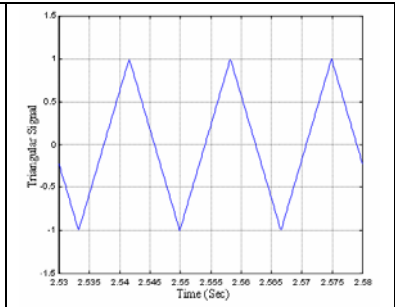


Fig. 12. Simulation result of Triangular

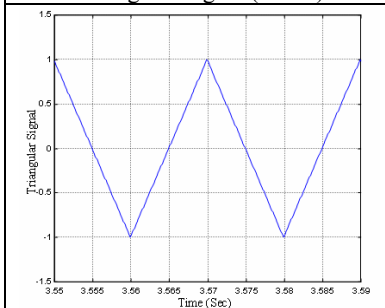


Fig. 13. Simulation result of Triangular Signal (50 Hz)

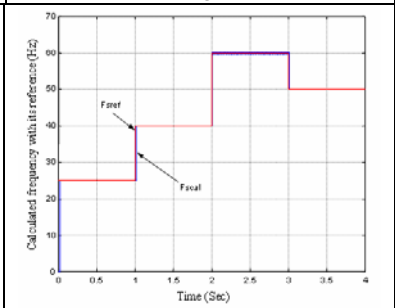


Fig. 14. Simulation result of calculated frequency of Triangular Signal with its reference

De-Interlacing Using Area Based Motion Compensation

Roman Khudeev, Svjatoslav Osipov, Vadim Afanasyev

Alparysoft R&D, Tomsk, Russia

Abstract — A motion compensated de-interlacing method with adaptive area based motion compensation is proposed to recover the defects of interlaced video sequence. GMC is used to recover the change of the picture due to both camera motions and local motions. During the processing of a frame the areas containing enough of so called “interlaced pixels” are a subject to mathematical correction only. This allows to decrease information loss. A part of a frame is saved without changes so introduced artifacts are decreased appreciably. The proposed algorithm could achieve higher image quality of interlaced video sequences than any other usual de-interlacing algorithm on progressive devices.

Index Terms — de-interlacing, area based motion compensation

I. BACKGROUND

For the moment, there are camcorders with progressive scan and interlace scan in the market [1]. When recording with the latter ones each frame consists of two half-frames also called fields. This method of recording allows to achieve smooth movement of objects when using a TV-set with interlace. The reason is that the output is 50 half-frames per second instead of 25 full frames. But in some cases it is necessary to get one full frame from two half-frames, generally, when processing video with a computer or getting a photo of a full frame [2-6].

When combining two half-frames into one frame an interlace effect appears on moving objects. This is because of a time delay between two half-frames which is approximately 16ms for NTSC standard and approximately 20 ms for PAL and SECAM standards [3]. A moving object is located displaced in adjoining half-frames (fig. 1). After combining two adjoining half-frames an interlace effect appears on moving object's edges [7] which affects both visual perception of video and processing aptitude of the video by various algorithms



Fig. 1

adversely. Because of this fact in some cases it is necessary to remove the interlace effect thus improving the quality of video. Usually special algorithms of video processing are used for this [5, 6, 8-13]. The process of interlace effect removing is called de-interlacing. The aim of this article is to describe some new de-interlacing methods and also to examine their advantages as compared with the old ones.

There are a number of publications about the de-interlacing problem [5, 6, 8-13]. In these works the following methods are examined: blend [5, 6, 9, 10], weave [5, 9], area based [5], motion blur [5], discard [5, 6], bob [5, 6, 9, 10, 13], adaptive [5, 6, 9], motion compensation [5], even only [9], greedy [9], MoComp [9], odd only [9], old game [9], DCDi [11], XAW [12]. The method described in this article may be called area based motion compensation according to the given terminology. The method of de-interlacing using motion compensated local spectrum was examined in [8]. This article uses other approach to motion compensation de-interlacing. The new methods are realized in Alparysoft Deinterlace Filter software [14].

II. THE METHOD OF INTERLACED AREA DETERMINATION

Restoration of a full frame from two half-frames using mathematical methods is usually made on the basis of one of the half-frames. The other half-frame is calculated from the basic one using one of interpolation methods. This approach leads inevitably to information loss right up to losing all the information of one of the half-frames. Video materials of medicine, map-making etc. are particularly sensitive to the information loss. So it is expedient to avoid using these methods in frame parts where superposition of adjoined half-frames does not lead to visible negative effects (see the area marked with a rectangle, fig. 2). It is advisable to find these areas before applying the methods of unwanted effects removal.



Fig. 2

Let's name the pixels of a frame which require to be corrected when the superposition of half-frames is performed with a word "interlaced".

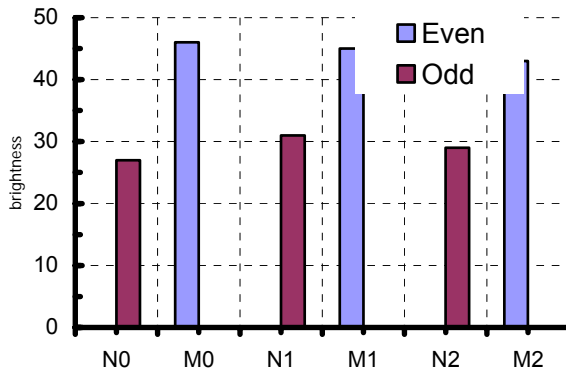


Fig. 3

It is necessary to clarify that when making a record in real-life environment objects of a scene including the moving ones usually differ by brightness and color from background. It is suggested to use the following method of interlaced pixel finding when examining brightness of a pixel or brightness of its color components.

Let's examine a pixel column in a frame which is made by combining two adjoining half-frames. Let's number them. Let N_x be the brightness values of pixel color components in odd rows. Let M_x be the same in even rows. In accordance with aforesaid, color component brightness allocation in the column for the areas which require correction could be as shown on fig. 3. Also see fig. 1.

If the following conditions are true then N_x pixel is interlaced:

$$\begin{aligned}
 N_{x-1} &\approx N_x \approx N_{x+1} \\
 M_{x-1} &\approx M_x \approx M_{x+1} \\
 |N_x - M_x| &> Tr,
 \end{aligned}
 \tag{2.1}$$

Tr is a threshold meaning minimal difference of color component brightness between object pixels and background pixels. In concordance with (2.1) criteria N1 pixel is interlaced on fig. 3.

In practice color characteristic can be neglected with respect to brightness for most tasks. Besides, human vision is organized the way in which brightness is perceived better than color [15].

During the following processing of a combined frame the areas containing enough of interlaced pixels are a subject to mathematical correction. This allows to decrease information loss. A part of a frame is saved without changes so introduced artifacts are decreased appreciably.

This approach also allows to save time of frame processing because the criteria of interlaced pixels finding are simple and demand less processing power in comparison with that required for the interlace effect removal. The following “expensive” processing is only applied to the interlaced pixels or the areas containing enough of them. The criteria referred above also suit for determining interlace effect existence in a frame.

III. THE METHOD OF INTERLACED AREA RECOVERY WITH MOTION COMPENSATION

The main point of the method is that a search of needed fragment in adjoining half-frame is performed in addition to mathematical methods of restoration of an image using pixels of the given half-frame. This allows to use maximum information of both half-frames.

In the first stage the restoration of one of the half-frames into a full frame using interpolation methods is performed. Let's examine a pixel column in a frame made by combining of two adjoining half-frames. Let's number them. Let Nx be the brightness values of pixel color components in odd rows which are contained in N half-frame. Let Mx be the same in even rows which are contained in M half-frame. Let the restoration of the full frame be performed on the basis of the N half-frame which contains odd rows. Then it is possible to find approximate values of pixel color components of M half-frame ($M0, M1$ etc., see fig. 4) using interpolation of pixel color components of N half-frame ($N0, N1$ etc., see fig. 4). Any interpolation method may be used. The simple average method is used in the example shown in fig. 4:

$$Y0 = \frac{X0 + X1}{2}. \quad (3.1)$$

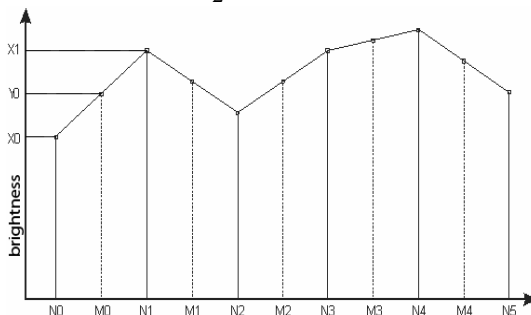


Fig. 4

In real-world problems the less rough interpolation methods are used. These methods also should be adapted to modern computers features to increase the speed of frame processing. The variables are named in accordance with the logic of fig. 4:

$$Y_1 = \frac{(X_1 + X_2) \cdot 5 - (X_0 + X_3)}{8}. \quad (3.2)$$

Thus the brightness characteristic of adjacent pixels influences the estimated characteristic 5 times more than that of the distanced ones.

In the second stage an 8x4 pixel block is chosen in the half-frame which was restored with an interpolation method. Practice shows that the chosen values of width and height of the block are optimal. The block should also contain enough interlaced pixels which were found as described above. Then a search of brightness characteristics aggregate of chosen block pixels of restored half-frame in the M half-frame is performed. The search is performed in some environment in the M half-frame around a block which corresponds to the chosen block in restored half-frame. During the search the criterion of blocks coincidence is the following:

$$\sum_{i=0}^{8.4} \Delta I_i^2 < Tr, \quad (3.3)$$

where ΔI is the brightness difference between appropriate pixels of compared blocks. I.e. total quadratic deviation of brightness of sought block should not exceed some Tr threshold.

The choice of mean-square deviation as a criterion allows to increase apprehensibility to the existence of some pixels in the block which have sizeable brightness deviation. Square of difference of brightness of such pixels and corresponding pixels of the initial block gives bigger values. This allows to exclude unwanted blocks. fig. 5, 6 contain blocks which meet the chosen conformity criterion. The blocks which are shown in fig. 7, 8 do not meet it. The size of blocks in the pictures is increased relatively to the real one advisedly for more clearness.

After finding the sought block the color values of its pixels are substituted to the place of pixels of chosen block of restored half-frame. If the block is not found (no block of given environment meets the criteria) then the values calculated in the first stage are saved.

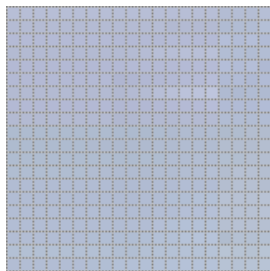


Fig.5

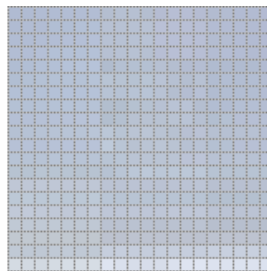


Fig.6

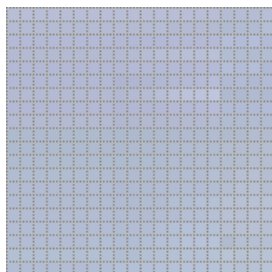


Fig.7

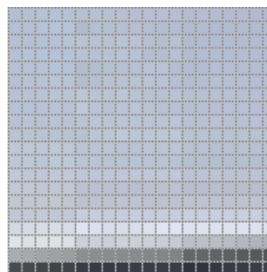


Fig.8

When the processing of all the blocks is finished the M half-frame is replaced with restored half-frame and N half-frame is taken unchanged.

Thus the combination of the methods described above (the method of interlaced pixels finding and the method of interlaced area recovery with motion compensation) allows to use the information of both half-frames and also to decrease artifacts which are inevitable when using mathematical methods, interpolation in particular.

REFERENCES

- [1] "Progressive scan vs. Interlace video", http://www.axis.com/products/video/camera/progressive_scan.htm
- [2] M. Tekalp. "Digital Video Processing", Prentice Hall, 1995.
- [3] Yao Wang, Joern Ostermann, and Ya-Qin Zhang, "Video Processing and Communications". Prentice Hall, 2002.
- [4] J. Watkinson, "The Art of Digital Video", 3rd edition, Focal Press, 2000.
- [5] "What is Deinterlacing? Facts, solutions, examples", <http://www.100fps.com/>
- [6] "Methods of deinterlacing. How to deinterlace video clips, divx movies?" <http://www.gromkov.com/faq/videoedit/deinterlace.html>
- [7] "Video Deinterlace Effect", <http://www.captureandconvert.com/video-effects/Video-Effects-video-deinterlace-effect.htm>

- [8] Chul Ryu, Seung P. Kim, "Deinterlacing Using Motion Compensated Local Spectra," *asilomar*, vol. 00, no. , p. 1394, 1995.
 - [9] "DScaler Help" <http://deinterlace.sourceforge.net/Help/>
 - [10] "NTSC, PAL & Interlace Explained", <http://nickyguides.digital-digest.com/interlace.htm>
 - [11] "DCDi", http://www.answers.com/main/ntquery;jsessionid=9igi8rap6ekdi?method=4&dsid=1512&dekey=DCDi&gwp=8&curtab=1512_1&sbid=lc02a
 - [12] "About XAW-Deinterlace", <http://xaw-deinterlace.sourceforge.net/index.php?sec=about>
 - [13] "Deinterlace DDI", http://msdn.microsoft.com/library/default.asp?url=/library/en-us/graphics/hh/graphics/dxvaref_d72180f0-84bc-4acf-b263-6f6c7e9f7b22.xml.asp
 - [14] Alparsoft Deinterlace Filter documentation, <http://www.alparsoft.com/products.php?id=8&item=6>
- "Human Color Perception", http://msdn.microsoft.com/library/en-us/icm/icm_06y6.asp

Acceleration of Algorithm of Fractal Image Compression

E.S. Pereguda

*Khabarovsk State Technical University, Faculty of Computer facilities,
136 Pacific str., Khabarovsk, 680035, Russia*

Abstract — In the paper, the problem of acceleration of fractal compression algorithm is considered. The analysis of reduction methods of calculations using DCT is resulted.

Index Terms — Fractal compression, chaos, DCT

Fractal image compression is one of the most exotic technologies in the computer image processing. It is based on fractals – specific structures, studying in Theory of Chaos. Any image is the chaotic set of pixels structured definitely. The main question is how to make the fractal expression describing the image. Michael Branslye was the first, who pay attention to the question and specified the image as attractor of the certain fractal. His post-graduate student Arnaud Jacquin has developed an algorithm based on local iterative system of functions. The algorithm is based on search of local self-similarity of separate image elements. For this purpose, the image is partitioned into separate blocks, and among them it is necessary to find the most conterminous. Moreover, it is necessary to make the following operations for this purpose: affine transformations and brightness displacement. The basic affine transformation is compression of the block. The general expression described in [1]:

$$F \approx G(F) + H,$$

where $G: R^2 \rightarrow R^2$ is an operator of affine transformation with all set of the image blocks, H is brightness displacement. Taking into account that in most cases this equation has no exact decision, it is possible to describe it in more strict kind:

$$F = G(F) + H + \varepsilon,$$

where $\varepsilon \in R^2$ is some error of the image. Let \tilde{F} be the exact decision, then

$$F - \tilde{F} = G(F) + H + \varepsilon - G(\tilde{F}) - H = G(F - \tilde{F}) + \varepsilon,$$

whence follows through Cauchy – Bunaykovski inequality:

$$\|F - \tilde{F}\| \leq \|G\| \cdot \|F - \tilde{F}\| + \|\varepsilon\| \text{ or } \|F - \tilde{F}\| \leq \frac{\|\varepsilon\|}{1 - \|G\|}.$$

This expression is meaningful only under condition of $\|G\| < 1$ that means that transformation should be compressing. We shall notice from a condition displacement of brightness H drops out.

The general algorithm of search consists in minimization of expression:

$$\sum_i \sum_j (s \cdot d_{ij} + o - r_{ij})^2,$$

where d_{ij} and r_{ij} are pixels of two compared blocks of the image titled domains and ranges; s is the scaling factor of brightness; o is brightness displacement. In addition, the domain d sizes exceed the range r size, thus the compressing condition is carried out. The purpose is reduction of calculations of the given algorithm.

First of all, for algorithm realization we decide a question about optimum partition of the image on ranges and domains. Splitting on quadtree can be considered enough convenient, but global partition is resulting in substantial growth of run time. Certainly, if the image has the big areas with uniform distribution of energy, such algorithm will be effective. Nevertheless, such images meet seldom and have more likely artificial character. For this reason at the initial research the decision to refuse from splitting quadtree was accepted and will be limited only to the sizes 8×8 for ranges and 16×16 for domains. Such range size will provide satisfied quality and give an opportunity for additional splitting.

The next problem has consisted in limitation of pixel values, which lays in a narrow range from 0 up to 255, hence, is necessary to check of approximation on $0 \leq (s \cdot d_{ij} + o) \leq 255$. This range is very narrow and integer. Check the condition at algorithm realization results in impossibility to make conveyor of algorithm the processor. It has induced to transition of the analysis from integer to real through DCT.

The following step is analysis of operations necessary for processing each pixel. It will need two multiplications for 63 points in all eight affine transformations, i.e. 1008 multiplications to one check of similarity. It is too prodigally. However, as it specified earlier, convergence of the image to attractor is defined only by affine

transformation G , but not brightness. Thus, it is possible to call into question necessity of operation $s \cdot d$ at the analysis though s is necessary at restoration. As s is the scaling brightness factor, the algorithm compares quantity and quality. Having refused scaling it is possible to analyze only qualitative characteristics. In [3] the beautiful proof of the Euclidean metrics minimization for the normalized vectors is submitted. Thus, the problem consists in a finding of the minimal corner between normalized vectors. At this realization, the number of multiplications decreases on half. Researches have shown that refusal from initial condition $0 \leq s < 1$ give an opportunity to form image with sharp transitions of the image that was impossible under a former condition. The use of affine transformations to DCT is process or multiplication on (-1), or to transposing matrixes of DCT coefficients and possible to make the table of transformations [2]:

	Spatial Domain	DCT Domain
1	identity	$I_0(F(u, v)) = F(u, v)$
2	reflection about mid-vertical axis	$I_1(F(u, v)) = (-1)^V F(u, v)$
3	reflection about mid-horizontal axis	$I_2(F(u, v)) = (-1)^u F(u, v)$
4	reflection about first diagonal	$I_3(F(u, v)) = F(v, u)$
5	reflection about second diagonal	$I_4(F(u, v)) = (-1)^{u+v} F(v, u)$
6	rotation through $+90^\circ$	$I_5(F(u, v)) = (-1)^u F(v, u)$
7	rotation through $+180^\circ$	$I_6(F(u, v)) = (-1)^{u+v} F(u, v)$
8	rotation through -90°	$I_7(F(u, v)) = (-1)^v F(v, u)$

Obviously at reflection along horizontal, vertical or simultaneously all even harmonics are always multiplied on 1 i.e. if to compare the reflected images all their even harmonics will coincide. Thus, there is no necessity to make all eight transformations. It is enough to compare only even harmonics of the direct and transposed matrixes, and based on it to make a decision it is doing to rotate the image. Thus, the number of operations of multiplication can be reduced at twice (or four if will be transformation the image only on even DCT coefficients). Last operation is classification of ranges and domains along size of normality DCT vector and on three low-frequency coefficients. In the first case if the length of vector less than the threshold value, the range can be approximated constant brightness and s is equal 0 and it can be not analyzed, and the domain can be simply off from list for the analysis. If the image will consist of areas with constantly brightness, the speed of analysis considerably increases.

Thus, acceleration of analysis and time reduction is significant, though loss of quality is appreciable. For example, the image "Lena" is coded for 1 second, thus the compression degree is 14 times. Quality is not high, though in time of development of algorithm the emphasis was done on reduction of calculation time and simultaneously on preservation of identifiability. The aspiration to reduce an operating time until 1 second is caused by attempt to step over a psychological barrier because in many videoconference systems with low rate with 1 frame per second is sufficient. Resources of the given algorithm still are significant enough. For DCT the algorithm with rate $O(n^2)$ has been used, that extremely is not effective, however its coefficients have been spread out on usual basis that has reduced speed only in 2 times, instead in 4 as it would be possible at transformation on even DCT coefficient basis. In addition, speed can be increased if the first minor of DCT matrix takes for the analysis only. Thus it is equivalent to reduction of the image scale that will allow to reduce of the analysis time still twice. The algorithm is carried out in C++, but translation of algorithm into Assembler via MMX technology could increase productivity also.

REFERENCES

- [1] G. Davis, "Implicit Image Models in Fractal Image Compression". Proc. of SPIE Conf. on Wavelet Applications in Signal and Image Processing IV, Denver.
- [2] Yao Zhao, Baozong Yuan, "A Hybrid Compression Scheme Combining Block-based Fractal Coding and DCT".
- [3] Dietmar Saupe, Raouf Hamzaoui, Hannes Hartenstein, "Fractal Image Compression. An Introductory Overview".

Old Movie Recovery

Roman Khudeev

Alparysoft R&D, Tomsk, Russia

Abstract — In the paper, a method of video restoration from films is described. It is necessary to take into account that the given method should be applied for the films storing on a film only, not on digital or analogue tape. This is because of the fact that the artifacts on tape have other nature and it is necessary to use other algorithms to remove them.

Index Terms — de-noising, noise reduction

There are several algorithms allowing to decrease noise on video and also remove various artifacts from video. The description of these algorithms can be read in [1-9]. These methods can be applied for digital video filtering but we will examine the way of video film restoration.

When storing video on film the last experiencing various physical impact from environment and receives different damages which leads during capturing to various artifacts on video. This decreases final video quality. These artifacts clearly visible on old films and they are visible as dark or bright spots and lines of different configuration. After the capturing of films the video can be processed with special algorithms and the lost areas could be recovered using the neighboring frames information.

As the film is the physical sequence of frames on stripe which is convolute in roll so the specificity of damage of a film is that almost impossible to get equal damage in neighboring frames. I.e. the damage is unique for each frame. The given method uses this specific and allows to recover frames effectively.

At first it is necessary to divide all the video into scenes as the most effective recovering is possible when using neighboring frames of one scene because the most information is doubling. At the moment there are algorithms which are able to determine scene change. The principle of their work is that the previous frame is divided into blocks and for each block on the next frame the similar block is seeking. If the number of blocks for which the equal block was found exceeds some threshold when the scene is the same. If the similar block number is not great then there is scene change.

The following algorithm parameters of scene change determination show its effectiveness in practice:

An image should be divided into blocks 8x8 size.

Radius of search of similar blocks is not exceeded 16 dots for most videos. But for the video with fast motion this number could be bigger in some cases.

Range of blocks similarity is determining as sum of square of difference of brightness of all 64 dots of blocks of compared frames, i.e.

$$\text{Err} = \sum_{i=0}^{63} (A_i - B_i)^2, \quad (1)$$

where Err is total error for a block; A_i is dot i brightness of the first frame; B_i is dot i brightness of the second frame.

If Err of the current block less than the threshold then the given block was found on a compared frame. With the change of the block threshold and with the percentage correlation of found blocks in which the scene was changed it is possible to tune the algorithm of scene change determining for various video.

These methods are effective enough for use in various codecs for the place of scene change determining but for our aims it is necessary to make corrections. The point is that some frames could be damaged severely especially the ones located in the places where the film was glued. So the method described above determines a severely damaged frame as a scene change. And there will be no chance to restore it in future. So it is necessary to compare not only neighboring frames but longer frame sequences. An example (fig. 1, 2) shows video sequences which has severely damaged frames.

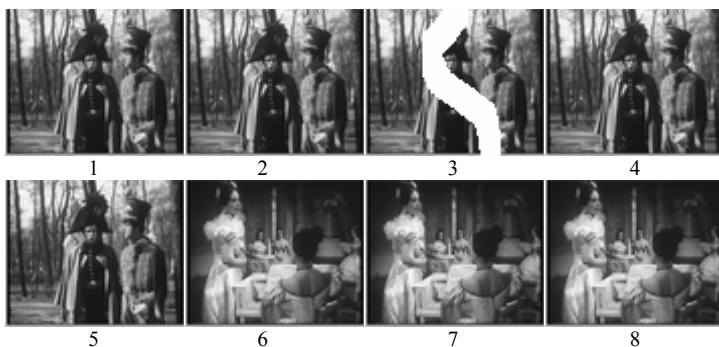


Fig. 1.

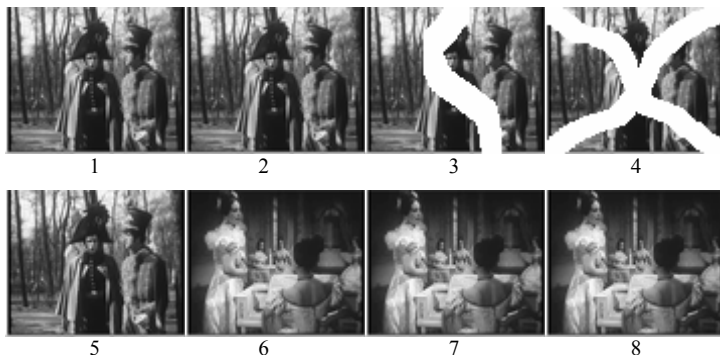


Fig. 2.

In both examples the scene change happens after the 5th frame, but standard algorithms will determine the scene change after 2nd, 3rd and 5th frames for fig. 1 and after 2nd, 3rd, 4th and 5th frames for fig. 2. If sequences of frames are compared but not neighboring frames then it is possible to determine that 1st-5th frames regard to the first scene and 6th, 7th, 8th frame regard the second one. Human is not able to percept an information for the time of tens or even hundreds of milliseconds so in real video a scene can not be shorter than 5-10 frames. More than that the damaged frames is not contain the similar damages these frames will not be identified as a separate scene. So if there are out-of-order frame sequence or separate frames not similar to each other then they could be identified as damaged frames. If previous and next frames are similar then the damaged frames are of the current scene, on the contrary the damaged frames are of either previous scene or next scene. This depends the scene the frames of which more similar to the damaged frames.

After the scenes determination it is possible to restore the whole frames or its parts in sequences of one scene. As it was described above the film damages have characters. It can be white or dark spots or dots and also dark or bright lines of various configuration caused by scratches on film. These damages with liberal share of probability are unique for each frame. Fig. 3 and 4 contain an example of the damage of this kind.

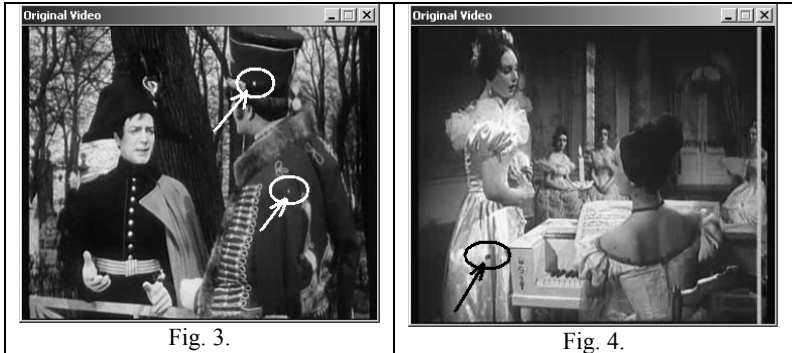


Fig. 3.

Fig. 4.

Damaged parts recovery consists of two stages. The first one is the area determination which should be recovered and the second one is filling them with the appropriate information. To find the area of film damage we can issue that there are only small differences between frames of one scene. This is because of the fact that when recording 25 fps between the neighboring frames there is 40 ms. This time is not enough for physical objects to change. We certainly can not say it about such events as explosions and other ones which are changing objects in a short time. If we are talking about slow camera turning, focus changing or object inside of the frame movement then the changes in frame will be small. And these changes can be tracked. The essence of damaged areas searching is that the frame is divided into blocks and the search of the similar block is performing in the neighboring frame. If such a block was found then this block does not contain damages and we could track to other block. If the block was not found then either the object changed a lot or there are damages of the film. If the object is changed then the similar blocks will not be on the following frames of the scene too. If there are damages then following frames will contain these blocks and so it is possible to identify the damage location.

For the given method realization the same algorithm may be used as there was used for scene change determination. So a frame should be divided into blocks 8x8 size and for each block looking for the similar blocks in the neighboring frames. If the block contains defects then part of its dots will be different a lot by brightness from the dots of neighboring frame. And then squaring the value of the block will be big enough to find the block needed. This

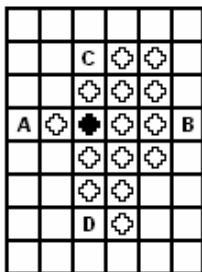


fig. 5

block is marked as possibly damaged. In the following text these blocks will be marked as Bb (bad blocks). The blocks there are no damages we mark as Nb (Normal block). After the whole frame processing some of its blocks could be marked as possibly containing damages Bb. These parts should be processed additionally. If the block contains the damage which can be seen by eye then the damaged area should differ a lot by brightness from the neighboring areas. Or human will not be able to differ the damage from the background and there are no need to recover such a damage. So with the second pass we should perform analysis of brightness of such blocks. For doing this it is needed to do per line scan of these blocks we should find the areas of these blocks where the brightness of neighboring pixels differ a lot. If absolute value of brightness difference of neighboring dots (2) exceed the threshold then where will be the damage border:

$$abs(A_i - A_{i+1}) > Tr, \quad (2)$$

where A_i is i dot brightness; A_{i+1} is $i+1$ dot brightness; $abs(A_i - A_{i+1})$ is absolute value of difference of neighboring dots; Tr is damage border threshold.

All the dots which are located between the border lines inside the damaged block are the damages and they need to be restored.

When the damaged areas were found they need to be restored. For doing this we need to use information from the neighboring areas of the same frame and also from the neighboring frames. On the first stage with the interpolation methods we should recover damaged pixels using current frame information. Fig.5 shows an example of the area which contains damages. The empty cells shows normal dots, the circumference cells shows damaged dots and circle cells shows current dot which is currently restored. For its restoration the information from the normal dots (A, B, C, D) will be used. These are the nearest normal dots upon horizontal and vertical to the current dot.

The brightness of the current dot or the brightness of each color component can be calculated according to the formula (3):

$$A_i = (X_i + Y_i) / 2, \quad (3)$$

where A_i is desired dot brightness; X_i is calculated according to formula 4; Y_i is calculated according to (5).

$$X_i = (A * Lb + B * La) / (La + Lb), \quad (4)$$

where A is A dot brightness; B is B dot brightness; La is the distance in pixels from the desired dot to A dot; Lb is the distance in pixels from the desired dot to B dot.

$$Y_i = (C * Ld + D * Lc) / (Lc + Ld), \quad (5)$$

where C is C dot brightness; D is D dot brightness; Lc is the distance in pixels from the desired dot to C dot; Ld is the distance in pixels from the desired dot to D dot.

The given formulas allow increasing influence of the closer dots to the desired dot and decreasing influence of the far dots. So it is possible to restore the damaged area upon the data of the current frame. If there is possibility to use data from neighboring frames it is desirable to make additional correction of recovered dots values. It is needed to sum all the vectors of block displacement which are located around the damaged area and get the vector of the object movement where the damages exist. Knowing where was the damaged area in the previous frame and where it is located in the next frame it is possible to calculate every damaged dot as simple average between previous and following dots (6):

$$A_i = (A_{i-1} + A_{i+1}) / 2, \quad (6)$$

where A_i is desired dot brightness; A_{i-1} is previous frame dot brightness; A_{i+1} is next frame dot brightness.

To get the final value of the dot brightness it is possible to us both brightness value according to data inside the frame and brightness value according to neighboring frames data. The degree of influence of these values to the final value can be set by user or can be set up during realization of the method.

After the brightness values calculation of damaged dots the restored areas can not be seen from the objects around them. This will increase the quality of perception of restored films.

REFERENCES

- [15] M. Tekalp. "Digital Video Processing", Prentice Hall, 1995.
- [16] Yao Wang, Joern Ostermann, and Ya-Qin Zhang. "Video Processing and Communications", Prentice Hall, 2002.
- [17] J. Watkinson. "The Art of Digital Video", 3rd edition, Focal Press, 2000.
- [18] "Human Color Perception", http://msdn.microsoft.com/library/en-us/icm/icm_06y6.asp
- [19] J.V. Lorenzo-Ginori, K.N. Plataniotis, A.N. Venetsanopoulos, "Nonlinear filtering for phase image denoising". IEEE Proceedings on Vision, Image and Signal Processing. Vol. 149, Issue 5, Oct. 2002.
- [20] D. Teytelman, E.H. Feria, "A simple real-time digital video noise reduction system". Proceedings of the IEEE National Aerospace and Electronics Conference NAECON 1994, 23-27 May, 1994, vol.1, pp. 507-511.

- [21] N. Gupta, M.N.S. Swamy, E.I. Plotkin, "Low-complexity video noise reduction in wavelet domain". IEEE 6th Workshop on Multimedia Signal Processing, 29 Sept. 1 Oct. 2004, pp. 239– 242.
- [22] A. De Stefano, P.R. White, W.B. Collis, "An innovative approach for spatial video noise reduction using a wavelet based frequency decomposition". 2000 International Conference on Image Processing. Proceedings. Vol. 3, 10-13 Sept. 2000, pp. 281-284.
- [23] A. Amer, H. Schroder, "A new video noise reduction algorithm using spatial subbands". Proceedings of the Third IEEE International Conference on Electronics, Circuits, and Systems ICECS '96, Vol. 1, 13–16 Oct., 1996, Pp. 45– 48.

A New Flood-Fill Algorithm for Closed Contour

Roman Khudeev

Alparysoft R&D, Tomsk, Russia

Abstract — In this article, a new flood fill method is described. The method is fast and can be applied to both simple and self-crossing contours. It also can be used to fill the area outside the given contour.

Index Terms — filling of contour

There are several ways to make flood-fill for closed contour [1-5], but these variants demand the large calculations near contour and as a result because of low processing speed. More existent algorithms do not allow to fill complicated contours which contain self-crossings.

The suggested variant is characterized by simple working logic, simple realization and high processing speed. The given method does not use trigonometric functions, multiplication and division operations and recursive algorithms. In contrast to recursive algorithms in which the quantity of verification reaches 4 or even 8 (depend upon algorithm and contour type) for each dot of the contour the quantity of verification in our algorithm in average does not exceed 2 for each dot of the contour. This quickens lot the process of contour flood fill for the cases in which the quantity of dots inside the contour greatly exceeds the quantity of the contour dots. More than that our method allows to fill self-crossing contour both the whole one and any of its parts.

So, the task is:

- There is an array of dots X, Y size.
- There is closed 4 or 8 connected contour. The color of its dots differs from the background (fig. 1).
- It is necessary to fill all the areas which are located inside or outside the given contour.

The description of the algorithm is following.

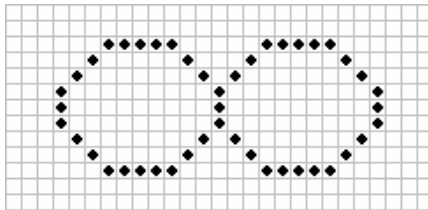


Fig. 1.

The essence of the algorithm is that it is necessary to build other contour (external contour) over the given one (internal contour). And then it is necessary to fill the areas per line in which between two neighboring dots of the external contour there is at least one dot of the internal contour. For doing this it is necessary to make the following steps:

1. It is necessary to find any dot of external contour. This dot can be set or it is necessary to scan an image per line until get to one of the external contour dots (fig. 2).

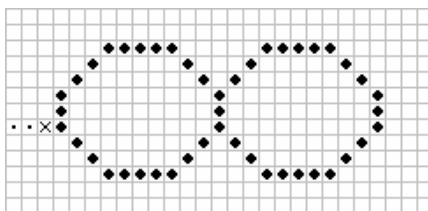


Fig. 2.

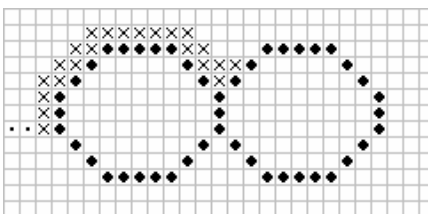


Fig. 3.

2. Then we build external contour. For doing this we should go around the given contour in series and any direction from the point which we had found in item 1. During this we should mark the dots of the external contour (fig. 3).

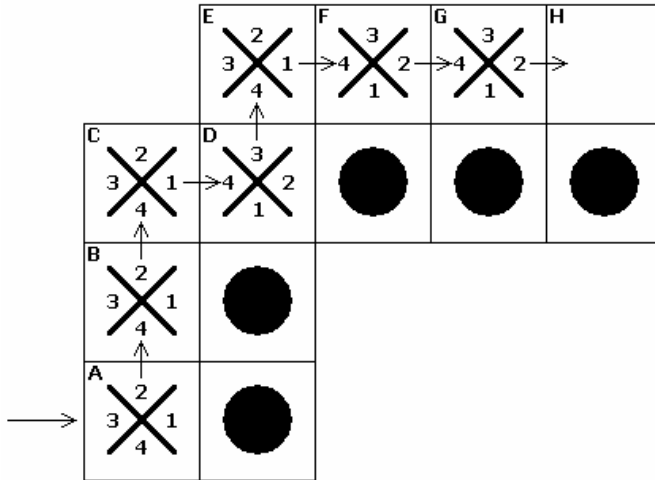


Fig. 4.

The algorithm of external contour building can be as follows: we have the first dot of the external contour (marked with letter A on the fig. 4). It was found during scan per line. For this dot and the following dots it is necessary to determine any “free” direction and make a step in this direction and mark this dot as a next dot of the external contour. Then this should be repeated until the external contour will be completed. The “free” direction is one of four directions which does not lead to a dot of the internal contour when we made a step. The direction is “free” also when we get to a dot of the external contour when we make a step. The examination is directions must be done either clockwise or anticlockwise always. The sequence of the examination of directions for A-G dots of the external contour marked with digits on fig. 4. At first the direction 1 must be examined then 2, 3 and 4. The rule for choosing the direction 1 is the following: the direction is the same as the direction to the closest dot of the internal contour for the first dot; for all the rest of the dots the direction 1 is the next direction anticlockwise from the direction we are coming from, i.e. the direction we are coming from always is number 4. To clarify the process fig. 4 shows the sequence of the examination of directions for several dots of the external contour. The rules described above allow to build the external contour with great speed, i.e. with minimal quantity of examinations of “free” directions.

The process of the external contour building will be finished when the current dot coordinates is the same as the first dot coordinates (fig. 5).

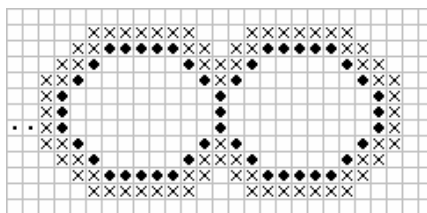


Fig. 5.

3. Now it is time to scan per line the rectangle in which the contour is inscribed. When at least one dot of the internal contour is between two neighboring dots of the external contour we should fill a raw of dots part which is located between two neighboring dots of the external contour. If it is necessary (e.g. the flood fill color is not the same as the contour color) it is possible to exclude from filling the internal contour dots (fig. 6, 7).

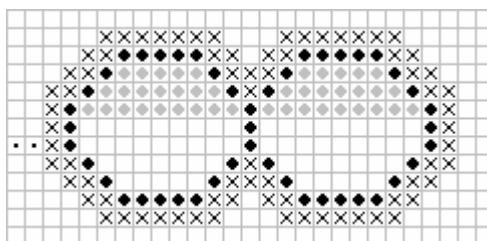


Fig. 6.

The same principle is for filling all the dots outside the given contour. For doing this after the external contour building it is necessary to scan per line and if there are no dots of the internal contour between the edge of the image and the dot of the external contour or if there are no dots of the internal contour between two neighboring dots of the external contour then all the dots can be filled with the filling color.

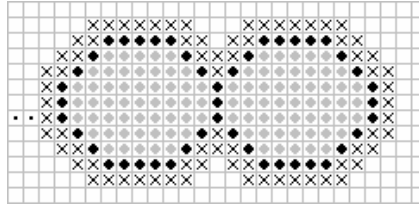


Fig. 7.

If it is necessary to fill the area inside the contour it is possible to do it upon the same principle. But in this case the given contour should be considered as the external one. Then the internal contour is built and if there are no dots of the external contour between two dots of the internal contour then all the dots between the dots of the internal contour can be filled with the color of filling.

So the given algorithm in spite of other ones allows to fill all the internal areas both the simple contour and self-crossing one of any configuration. Also it is possible to fill any area of a self-crossing contour. More than that our algorithm works faster for the contours which have much more dots inside the contour than in the contour.

REFERENCES

- [1] J. Encarnacao, „Einführung in die Graphische Datenverarbeitung“. Eurographics '89. Tutorial Notes 1. Hamburg, FRG, September 4–8, 1989. 122 p.
- [2] D.F. Rogers, “Procedural Elements for Computer Graphics”, McGraw-Hill, Boston, MA, 1998.
- [3] P. Shirley, “Fundamentals of Computer Graphics”, AK Peters Ltd, 2002.
- [4] <http://alglib.sources.ru/graphics/fillarea.php>
- [5] <http://algotlist.manual.ru/graphics/fill.php>

Method of Estimation of the Definition in Photo-Realistic Images

S.V. Say

*Khabarovsk State Technical University
136, Tikhookeanskaya st., Khabarovsk, 680035, Russia
Tel.: (4212)358313, e-mail:sai@evm.khstu.ru*

Abstract — In the paper, original method of estimation of the definition in photo-realistic images founded on the analysis of point objects distortions in equal contrast space of brightness is offered.

Index Terms — Image, brightness, JPEG

At present, standard specifying digital photo and video quality does not exist, so many images is offered in "compact packing", but with low quality. What quality of the images is necessary? Restrictions on transmission channels and information stores bring about searching for the half-way decisions between degree of the image compression and their quality. The problem is solved by following way. Analysis of image quality is carried out on the first stage in used system of the coding and transmissions photo or video material. If image quality does not correspond to the given requirements on the second stage, the optimization of the compression algorithm under known restrictions on transmission channel or information store volume is executed. If optimization does not allow to reach the required quality, then in this case half-way decision is offered in the manner of recommendation at the option parameter of the transmission channel or the information store volumes.

Analysis of the existing methods of estimation of the image quality allows the following.

1. The visual estimation quality image is subjective and requires the large expert operations.
2. The estimation quality images on base of the methods of the distortion signal measurements on test table, used in analog television, in digital system usually brings about inadequate result to visual

estimation.

3. Most often used root-mean-square (RMS) criterion does not give the objective estimation to visual definition and sharpnesses, since eye in process of the perception processes the image on local sign, rather than averages it termwise.

Thereby, the problem of searching for of the objective quality image criterion is actually.

Supposing that inaccuracy of the scanner is minimum, shall value the influence of inaccuracy of the compression algorithm on example of JPEG standard. Experience shows that increase degree compression in the most essential distortion reveal itself on fine structure of the image consisting of point object. Under greater factor of the compression contrast object falls to such extent that they become not distinguished and, herewith, image loses definition.

The essence of the method is following. Recognition point object source scene is executed on first stage on:

$$d = |W_{i,j+1}^* - (W_{i,j}^* + W_{i,j+2}^*)/2| \geq P_1; \quad |W_{i,j}^* - W_{i,j+2}^*| \leq P_2; \quad (1)$$

where $W_{i,j}^* = 25Y_{i,j}^{1/3} - 17$ is brightness index of (i, j) element of the image, computable in equal contrast space; d is contrast of the point object comparatively nearby element in horizontal direction; P_1 and P_2 is parameters assigned number minimum threshold visions on brightness.

If condition (1) is carried out consider that object is discovered and executed estimation of the distortion on following:

$$\varepsilon = 100 \left(|d - \tilde{d}| + \sigma \right) / d, \quad (2)$$

where ε is normalized mistake; \tilde{d} is the contrast of the point object of the decoded image; $\sigma = \sqrt{(W_{i,j}^* - \tilde{W}_{i,j}^*)^2 + (W_{i,j}^* - \tilde{W}_{i,j+1}^*)^2 + (W_{i,j}^* - \tilde{W}_{i,j+2}^*)^2}$ is standard deviation of brightness element source and decoded fragment of the images.

Similarly recognition and estimation of the distortion point object is executed in vertical direction. From expression (2) follows that distortions of the point object are valued in percent attitude to source contrast d that can bring about ambiguous visual estimation of definition of the image with low and high contrast.

For the reason increasing of objectivity estimation is offered to analyze distortion point object with contrast close to threshold of the visual perception. In particular in work [1], it is shown that threshold

of the contrast on brightness for small details with size not more 1-2 pixels is 4..6 minimum thresholds. So parameter P_1 is chose within 10...20 that in 2...3 times exceeds threshold of the contrast. Parameter $P_2 = 2...3$ is chose from condition that differences on brightness between nearby element of the point object must be noticeable for eye.

On the last stage the average of the distortion discovered point object estimation is calculated on the whole area of the image analyze and on its importance is defined rating quality. As scales estimation is chose 10-point scale quality, used in Adobe Photoshop when performing JPEG. Dependence of average importance of the error is brought in table 1 from rating quality q got after processing 15 photo-realistic images.

Table 1

Rating	Low			Medium			High		Maximum	
	1	2	3	4	5	6	7	8	9	10
q	1	2	3	4	5	6	7	8	9	10
$\bar{\varepsilon}$ %	60	56	50	44	42	40	30	20	11	6

Experiment has brought about the following result. At compression of photo-realistic images by JPEG with given parameter quality q , deviation in result estimation for different images (the large plan, average plan, texture and others) does not exceed 5-10%. Use the standard method founded on calculation of the root-mean-square mistake (RMS) under equal parameter quality gives deviation up 30-40%. Thereby, proposed method is objective and allows more exactly value distortions the small details and consequently definition of images.

Thus, designed method is ready not only for analysis of inaccuracy of the JPEG algorithm, but also for any algorithm of the image compression. In this case, it is simply to compare of the $\bar{\varepsilon}$ with rating quality. Also, the method shall use for analysis of definition of the in I-frames dynamic video sequences used in MPEG standard.

REFERENCES

- [1] Say S.V. "Quality of the transmit and reproducing the small details color television images". Vladivostok: Dalinauka, 2003. – 160 p.

Contents

The Usage of Mobile Agents for Management of Data Transmission in Telecommunications' Networks <i>T. Orzechowski</i>	5
A Convolutional Code Decoder Design Using Viterbi Algorithm with Register Exchange History Unit <i>V. P. Pribylov, A.I. Plyasunov</i>	10
Formal Interpretation of Network Tasks of Model OSI <i>A.A. Kiselev, S.N. Novikov</i>	16
The Construction of Wireless Network Model with Security and Performance Criteria (Security Matrix Based) <i>R. Sutormin, D. Pochufarov</i>	23
The Analysis of Probability-Time Characteristics of a Telecommunication Network <i>S. N. Novikov, A.A. Burov</i>	26
Automatic Detection of Local and Global Software Failures <i>P. Hazy, R. E. Seviara</i>	30
Design of the Steganography System Based on the Version 4 Internet Protocol <i>E.O. Savateev</i>	36
Cryptographic Data Security in Wireless Networks Based on Biometrical Passport <i>D. V. Vishnyakov, A. G. Serdyukov</i>	50
Tensors Analysis for Investigation Next Generation Network <i>D.U. Ponomarev</i>	53
A Protection Profile and Its Content <i>O. Solonskaya</i>	58
Study Sensing Properties to CH ₄ of Pt/SnO ₂ :Sb Thin Film Gas Sensor in Pulsing Mode <i>O.V. Anisimov, N.K. Maksimova, S.S. Schogol, R.V. Chernykh, E.V. Chernikov</i>	63
Diffusion of Chromium into GaAs as a Way to Detector Material Making <i>M.V. Ardyshev, I.A. Prudajev, S.S. Khudkov</i>	68

Detectors for the X-Ray Testing Systems <i>G.I. Ayzenshtat, M.D. Vilisova, M.A. Lelekov, A.I. Ivashchenko, D.Yu. Mokeev, L.P. Porokhovnichenko, O.P. Tolbanov, L.G. Shapoval</i>	72
Analysis of Free-Carrier Charges Distribution in the n-GaAs Monocrystals Used at Formation of the High-Resistance Material for the Ionizing Radiation Sensors <i>D.L. Budnitsky, O.B. Koretskaya, V.A. Novikov, O.P. Tolbanov</i>	78
Study of Particularities for Metal Contact Formation to the Semiconductor High-Resistance GaAs:Cr <i>D.L. Budnitsky, A.D. Lychagin, L.S. Okaevich, O.P. Tolbanov</i>	83
The Influence of Thermal Annealing on Sensitivity of Silicon MOS-Diodes to Reducing Gases <i>V.I. Baljuba, V.Y. Grisyk, T.A. Davidova, V.M. Kalygina, S.S. Nazarov, A.V. Panin, L.S. Khudkova</i>	88
New Photovoltaic Gamma and X-Ray Detector <i>G.I. Ayzenshtat, M.D. Vilisova, E.P. Drugova, D.Y. Mokeev, L.P. Porokhovnichenko, V.A. Chubirko</i>	94
The Detected Block for Systems of Nondestroying Testing Based on the GaAs Detectors <i>I.I. Nadreev, S.V. Kasyanov, S.A. Ryabkov, O.P. Tolbanov, A.V. Tyazhev</i>	98
Estimation of GaAs Detector System Characteristics for Low Dose Mammography <i>M. V. Bimatov, I. Ph. Nam, A.V. Tyazhev</i>	102
Detector Structures Based on Epitaxial Gallium Arsenide Compensated by Chromium <i>M.D. Vilisova, O.P. Tolbanov, D.Y. Mokeev, E.P. Drugova, V.A. Chubirko, L.P. Porokhovnichenko, I.V. Ponomarev</i>	107
Gamma Quantum and Alpha Particle Counters Based on GaAs Detectors <i>M.A. Rozhnev, S.A. Ryabkov, D.Yu. Mokeev, A.V. Tyazhev, A.N. Zarubin</i>	111
Impulse Response of GaAs Radiation Imaging Detectors <i>A.V. Tyazhev, R.A. Ryzhov</i>	116
Methods of Design Improvement of Balun Transformer with Additional Balancing Lines Using Microstrip Lines with Front Coupling <i>S. A. Goncharov, V. I. Sedinin</i>	121

Advanced Large Distance Optical Free-Space Link on the Infrared Diode in Nanosecond Pulsed Mode <i>E.D. Golovin, O.V. Stukach</i>	126
Inductive Voltage Divider Simulation in MATLAB <i>V.L. Kim, R.G. Dulbinov</i>	135
The Electric Circuit Property for Use in Blocks of Data Mining and Processing <i>G.I. Peredelsky, A.C. Romanchenko, U.V. Didenko</i>	141
Digital Calculation of Frequency of Periodical Signal (Sinusoidal and Triangular) <i>T. Benslimane, B. Chetate</i>	146
De-Interlacing Using Area Based Motion Compensation <i>R. Khudeev, S. Osipov, V. Afanasyev</i>	152
Acceleration of Algorithm of Fractal Image Compression <i>E.S. Pereguda</i>	159
Old Movie Recovery <i>R. Khudeev</i>	163
A New Flood-Fill Algorithm for Closed Contour <i>R. Khudeev</i>	170
Method of Estimation of the Definition in Photo-Realistic Images <i>S.V. Say</i>	175

Author Index

Afanasyev 146, 152	Nadreev 98
Anisimov 63	Nam 102
Ardyshev 68	Nazarov 88
Ayzenshtat 72, 94	Novikov 16, 26, 78
Baljuba 88	Okaevich 83
Benslimane 146	Orzechowski 5
Bimatov 102	Osipov 146, 152
Budnitsky 78, 83	Panin 88
Burov 26	Peredelsky 141
Chernikov 63	Pereguda 159
Chernykh 63	Plyasunov 10
Chetate146	Pochufarov 23
Chubirko 94,107	Ponomarev 53, 107
Davidova 88	Porokhovnichenko 72, 94, 107
Didenko141	Pribylov 10
Drugova 94, 107	Prudajev 68
Dulbinov 135	Romanchenko 141
Golovin 126	Rozhnev 111
Goncharov 121	Ryabkov 98, 111
Grisyk 88	Ryzhov116
Hazy 30	Savateev 36
Ivashchenko 72	Say 175
Kalygina 88	Schogol 63
Kasyanov 98	Sedinin 121
Khludkov 68	Serdyukov 50
Khludkova 88	Seviora 30
Khudeev 152, 163, 170	Shapoval 72
Kim 135	Solonskaya 58
Kiselev 16	Stukach 126
Koretskaya 78	Sutormin 23
Lelekov 72	Tolbanov 72, 78, 83, 98, 107
Lychagin 83	Tyazhev 98, 102, 111, 116
Maksimova 63	Vilisova 72, 94, 107
Mokeev 107, 111	Vishnyakov 50
Mokeev 72, 94	Zarubin 111

IEEE International Siberian Conference on Control and Communications (SIBCON-2005). Proceedings. – Tomsk: The Tomsk IEEE Chapter & Student Branch. Russia, Tomsk, October 21–22, 2005.

General Editor: Oleg Stukach
Editor: Nataly Golikova

Printed in the Tomsk State University of Control Systems
and Radioelectronics

Address: TUCSR, 40, Lenin Avenue,
Tomsk, 634050, Russia
<http://ieee.tusur.ru>

IEEE Catalog Number: 05EX1091
ISBN: 0-7803-9219-1
Library of Congress: 2005925121